8-17-2016 12:00 AM

Analysis and Mitigation of Temporary Over-Voltage (TOV) Phenomenon in Unintentionally Islanded Grid-Connected Photovoltaic (PV) Inverters

Md Maruful Islam
The University of Western Ontario

Supervisor
Dr. Amirnaser Yazdani
The University of Western Ontario

Graduate Program in Electrical and Computer Engineering
A thesis submitted in partial fulfillment of the requirements for the degree in Master of Engineering Science

Abstract

Grid-connected photovoltaic (PV) solar systems, like other inverter-based distributed generators, can cause temporary over-voltages (TOVs), especially subsequent to faults and unintentional islanding incidents, and can damage equipment and customers within the host distribution network. Thus, this thesis aims to study the phenomenon and propose corrective measures for it. Thus, the thesis first presents detailed models for a conventional single-stage PV system and a modified single-stage PV system. The conventional system uses a Δ/YG isolation transformer, whereas the modified system, proposed in the literature, assumes a Y/YG isolation transformer that is effectively-grounded by an additional half-bridge leg energized by the dc-link of the voltage-sourced inverter (VSI) of the PV system. Moreover, the thesis proposes two TOV mitigation schemes that augment the basic controls of the conventional and modified single-stage PV systems, respectively. Further, the thesis models a two-stage PV system that adopts the same TOV mitigation scheme as that proposed for the conventional single-stage system. Then, the TOV caused by the two-stage system is evaluated, with and without the TOV mitigation scheme. It is shown that the proposed TOV mitigation schemes are effective. The thesis also compares the TOVs caused by the three aforementioned PV systems, with and without the TOV mitigation schemes, and concludes that a two-stage PV system without a TOV mitigation scheme produces smaller TOVs than its single-stage counterparts without TOV mitigation schemes. Similarly, a two-stage PV system with its TOV mitigation scheme produces smaller TOVs than its single-stage counterparts with their respective TOV mitigation schemes. The performance of the PV systems and the effectiveness of the TOV limiting schemes are evaluated through time-domain simulation studies conducted in the commercial grade PSCAD/EMTDC software environment.

Keywords: Distributed Generator (DG), DC-DC Boost Converter, Ground Fault, Islanding, Maximum Power Point (MPP), Photovoltaic (PV) Inverter Systems, Single-Stage PV System, Two-Stage PV System, Temporary Over-Voltage (TOV), TOV Limiting Scheme, Voltage-Sourced Inverter (VSI).

Dedication:

To my Mom,

Jannatun Tazri Shamonti,

and Soma & Manisha Chakraborty.

Acknowledgments

I would like to express my sincere gratitude to my supervisor, Prof. Amirnaser Yazdani, for the continuous support of my graduate study, for his valuable supervision, immense knowledge, and encouragement in my research work. His constructive guidelines and friendly attitude has been a constant source of motivation for hard work and sincerity. His guidance helped me in all the time of research and writing of this thesis.

I am also grateful to Dr. Mohammad Dadash Zadeh, Dr. Rajiv K. Varma, Dr. Jin Jiang, Dr. Hisham Mahmood, and Dr. Firouz Badrkhani Ajaei, for sharing their valuable knowledge during my graduate course studies. In addition, I must express my very profound gratitude to Dr. Quazi Rahman for providing me with unfailing support and continuous encouragement throughout my years of graduate study. I would like to thank Dr. Hamidreza Ghoddami for his technical support on this thesis.

I would like to acknowledge the financial support provided by the University of Western Ontario and Natural Sciences and Engineering Research Council of Canada (NSERC).

I thank my fellow labmates Tirath, Hasan, Hadi, Hessam, and Rahim for their constructive suggestions, excellent company and constant support.

I am immensely grateful to Soma Chakraborty and Manisha Chakraborty for their financial support and encouragement towards pursuing my higher study. Last but not the least, I would like to thank my parents and to my brother and sister for supporting me spiritually throughout writing this thesis.

Contents

List of Figures

List of Tables

List of Appendices

Convention for Notations

For clarity and consistency, the following is used in this thesis.

- Circuit parameters are denoted by upper-case letters, for example, C, L_f.
- Instantaneous voltages and currents, and variables and signals are denoted by lower-case letters, for example, i, v_s, v_{tabc}, etc.
- Real and Reactive powers are denoted by upper-case letters, for example, P_t, Q_t, P_s, Q_s, P_g, Q_g, etc.
- dq-transformed variables are denoted by lower-case letters and accompanied by applicable subscripts, for instance, i_d, m_q, v_{sd}, etc.
- Laplace transformed variables are denoted by upper-case letters and accompanied by (s), e.g. $I_{dref}(s)$.
- Subscript t denotes an inverter phase terminal variable.
- Subscript s denotes an inverter ac-side variable.
- Subscript g denotes a grid-side variable.
- Subscript d denotes a d-axis variable.
- Subscript q denotes a q-axis variable.

Nomenclature

v_{pv}	PV *generator* terminal voltage
v_{dc}	DC-link voltage
v_{tabc}	Inverter phase terminal voltages
v_{sabc}	Inverter ac-side phase voltages
v_{gabc}	Grid-side phase voltages
v_l	Load voltage
i_{pv}	PV *generator* output current
i_{tabc}	Inverter phase terminal currents
i_{abc}	Inverter ac-side phase currents
i_{gabc}	Grid-side phase currents
i_L	Inductor current of the dc-dc boost converter
i_l	Load current
P_{pv}	PV *generator* power
P_s	Real power output of the PV system
Q_s	Reactive power output of the PV system
R	Interface resistance
L_f	Filter inductance
C	DC-link capacitance
C_{pv}	PV *generator* terminal (input) capacitor
C_f	Filter capacitance
B_r	PV inverter disconnect breaker
B_g	Utility-interface disconnect breaker
ρ	dq-frame reference angle
ω	dq-frame angular speed
$m_{dq,max}$	Maximum saturation limit of the inverter dq-frame modulating signals
$m_{abc,max}$	Maximum saturation limit of the inverter abc-frame modulating signals
$F(s)$	Transfer function of the current-controller feedforward filter
$H(s)$	Transfer function of the PLL filter
$T(s)$	Transfer function of the low-pass filter (LPF)

List of Abbreviations

ANSI	American National Standards Institute
APAC	Asia-Pacific
CSA	Canadian Standards Association
DG	Distributed Generator
EMTDC	Electromagnetic Transients including DC
EPIA	European Photovoltaic Industry Association
FACTS	Flexible AC Transmission Systems
HBC	Half-Bridge Converter
IC	Incremental Conductance
IEA	International Energy Agency
IEEE	Institute of Electrical & Electronics Engineers
LPF	Low Pass Filter
LV	Low Voltage
MEA	Middle East and Africa
MPP	Maximum Power Point
MPPT	Maximum Power Point Tracking
MV	Medium Voltage
NEC	National Electrical Code
PCC	Point of Common Coupling
PFC	Power Factor Correction
PI	Proportional-Integral
PLL	Phase-Locked Loop
PSCAD	Power System Computer-Aided Design
p.u.	Per-Unit
PV	Photovoltaic
PVPS	Photovoltaic Power Systems Programme
PV-STATCOM	Photovoltaic (Inverter) Static Synchronous Compensator
PWM	Pulse-Width Modulation
STATCOM	Static Synchronous Compensator
TOV	Temporary Over-Voltage
VCO	Voltage-Controlled Oscillator
VML	Vector Magnitude Limiter
VSI	Voltage Sourced-Inverter
Wind-STATCOM	Wind turbine (Inverter) Static Synchronous Compensator
YG	Grounded Wye

Chapter 1

Introduction

Recently, the energy production of the world is in transition stage, shifting from conventional to renewable forms of energy sources to deliver power to the grid. Among renewable forms of energy sources, large-scale power generation from photovoltaic (PV) solar systems are considered to be an attractive option in distributed generation applications, due to its cost-effectiveness, technical and environmental benefits [1–7]. Thus, the multi-megawatt distributed PV systems and their interconnection into distribution networks have increased in a growing number of countries around the globe [4], [8–10]. However, large number of distributed PV systems connected with the grid introduces many technical challenges. This chapter presents an overview of the recent proliferation of the distributed PV systems and their key technical challenges related to their integration with distribution networks. In addition, the chapter presents the main goals and contributions of the thesis.

1.1 Background and Motivation

1.1.1 Development of PV Solar Systems

According to the photovoltaic power systems programme (PVPS) annual report of international energy agency (IEA) and europian photovoltaic industry association (EPIA) data, the year 2015 has seen close to 50 GW of additional grid-connected PV solar systems installed worldwide; approximately 25% above from the total installed capacity in the year of 2014 and raising the cumulative installed capacity close to 230 GW [9], [10]. Figure 1.1 and Figure 1.2 present the grid-connected capacities which best describe the role of PV solar power in the energy system. Figure 1.3 illustrates that the total grid-connected PV solar system's installed capacity in 2019 could reach 540 GW with the

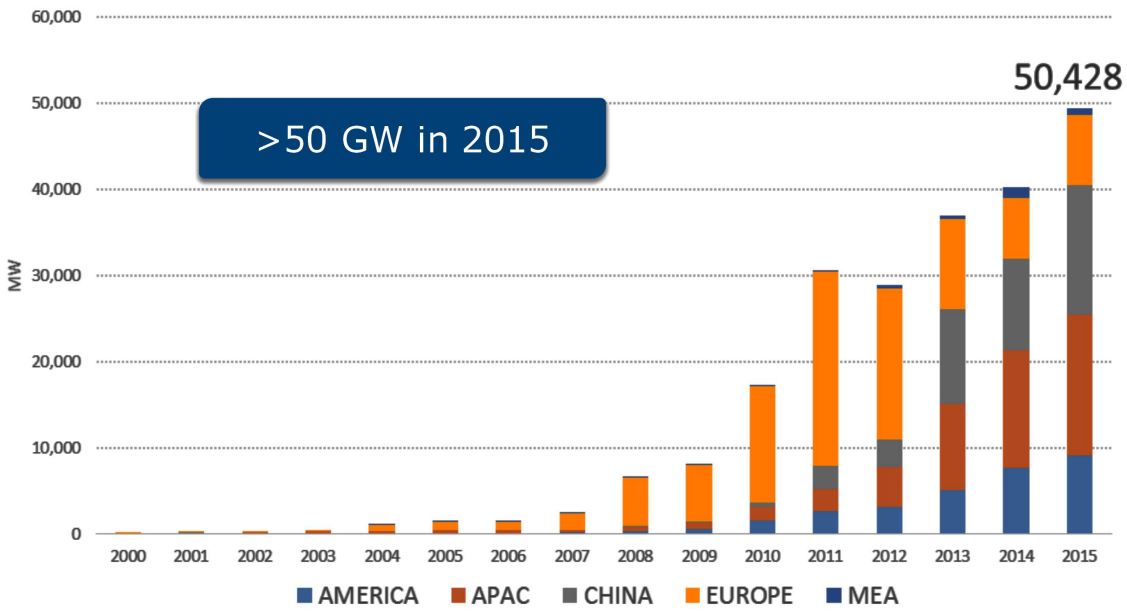

Figure 1.1: Global PV solar installed capacity for the year of 2015 [10].

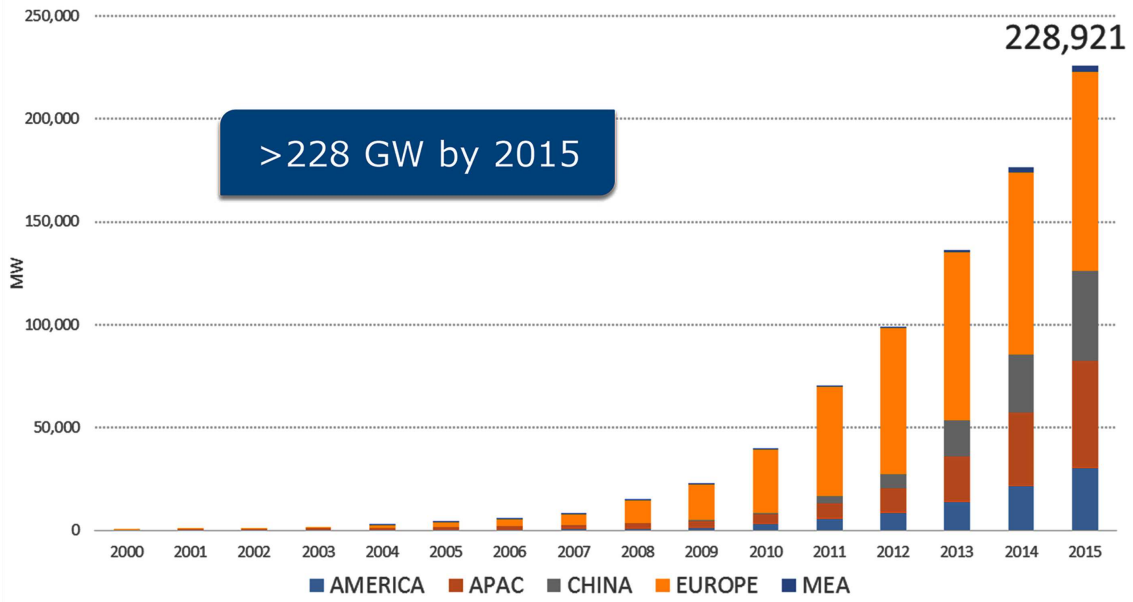

Figure 1.2: Global PV solar cumulative installed capacity from the year of 2000 to 2015 [10].

highest probability scenario being around 450 GW [10]. The proliferation of PV solar systems have led to decreasing costs due to both higher production of PV modules and improved efficiency of the other PV system components. Moreover, due to the incentives provided by many governments and the green-generation portfolio requirements, grid-connected PV systems with capacities in the order of several megavoltamperes (MVAs) installations are being increasingly installed worldwide [11].

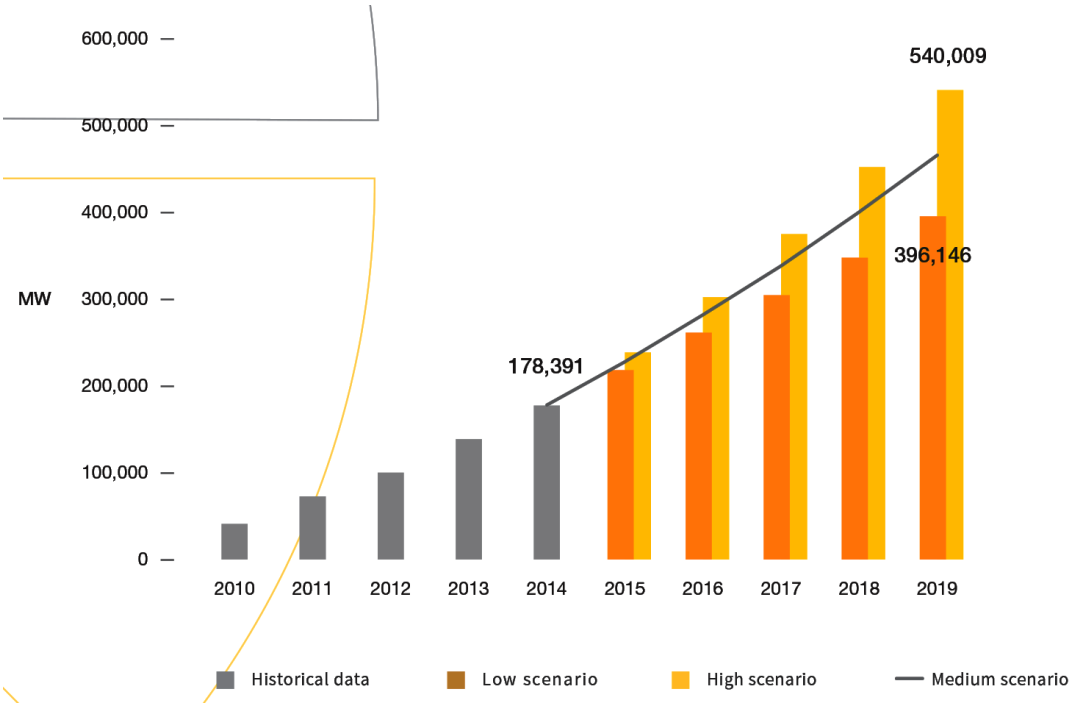

Figure 1.3: Global PV solar power cumulative market scenarios until 2019 [10].

Canada is one of the top ten countries in the world with respect to the total installed PV solar capacity. Since 2001, Canada's solar sector has been witnessing a significant growth in investments year after year. According to the national survey report of PV power applications in Canada, in 2014, the cumulative PV solar installed capacity had grown to about 1,843 MW [12]. Figure 1.4 illustrates the PV solar installed capacity in Canada.

1.1.2 Impacts of Distributed PV Systems

PV solar systems are normally interfaced with the medium-voltage (MV) and low-voltage (LV) distribution networks. While high penetration of PV systems into distribution networks provide benefits such as fulfilling additional load demands, and hence reducing the transmission network expansion and losses, PV systems can affect the host distribution networks and introduce technical issues such as over-voltages, temporary over-voltages (TOVs) subsequent to ground faults and unintentional islanding incidents, reverse power flows, low fault current contributions, and injection of harmonic currents [7], [14–26]. The following subsections briefly discuss the issues related to inverter-based distributed generators (DGs) (including PV).

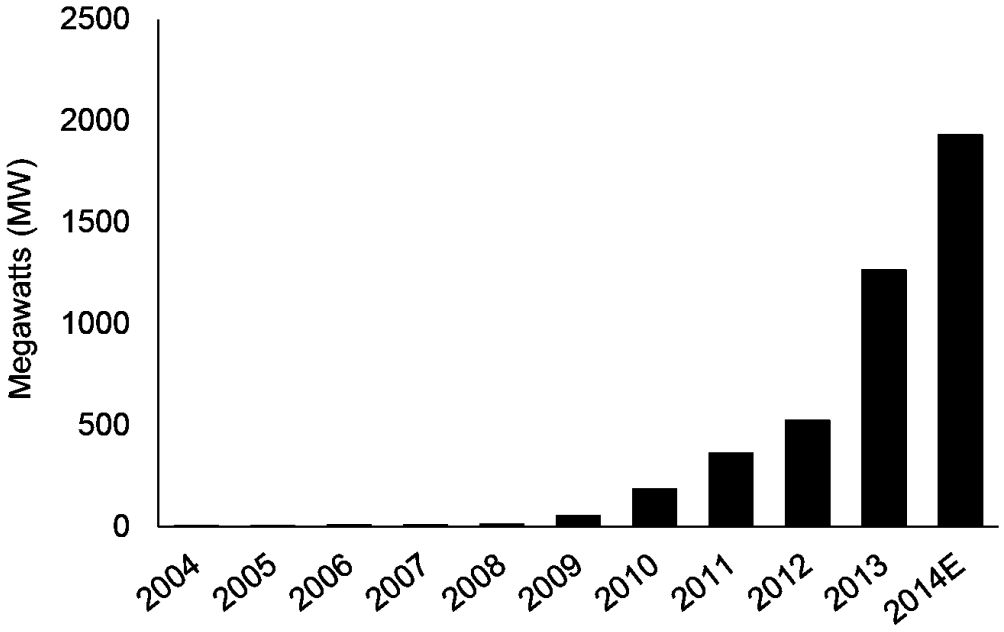

Figure 1.4: PV solar installed capacity in Canada [13].

Over-Voltages

One of the most well-known characteristics of large-scale grid-connected PV systems is that they can cause over-voltages. The effect of an over-voltage is particularly evident and problematic when large PV plants are connected near the end of a long, lightly loaded feeder. This issue is known as over-voltage problem caused by inverter-based DGs [14], [15], [21]. Figure 1.5 shows an example of a voltage rise condition for a very large PV system connected at the end of a feeder that transmits power to a substation. For a large PV system connected near the end of a feeder, the voltage rise can be significant, raising the voltage above the *ANSI Range-A* upper limit of +5% [22]. The authors in [16] report that the variations in the solar irradiance can also cause substantial swings in the output power of PV systems and, consequently, on the feeder voltages. A number of prior work [27–31] have studied TOVs caused by inverter-based DGs. Distributed PV systems can also cause TOVs, particularly subsequent to ground faults and unintentional islanding incidents [30], [31].

In [27], [28], [32], another form of over-voltages, that is, resonant over-voltages during islanding incidents, has been studied. During accidental islanding of a DG, interaction between the generator and power-factor correction (PFC) capacitors can cause series resonance [27]. Moreover, interaction of the induction and synchronous generators with feeder capacitor bank can excite ferroresonance and, as such, over-voltages can reach up to 3 per-unit (*p.u.*) [33], [34]. Over-voltages due to lightning strikes, however, are not

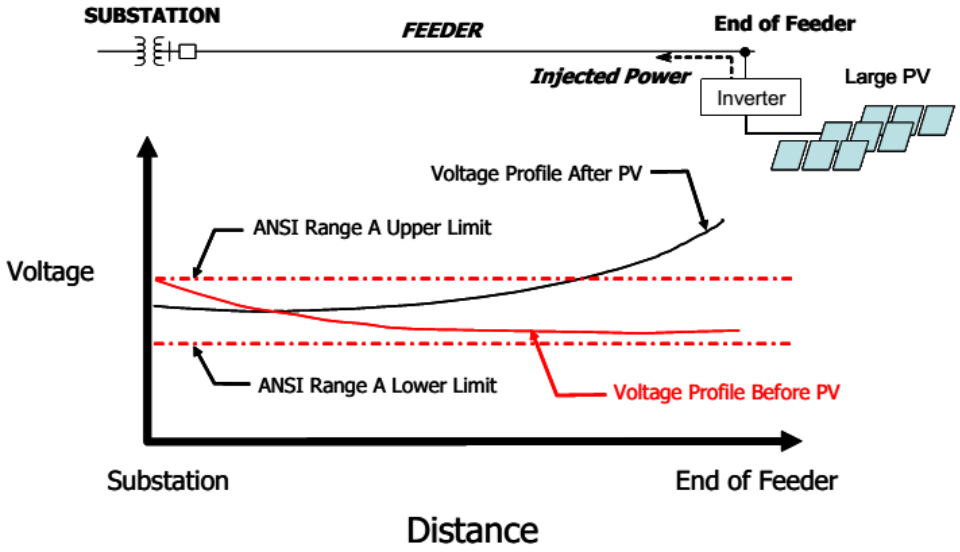

Figure 1.5: Voltage rise resulting from a very large PV system connected at the end of a feeder that transmits power to a substation [22].

due to DGs; rather, they are a direct threat to DGs [27]. Thus, care must be taken to protect the DGs against over-voltages caused by lightning strikes.

Over-voltages can reduce the life of utility equipment and customers, and they can damage the DG itself. IEEE and CSA standards [35–38] specify the requirements relevant to the performance, operation, testing, safety, and maintenance of DGs. The underlying philosophy of the aforementioned standards is that, a DG should not negatively affect the grounding and protection schemes or the power quality of the distribution system, and it must disconnect, as quickly as possible, under abnormal operating conditions. Care must be taken to ensure that the voltage variations fall within the acceptable magnitudes (for example, ±6% of nominal value is permitted in [20]). Reference [39] discusses possible solutions to the voltage rise problem, such as limiting the output power of DGs, control of the reactive power, incorporation of storage systems, use of flexible ac transmission systems (FACTS) devices, etc.

Reverse Power Flow

The introduction of the PV systems can change the dynamic of the network because power may flow in both directions. When the PV generation at its highest and the feeder load demand is at its lowest, the power flow can be reversed, and the feeder will start exporting power to the neighboring feeders. Since distribution feeders are typically designed for unidirectional power flow, this phenomenon can affect the over-current protection coordination and operation of line voltage regulators as they are not

designed for both forward and reverse power flow conditions [14].

Reference [15] suggests that, for a small number of feeders, to detect and stop the reverse power flow, reverse power detection relays can be installed. Reverse power flow most likely occur during the daytime and, therefore, specific studies must be conducted on a feeder-by-feeder basis to select the most adequate protection strategy and design, if a high penetration of utility-scale PV system is expected.

Unintentional Islanding

Islanding refers to the scenario where a part of the utility system, including DGs and local loads, is accidentally or purposefully disconnected from the upstream network, for maintenance purpose, equipment failures, or faults. Figure 1.6 illustrates the islanding situation.

As shown in Figure 1.6, an island can take place by accident when a recloser opens and isolates a section of the power system with an energy source. The aforementioned operation can impact the DG equipments and customer loads within the islanded zone because of poor power quality. Risks also arise for technicians who work on the lines, as well as for the general public who may be exposed to energized conductors [15], [40].

Modern electronically-coupled DGs generally employ current-controlled voltage-sourced inverters (VSIs). Therefore, islanding can lead to voltage/frequency instabilities, which, in turn, result in inverter shut down by its protection mechanisms. This is commonly referred to as the passive anti-islanding protection. A number of works [41–43] present reviews of techniques implemented or proposed for islanding detection.

Short-Circuit Current Contribution

In the radial distribution systems, protection schemes are based on the principle that power and fault current due to short circuit, flow from the utility energy sources to the loads and were developed without considering the possible impact of the DGs (PV, wind, battery etc.). Therefore, recent high volume of PV systems introduce new sources of fault current that can change the direction of current flow, increase the fault current magnitudes and, as such, affect the performance for certain types of over-current protection schemes.

Figure 1.7 shows that the current flowing to the adjacent feeder fault location is not only from the 115 kV utility energy source but also from the various DGs and PV systems. In [22], the aforementioned problem has been addressed and provides possible solutions such as the use of local short circuit current limiting capability in the inverter

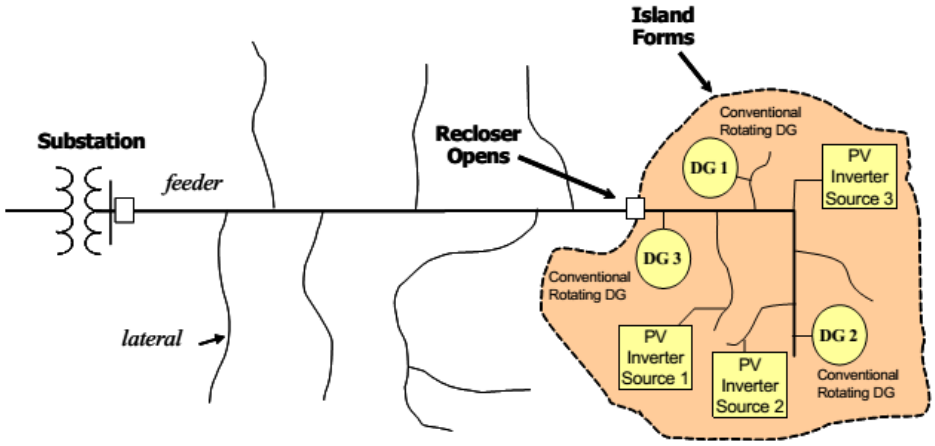

Figure 1.6: Example of an island composed of conventional rotating machine energy sources and PV inverter sources [22].

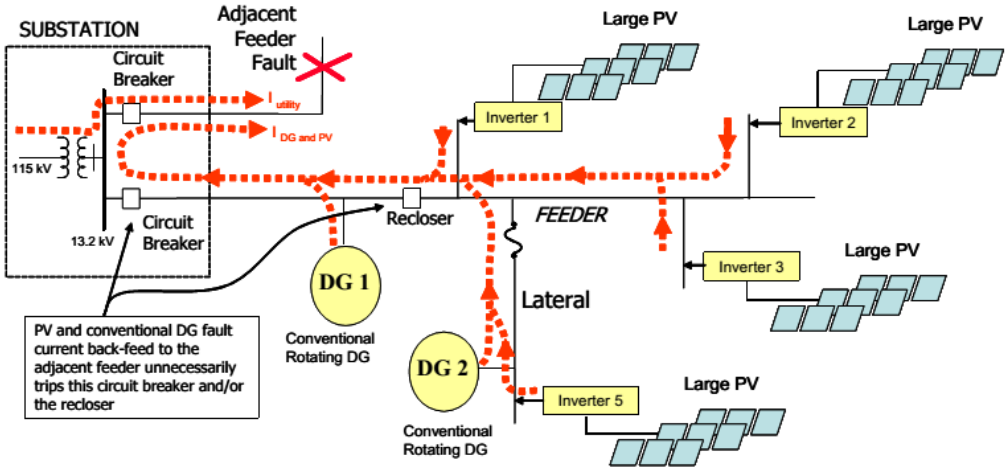

Figure 1.7: Example of how high penetration of DGs can affect protection devices [22].

control architecture and the use of directional over-current blocking and/or special transfer tripping schemes.

Harmonics

Harmonics are currents or voltages with frequencies that are integer multiples of the fundamental power frequency [15]. Harmonic generation by the PV is a major concern for utilities. A number of works [23–26] have focused on PV systems, with an emphasis on their harmonic interactions with the distribution network and their impact on the power quality [19], [21], [24], [26]. If the PV inverters are not designed optimally, harmonics may be injected into the network and can cause significant distortion in point of common

coupling (PCC) voltages. IEEE standards [37], provide guidelines on harmonic limits at the PCC. To prevent harmonics penetrated into the power network, a low pass filter can be used with the PV system.

1.2 Literature Pertinent to Temporary Over-Voltages

Temporary Over-Voltages on Distribution System

Increasing number of inverter-based DGs connected to the MV and LV distribution networks can causes temporary over-voltage (TOV), especially during single-line-to-ground faults and islanding incidents. Distributed PV systems are no exception, and traditional mitigation measures for rotating generators does not directly applicable in inverter-based PV systems.

Reference [29] reviews the mechanisms that cause TOV by the inverter-based DGs. These mechanisms are: ground potential rise, derived neutral shift, inductive coupling of fault currents, high generation to load ratio, interruption of inductive current, and over-modulation or saturation of inverter current-control scheme. The literature has identified two key mechanisms by which a distributed PV system can cause TOVs [27], [29], [31], [32], [44]. The first mechanism for the TOV is the neutral voltage displacement or the derived neutral shift. The mechanism applies to a three-wire *delta*-connected system, an ungrounded *wye*-connected system, or a *wye*-connected system with a large grounding impedance [45], [46]. Under the aforementioned condition, severe over-voltage occurs that can go up to 1.73 *p.u.*, and if the distribution network permits the pre-fault voltage as high as 1.05 *p.u.* (ANSI voltage regulation allowance), the over-voltage could go as high as 1.82 *p.u.* [27]. The second mechanism is known as interruption of significant power export, which takes place during an unintentional islanding. The TOV caused by the second mechanism could be more serious, if there exist a single-line-to-ground fault in the islanded zone. The authors in [46] reported that the TOV on the healthy phases could go up to 1.5 *p.u.*

In [47], the test results of several commercial inverters have been presented, with an emphasis on the TOV generated by the inverter systems during grid disconnection. This paper reports phase-to-ground TOVs up to 2.3 *p.u.* and lasted as long as 5 cycles. Reference [30] reports a field test that has studied the TOV caused by several commercial PV inverters. Test result reveals that, the inverter generates TOV due to ground faults with a magnitude of about 3.58 *p.u.*, and as such, damages electronic equipments in the PV systems and revenue meters.

A number of works have been studied on the mitigation of TOVs caused by the distributed PV systems [29], [31], [46], [48–55]. Reference [29] investigates the behavior of synchronous generators and the PV systems during a single-line-to-ground fault. This paper explains why IEEE 142 "effective grounding" requirements [48] do not work in the distributed PV systems. Research works in [31], [44], [49–53] also report the practice of "effective grounding" in the inverter-based DG system is inefficient and inadequate. Surge arresters are designed to prevent transient over-voltage due to lightning strikes for short period of time and they are ineffective to long-lasting TOV caused by PV systems. Reference [29] also provides several suggestions in order to mitigate TOV problem; such as, use of current-mode control for the inverters, selection of PV generator power rating close to the local load, proper selection of the winding configuration of isolation transformer etc.

Reference [46] has developed a modified single-stage grid-connected PV system model and proposed a mitigation strategy. The model uses a half-bridge converter and Y/YG isolation transformer and the function of the mitigation strategy is to limit the TOV by regulating the modulating signal of the central inverter. However, when applied in the conventional single-stage PV system, the TOV is limited to about 1.5 *p.u.*, which is still damaging and, above the standard level (for example, the Hydro One Networks Inc. defined that the maximum TOV caused by the inverter-based DGs should not exceed 1.3 *p.u.* [20]). Reference [56] has elegantly developed a control strategy for islanded operation of a single-stage DG; the control strategy is based on the current-mode control during grid-connected operation and the voltage-mode control during islanded operation. This paper, however does not report any TOV analysis during the worst case scenario, such as, during a single-line-to-ground fault and an islanding incident.

In [57], a control strategy has been presented to ensure seamless power transfer between the grid-connected mode and the islanded mode. A voltage-mode control employs in both grid-connected and islanded modes. The authors in [57] use islanding detection strategy and reported no transients in the local load voltage and current, even before the islanding is detected. However, this paper does not provide any TOV analysis caused by a single-line-to-ground fault followed by an islanding incident. In [58], author uses existing solar PV farm as PV-STATCOM and wind farm inverter as Wind-STATCOM to regulate steady state voltage and to suppress TOV so that the connection of the solar PV farm and wind farm can be increased. However, the author does not reported any TOV analysis during an unintentional islanding incident.

Despite the need, however, no comprehensive study has thus far been reported for two-stage grid-connected three-phase PV systems, from the viewpoint of TOV analysis.

In [59], a PV/battery unit is connected to the inverter through the dc-dc boost converters. Authors in [59] assumes that the PV/battery unit is in the islanded microgrids and uses a decentralized control strategies for the PV/battery unit. The PV/battery unit is controlled as voltage sources while a power curtailment control loop is used to modify the PV operating point to match the load autonomously whenever the PV power is higher than the load. This paper, however, does not provide any TOV analysis. In [60], a wind-photovoltaic-storage hybrid system is used for grid-connected and off-grid (islanded) operations. The PV unit is connected to the VSI through a dc-dc boost converter. Along with a grid-loss detection algorithm, authors in [60] propose a power management strategy for the hybrid system in order to ensure safe transition from grid-connected operation to off-grid (islanded) operation, but does not provide any analysis of the TOV during the transition period from grid-connected mode to islanded mode. The authors in [61] present new control strategies for a two-stage grid-connected PV system that allow the inverter to remain connected to the grid under faults. Reference [61], however, does not report any TOV analysis during an islanding scenario in the two-stage grid-connected PV system.

Grid-connected PV systems should comply with standards and grid codes and utility requirements for safe and steady operation. For example, the PV system must produce high quality power and not exceed harmonic levels set by the IEEE standards [37], [62]. In Ontario, Hydro One Networks Inc. has defined a number of design requirements. One of the requirements is based on the level of TOVs caused by the DGs. According to the Hydro One Networks distribution system, the maximum TOV at the PCC shall not exceeds 1.3 $p.u.$ [20]. According to the German grid code [63], which is used as a reference code for various studies, the PV systems connected to the MV distribution network should provide dynamic grid support in order to maintain the stability and may also remain connected to the network during faults.

The limiting curves of voltage for the inverter-based DG system are shown in Figure 1.8. As Figure 1.8 indicates, the inverter-based DG systems should not get disconnected before 150 ms even if the voltage drops to about zero. The system voltage stability should not get affected if the voltage drops above the borderline 1. There is no requirement for the inverter-based DG systems to remain connected to the grid if the voltage drop is below the blue line [63]. Moreover, the inverter-based DG systems and in this case the PV system is recommended to be capable of decreasing its real power output in case of an over-frequency condition in the network. Figure 1.9 clearly illustrates the real power reduction required from an inverter-based DG system to support the network frequency.

Based on the literature review work presented above, in order to study the TOV caused by

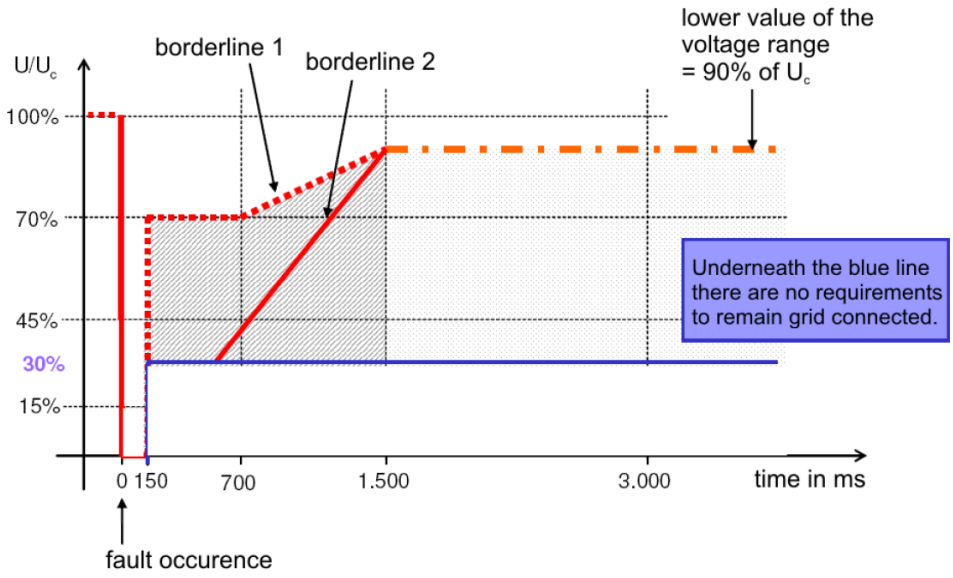

Figure 1.8: Limiting curves of voltage for the inverter-based DG system connected at MV level in the event of a network fault [63].

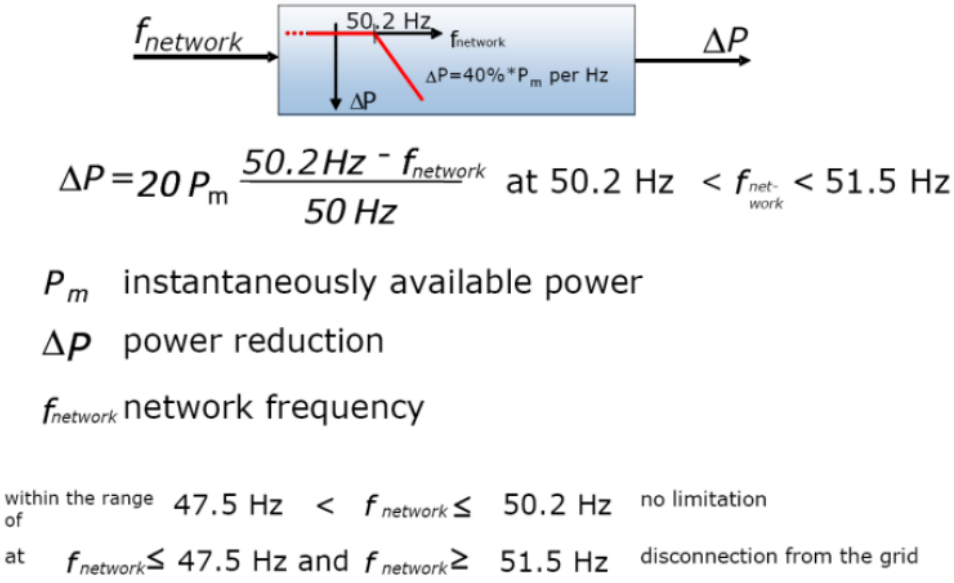

Figure 1.9: Real power reduction required from the inverter-based DG system connected at MV level in case of over-frequency [63].

singe-stage and two-stage PV systems, a proper model is required for both PV systems. The main aim of this thesis is to discuss the reasons behind the TOV caused by the PV systems as well as proposes corrective measures to mitigate the TOV.

1.3 Thesis Objectives and Scope

The overall aim of this thesis is to study and characterize TOVs caused by grid-connected PV systems, and to propose corrective measures to mitigate the TOV problem through the built-in software of the PV system. The scope of this thesis, however, is limited to PV systems with single-stage and two-stage three-phase central dc-ac inverters.

In this thesis a detailed, switched models of single-stage and two-stage PV systems have been used. However, an ideal model has been assumed for the isolation transformer. The PV system is assumed to be connected with a host CIGRE benchmark MV distribution network [64], and the network lines have been modeled as series RL branches. Further, the network loads and local loads are modeled as voltage-dependent real-/reactive-power sinks. Moreover, the model uses an under-/over-voltage relay and a low-/high-frequency relay, to disconnect the PV system during abnormal operating conditions. However, no islanding detection scheme has been assumed. Furthermore, the thesis assumes that no corrective measure is taken for the TOV on the part of the host utility network.

The more specific objectives of the thesis are:

- To study and characterize TOVs caused by a conventional single-stage grid-connected three-phase PV system in which a widely utilized Δ/YG isolation transformer is used, and to propose a TOV limiting scheme for the PV system.

- To investigate the TOV in an effective grounding system, a modified single-stage grid-connected three-phase PV system with a Y/YG isolation transformer will be utilized, and to propose a TOV limiting scheme for the PV system.

- To study and characterize the TOVs caused by a two-stage grid-connected three-phase PV system, and to apply the proposed TOV limiting scheme (which is used for the conventional single-stage PV system) in the two-stage PV system.

- To compare the single- and two-stage PV systems from the viewpoint of TOV, with and without the proposed TOV limiting schemes.

1.4 Methodology

To achieve the objectives of this thesis, the PV *generator* configuration and the single- and two-stage PV system structures are studied and appropriate control schemes for the inverter and for limiting the TOV caused by the PV system are used. The single- and two-stage PV systems are modeled in detail in the commercial grade software, power systems computer aided design using electromagnetic transients including dc (PSCAD/EMTDC). The performance of the PV system models and the effectiveness of the TOV limiting schemes are evaluated through a fairly comprehensive set of case studies, conducted in the PSCAD/EMTDC software environment.

1.5 Thesis Outline

The remainder of this thesis is organized as follows:

- In Chapter 2, first, the mechanisms behind the TOVs caused by PV systems are described. Then, a conventional single-stage grid-connected three-phase PV system interfaced with a CIGRE benchmark MV distribution network is studied. A widely used Δ/YG isolation transformer is utilized in the conventional single-stage PV system. The inverter dc-link voltage controller and the inverter current-control scheme in the *dq*-frame are presented. Thereafter, to evaluate the performance and robustness of the system, and to investigate the TOV caused by the single-stage PV system, Chapter 2 demonstrates a number of cases for both faulted and normal operating conditions by time-domain simulation studies conducted in the PSCAD/EMTDC software environment.

  To evaluate the TOV in an effective grounding system, Chapter 2 also utilizes a modified single-stage grid-connected PV system. The modified system employs a half-bridge converter (HBC) and a Y/YG isolation transformer. Through time-domain simulation studies, Chapter 2 shows that the effective grounding system may not mitigate TOVs.

  Furthermore, to limit the TOV, a TOV limiting scheme is proposed for the conventional single-stage PV system. In the case of detected over-voltage, the proposed TOV limiting scheme limits the over-voltage on any of the three phases. Moreover, a TOV limiting scheme for the modified single-stage PV system is proposed to reduce the magnitude of the TOV. The effectiveness of the TOV limiting schemes are evaluated by time-domain simulation studies in the PSCAD/EMTDC software environment.

- Chapter 3 presents a two-stage grid-connected three-phase PV system, to further investigate the causes of TOVs. In the two-stage system, a dc-dc boost converter is used to control the PV *generator* terminal voltage and boosted to a voltage level slightly less than the dc-link voltage limit imposed by the national regulations. The boost converter also adopts a output voltage controller to control and prevent the dc-link voltage from rising during disturbances, such as network faults. The inverter uses the same dc-link voltage controller and the inverter current-control scheme in the *dq*-frame as those used in the single-stage PV system. However, different values are used in the controller compensators parameter.

  Chapter 3 also investigates the TOV caused by the two-stage PV system. Furthermore, the two-stage PV system employs the proposed TOV limiting scheme as that is used for the conventional single-stage PV system. The performance of the two-stage PV system and the effectiveness of the TOV limiting scheme are evaluated through a number of case studies on a detailed model of the system in the PSCAD/EMTDC software environment.

  Chapter 3 also demonstrates a comparative study of TOVs caused by the single- and two-stage PV systems with and without the proposed TOV limiting schemes.

- Chapter 4 presents the thesis conclusions with the suggestions for the future research work. The mathematical model and the PV *generator* parameters are given in Appendix A. The PV system parameters are given in Appendices B, C, and D.

1.6 Contributions

The main contributions of this thesis are:

- A conventional single-stage grid-connected three-phase PV system with its necessary components are modeled in the PSCAD/EMTDC software environment. Then, based on the developed model, the thesis studies the damaging TOV generated by the conventional single-stage PV system during a single-line-to-ground fault and an islanding incident. The thesis then proposes a TOV limiting scheme for the conventional single-stage PV system in order to limit the magnitude of the over-voltage on each phase.

- The thesis also studies the TOV caused by an effectively-grounded PV system. Thus, the thesis adopts a modified single-stage grid-connected three-phase PV sys-

tem from the literature. The thesis then proposes a TOV limiting scheme for the modified PV system, to further mitigate the damaging TOV.

- The thesis further models a two-stage grid-connected three-phase PV system in the PSCAD/EMTDC software environment, to evaluate the TOV during a single-line-to-ground fault and an islanding incident. Then the thesis adopts and evaluates the proposed TOV limiting scheme (which was used for the conventional single-stage PV system) also for the two-stage PV system.

- The thesis presents a comparative study of TOVs caused by the single- and two-stage PV systems, with and without the proposed TOV limiting schemes.

Chapter 2

TOV Analysis: Single-Stage PV Systems

2.1 Introduction

The focus of this chapter is to address, analyze and mitigate the damaging temporary over-voltages (TOVs) caused by single-stage PV systems. Though the TOV is primitive, the recent high penetration of PV generation into distribution feeders spurred utilities to do impact studies and, as such, the TOV caused by the PV systems need to be resolved for proper grid interconnections [7], [27–30], [44], [47], [65–68].

At first, this chapter presents the mechanisms, and characteristics behind the aforementioned TOV through an extensive literature review. This reveals that, neutral voltage displacement (during ground faults) and interruption of significant power export (during islanding incidents) are the two main reasons for the TOV caused by PV systems [27], [29], [31], [32], [44]. In order to investigate the aforementioned reasons behind the TOV, this Chapter presents a conventional single-stage grid-connected three-phase PV system with its associated components, control schemes, and the host CIGRE benchmark MV distribution network as grid. A widely used Δ/YG isolation transformer is utilized in the aforementioned conventional single-stage PV system.

Then, to evaluate the TOV in an effectively-grounded PV system, this chapter also adopts a modified single-stage grid-connected PV system [46]. The modified system employs a half-bridge converter (HBC) and a Y/YG isolation transformer. However, this chapter presents different controls for limiting the damaging TOVs. Through time-domain simulation studies, this chapter shows that the effective grounding system may not mitigate TOVs.

Furthermore, to limit the TOV, this chapter proposes a TOV limiting scheme for the conventional single-stage PV system. The proposed TOV limiting scheme limits the over-voltage on any of the three phases during ground faults and the following islanding incidents. This chapter also proposes a TOV limiting scheme for the modified single-stage PV system in order to reduce the magnitude of the TOV. A PI controller with an anti-wind-up technique [61] is utilized in each of the aforementioned TOV limiting scheme. The effectiveness of the TOV limiting schemes are evaluated by time-domain simulation studies in the PSCAD/EMTDC software environment.

It should be pointed out that, some grid codes, like the one in [63] defines that the PV systems require to connect to the network for a short period of time even after the fault. Therefore, the objective of the proposed TOV limiting schemes are to temporarily limit/reduce the magnitude of over-voltages during that short time interval.

2.2 TOV Caused by Distributed PV Systems

High penetration of DGs into distribution network has the potential to cause TOV problems [27], [31], [45], [46]. Among them, distributed PV system poses serious TOV problem since they are normally installed on the MV and LV side of the system, and potentially at any point on a feeder [31]. In the following section important mechanisms that cause the TOV by the PV systems are represented.

2.2.1 Important Mechanisms and Characteristics

The literature has identified two key mechanisms by which a distributed PV system can cause TOVs [27], [29], [31], [32], [44]. These mechanisms are described below.

- **Neutral Voltage Displacement or Derived Neutral Shift:**

  The first mechanism for the TOV is the neutral voltage displacement or the derived neutral shift. The mechanism applies to a three-wire *delta*-connected system, an ungrounded *wye*-connected system, or a *wye*-connected system with a large grounding impedance [45], [46]. In this mechanism, during a single-phase-to-ground fault, one point of the *delta*-connected system becomes ground referenced by the fault. This mechanism can be demonstrated by the phasor diagrams of Figure 2.1. As shown in Figure 2.1(a), during the pre-fault condition phase voltages are balanced and 120° apart and consequently neutral voltage, υ_n of the *delta*-connected system is zero. However, as Figure 2.1(b) shows, when a single-phase-to-ground fault strikes (in this case, phase–b is bolted to the ground), the voltage of the neutral

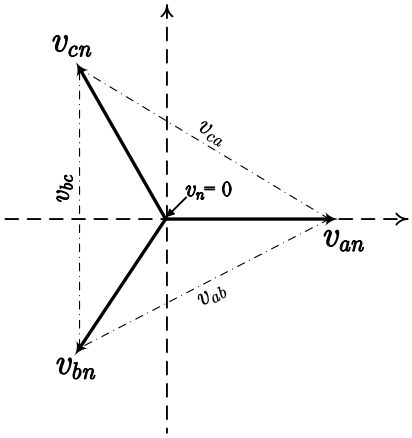

(a) Pre-fault condition

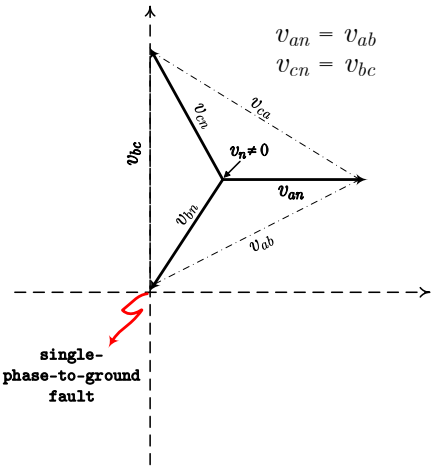

(b) During a single-phase-to-ground fault

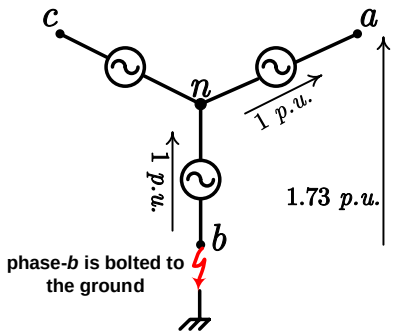

(c) Effect of neutral point shift on voltages

Figure 2.1: Illustration of neutral voltage displacement during a single-phase-to-ground fault by using voltage phasor diagrams.

point equals to that of the faulted phase. Therefore, the healthy phase voltages can be formulated as

$$\begin{aligned} v_{an} &= v_{ab} \\ v_{cn} &= v_{bc} \end{aligned} \tag{2.1}$$

Now, if a single-phase load is connected between any healthy phase (e.g. phase–a or phase–c) and the neutral, the load will see the line-to-line voltage (in this case, v_{ab} or v_{bc}). As shown in Figure 2.1(c), this type of over-voltage can go up to 1.73 $p.u.$ and if the distribution network permits the pre-fault voltage as high as 1.05 $p.u.$ (ANSI voltage regulation allowance), the voltage could go as high as 1.82 $p.u.$ [27]. Therefore, such a TOV poses a serious risk to loads and utility equipments.

- **Interruption of Significant Power Export:**

  The second mechanism is known as interruption of significant power export, which takes place during an unintentional islanding, where PV generation exceeds load [29], [45], [46], [68], [69]. The TOV caused by the second mechanism could be more serious, if there already exist a single-line-to-ground fault in the islanded zone. As shown in Figure 2.2, aforementioned condition occurs when an upstream utility protection circuitry detects a fault and opens the utility interface disconnect breaker and consequently, an island forms. During significant power export, output current of the PV *generator*, i_{pv} is larger than that required by the local load current, i_l, and thus the grid current, i_{grid} is positive. However, when the grid is disconnected from the PV system, i_{pv} becomes equal to i_l, meaning that i_l becomes much larger than before the pre-disturbance condition. According to Ohm's law, the load voltage, v_l will rise in proportion to the level of increase in i_l. If the total load impedance in the islanded zone is Z_{load}, total generation from the PV system is S_{PV}, the load power is S_{load}, and the nominal network voltage is $v_{nominal}$, then the magnitude of a TOV, V_{TOV}, can be formulated as [49]

$$V_{TOV} = v_l = i_{pv} Z_{load} \simeq \left(\frac{S_{PV}}{v_{nominal}} \right) \frac{v_{nominal}^2}{S_{load}} \tag{2.2}$$

  Equation (2.2) can be simplified as

$$\frac{V_{TOV}}{v_{nominal}} \simeq \frac{S_{PV}}{S_{load}} \tag{2.3}$$

  Therefore, from (2.3) it can be concluded that, during normal operation the amplitude of the TOV is proportional to the ratio of the total PV power generation to the total load.

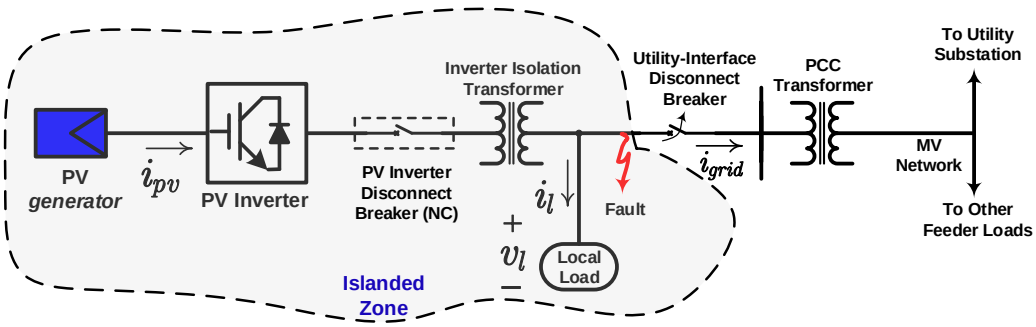

Figure 2.2: Schematic diagram illustrating the mechanism of the interruption of significant power export.

2.3 TOV Analysis: Conventional Single-Stage PV System

2.3.1 System Configuration and Principle of Operation

Assessing the TOV problem caused by the PV systems, a comprehensive PV system model is necessary. A comprehensive guidelines are reported in [70] for the grid-connected PV systems. A number of works have studied the dynamic models and the control of large-scale grid-connected single-stage three-phase PV systems [60], [71–74], [76–82]. Figure 2.3 illustrates a comprehensive single-line schematic diagram of a three-phase single-stage grid-connected PV system. As shown in Fig. 2.3, a PV *generator* is connected to the dc-side of a dc-ac power-electronic converter known as three-phase voltage-sourced inverter (VSI). The dc-side of the VSI is paralleled with the dc-link capacitor, C. As the diagram shows, each phase of the inverter ac-side terminals is interfaced with the CIGRE benchmark MV distribution network, at a point of common coupling (PCC), through a L_fC_f low-pass filter, an isolation transformer, T_r and a three-phase local load. The transformer, in this conventional PV system has a *wye* winding connection at the grid-side and a *delta* winding connection at the inverter ac-side in order to avoid triple-n harmonics of the magnetizing current.

Fig. 2.3 indicates that, the PV *generator* output current, i_{pv} and the terminal voltage, v_{pv} are utilized in the maximum power-point tracking (MPPT) scheme. The MPPT scheme generates the required dc-link voltage reference, v_{dcref} for the dc-link voltage controller. Fig. 2.3 also illustrates that the PV system employs a decoupled dq-frame current-control scheme [71]. The current-control is performed in a rotating dq reference frame whose d- axis makes a phase angle, ρ against the stationary α axis. Phase angle,

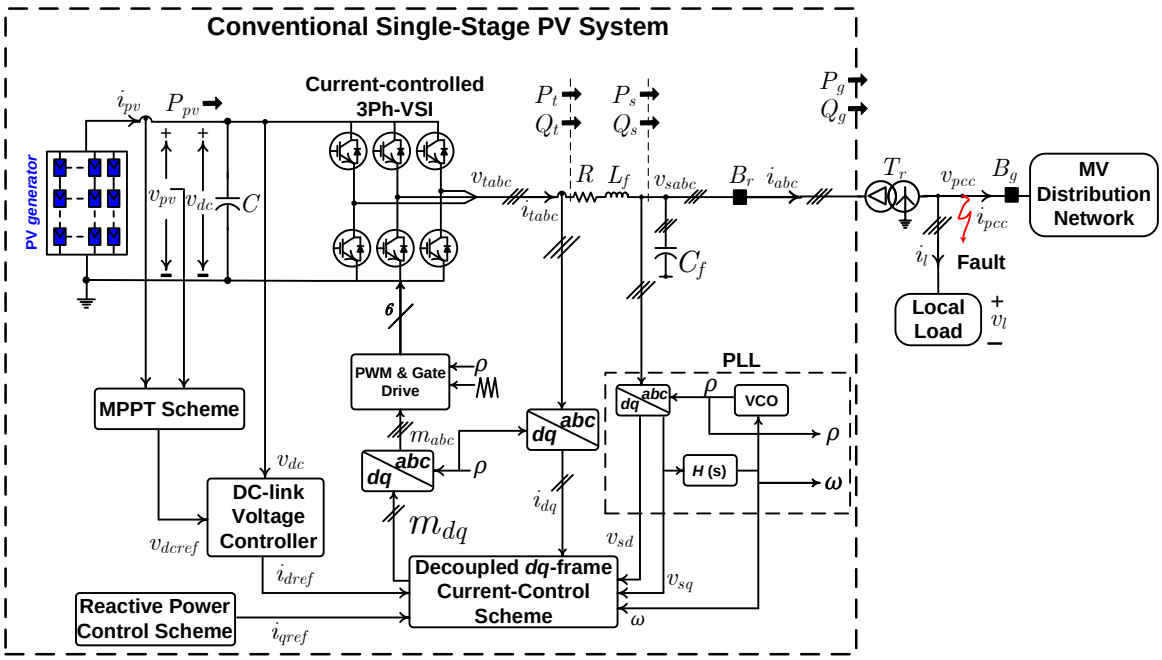

Figure 2.3: Schematic diagram of a conventional single-stage grid-connected three-phase PV system.

ρ and frequency, ω of the inverter ac-side voltages, v_{sabc}, are obtained by means of a phase-locked loop (PLL) [76]. The real- and reactive-power that the PV system delivers to the distribution network are independently controlled by the d- axis current, i_d and the q- axis current, i_q, respectively. The dc-link voltage controller issues the current command i_{dref} and the reactive-power control scheme issues the current command i_{qref}. The inverter current-control scheme ensures that i_d and i_q rapidly track their respective reference commands i_{dref} and i_{qref}. The inverter ac-side voltages, v_{sabc} are transformed to v_{sd} and v_{sq} by using the abc- to dq-frame transformation block [76]. The PLL also processes v_{sq} through the filter $H(s)$ in such a way that v_{sq} is forced to zero. All the control signals are processed by the current-control scheme which generates the dq-frame signals m_d and m_q. The inverter modulating signals, m_{abc} are obtained from m_d and m_q by using the dq- to abc-frame transformation block [76] and delivered to the pulse-width modulation (PWM) and the gate driver circuit for producing inverter gate pulses. The dq-frame modulating signals must be limited before being delivered to the converter PWM and the gate driver circuit, to ensure that $\sqrt{m_d^2 + m_q^2} \leqslant 1$, that is, the inverter can operate in the linear modulation region [75], [76].

A single-stage PV system can causes severe TOVs when a single-line-to-ground fault persists at the PCC [see Fig. 2.3] even after the islanding incident. Islanding incident occurs when the main three-phase utility-interface disconnect breaker, B_g opens and the

PV system is isolated from the host distribution network. Under the aforementioned condition, a TOV is the most severe when the PV generation exceeds local load. This thesis investigates the aforementioned scenario through simulation studies, as will be discussed in the respective section.

2.3.2 Inverter Current-Control Scheme

The singe-stage PV system of Figure 2.3 employs a decoupled dq-frame current-control scheme to ensure that the inverter ac current components, i_d and i_q are independently controlled and rapidly track their respective reference commands i_{dref} and i_{qref}. The current-mode control of the inverter also provides over-current protection [71] during network faults by limiting i_{dref} and i_{qref}.

As Figure 2.4 shows, i_d and i_q are the state variables, m_d and m_q are the outputs, and the inverter ac-side voltage components, v_{sd} and v_{sq} are the disturbances which are used as feedforward signals and processed through the low-pass filter, $F(s)$. Figure 2.4 indicates that, the factor ωL_f is incorporated to decouple the control of i_d and i_q. To regulate inverter ac-side currents, two compensators, $k_d(s)$ and $k_q(s)$, process the errors $e_d = i_{dref} - i_d$ and $e_q = i_{qref} - i_q$, and generate new control inputs, u_d and u_q. Thereafter, to produce m_d and m_q, the factor $2/v_{dc}$ is used to decouple the dynamics of i_d and i_q from those of v_{dc}. Inverter modulating signals, m_{abc} are obtained from m_d and m_q by using the dq- to abc-frame transformation block [76] and delivered to the pulse-width modulation (PWM) and the gate driver circuit for producing inverter gate pulses (not shown in Figure 2.4).

Since, both d- and q-axis current-control loops are identical, compensators $k_d(s)$ and $k_q(s)$ can also be identical. Thus, based on [76]

$$k_d(s) = k_q(s) = \frac{k_1 s + k_2}{s} \tag{2.4}$$

where k_1 and k_2 are the proportional and integral gains, respectively. If k_1 and k_2 are selected as

$$k_1 = \frac{L_f}{\tau_i} \tag{2.5}$$

$$k_2 = \frac{R}{\tau_i} \tag{2.6}$$

then i_d and i_q, independently track their respective setpoints, i_{dref} and i_{qref}, based on the following transfer function

$$\frac{I_d(s)}{I_{dref}(s)} = \frac{I_q(s)}{I_{qref}(s)} = \frac{1}{\tau_i s + 1} \tag{2.7}$$

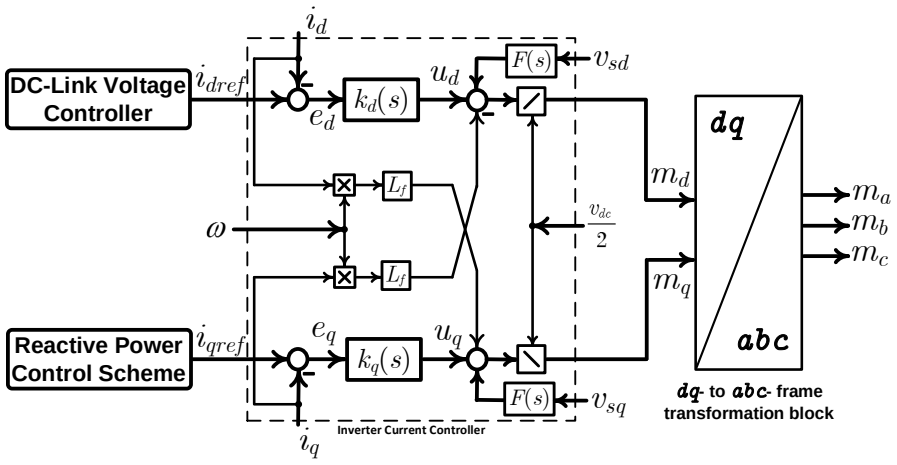

Figure 2.4: Block diagram of decoupled dq-frame current-control scheme.

where time constant, τ_i is a design choice. It should be noted that for fast current-control response, τ_i should be made small but adequately large so that $1/\tau_i$ is smaller than the inverter switching frequency. This can be done by proper tuning of the current-controlled parameters [76]. As it is mentioned earlier, i_d and i_q can be used to control the real- and reactive-power of the inverter, respectively. Thus, based on [71], the power components P_s and Q_s are written as

$$P_s = \frac{3}{2} v_{sd} i_d \tag{2.8}$$

$$Q_s = -\frac{3}{2} v_{sd} i_q \tag{2.9}$$

Dynamic Performance of the Inverter Current-Control Scheme

Consider the inverter decoupled dq-frame current-control scheme of Figure 2.3 with parameters $L_f = 30\ \mu H$, $R = 2.0\ m\Omega$, $v_{dc} \approx 460\ V$. The inverter switching frequency is 3060 Hz. The ac system frequency and inverter ac-side line-to-line rms voltage are 377 rad/s and 208 V, respectively. The transfer function of the low-pass filter is $F(s) = 1/(0.00005\text{s} + 1)$. The VSI is current-controlled with $\tau_i = 0.5\ ms$. Thus based on (2.5) and (2.6), once obtain,

$$k_d(s) = k_q(s) = \frac{0.06s + 4}{s}\ [\Omega] \tag{2.10}$$

Figure 2.5 illustrates the dynamic performance of the current-controlled scheme. Until $t = 0.3\ s$, the gating pulses are blocked and the inverter current-control scheme is inactive.

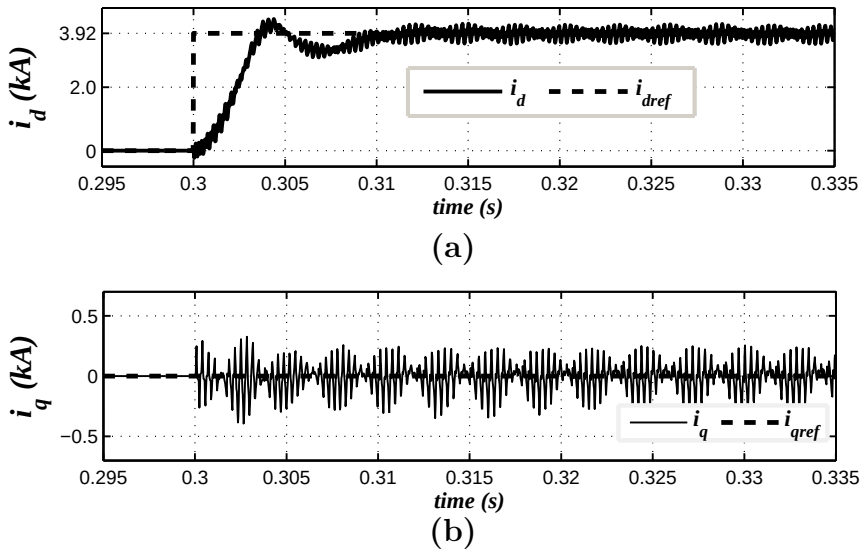

Figure 2.5: Dynamic response of decoupled dq-frame current-control scheme.

This permits the PLL to reach its steady state. At $t = 0.3\ s$, the gating pulses are unblocked and the inverter current-control scheme is activated. Figure 2.5(a) indicates that the d-axis current, i_d reaches its final value at about $t = 0.31\ s$. It is observed from Figure 2.5(b) that the q-axis current, i_q remains regulated at zero while i_d is changing from zero to about 3.92 kA. The ripples are observed on the current waveforms of i_d and i_q. It is worth explaining that these ripples are due to the PWM switching side-band harmonics of VSI ac-side currents. Figure 2.5 also verifies that i_d and i_q are well decoupled.

2.3.3 DC-Link Voltage Controller

Inverter dc-link voltage controller is responsible to control the dc-link voltage, v_{dc} and, provides protection for the dc-link capacitor and the inverter valves against over-voltage stress. Mathematical model of the dc-link voltage controller is adopted from [71]. As discussed in [71], a reduced-order model for the dc-link voltage dynamics can be written as

$$\begin{aligned} \frac{1}{2}C\frac{dv_{dc}^2}{dt} &\approx P_{pv} - \frac{3}{2}v_{sd}i_d \\ &\approx P_{pv} - \frac{3}{2}v_{sd}i_{dref} \end{aligned} \tag{2.11}$$

As (2.11) indicates, the dc-link voltage can be controlled by i_d. Since, τ_i is assumed to be a small value, $i_d \approx i_{dref}$ implies a fast operation of the inverter current-control loop.

As can be seen from Figure 2.6, the dc-link voltage compensator, $K_v(s)$, processes the error between v_{dc}^2 and its setpoint, v_{dcref}^2 to issue the current command i_{dref}. In turn, the inverter current-control scheme responds to the command based on (2.7). The signals $(3/2)v_{sd}$ and P_{pv} are delivered as feedforward compensation in order to mitigate the nonlinear effects on the control. It should be noted that, the feedforward compensation will be enabled if the factor $\gamma = 1$ is used and, as such, the effective control plant becomes

$$\frac{1}{2}C\frac{dv_{dc}^2}{dt} \approx u_v \tag{2.12}$$

where u_v is a new control input from the dc-link voltage compensator. It should be noted that if the factor $\gamma = 1$, then, the control plant becomes an integrator and $K_v(s)$ can be utilized as a proportional-integral (PI) compensator such as

$$K_v(s) = \frac{k_3 s + k_4}{s} \tag{2.13}$$

where k_3 and k_4 are the proportional and integral gains, respectively.

Figure 2.7 illustrates the inverter dc-link voltage controller response to stepwise change in dc-link voltage setpoint. The dc-link voltage setpoint, v_{dcref} is externally imposed. The initial $v_{dcref} = 350\ V$. As Figure 2.7 indicates, until $t = 0.3\ s$, the controller is disabled, the measured dc-link voltage is about $v_{dc} = 563\ V$. Thereafter, it tracks v_{dcref}. At $t = 0.55\ s$, the dc-link voltage setpoint is stepped up to 485 V. The controller quickly response to the step change and tracks the setpoint. The controller parameters are given in Table B.2.

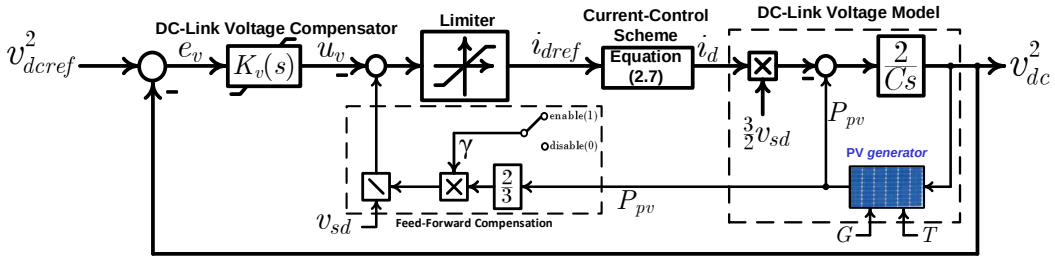

Figure 2.6: Block diagram of the dc-link voltage controller.

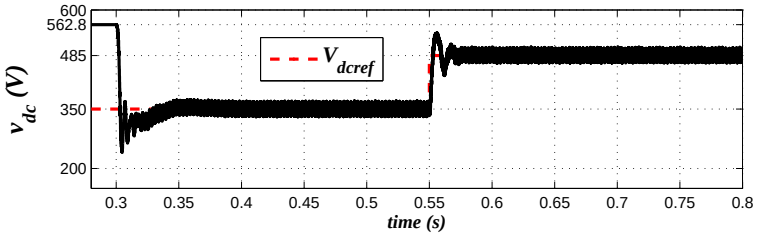

Figure 2.7: The inverter dc-link voltage controller response to stepwise change in dc-link voltage setpoint.

2.4 Study Cases and TOV Impact Analysis

At first, in this section, to demonstrate the performance of the conventional single-stage PV system, a number of study cases have been conducted on a detailed switched model of the system of Figure 2.3 in the PSCAD/EMTDC software environment [83]. Figure 2.8 indicates that, the single-stage PV system is interfaced with the CIGRE benchmark MV distribution network. As Figure 2.8 shows, the interfaced point is at BUS 3 which is referred to as the PV system terminal or the PCC. The PV *generator* rating is 1.0 MW and that is composed of $N_p = 300$ parallel-connected PV strings of $N_s = 18$ series-connected PV modules; each module is, in turn, assumed to be composed of $M_s = 54$ identical basic PV cells. The junction temperature of the PV cells is assumed to be $T = 40°C$, unless otherwise mentioned. In this thesis, the PV *generator* model is adopted from [71]. Other parameters of the PV *generator* are listed in Table A.1. The mathematical model of the PV *generator* is presented in Appendix A. The MPPT scheme employs the incremental conductance (IC) algorithm [84], [85]. Both the inverter and isolation transformer, T_r ratings are assumed as 1.0 MVA. The local load shown in Figure 2.3 is modeled as voltage-dependent real-/reactive power sinks; implemented in PSCAD/EMTDC by using standard components available in the software master library. The MV voltage distribution network and its load parameters can be extensively found in [64] and [86].

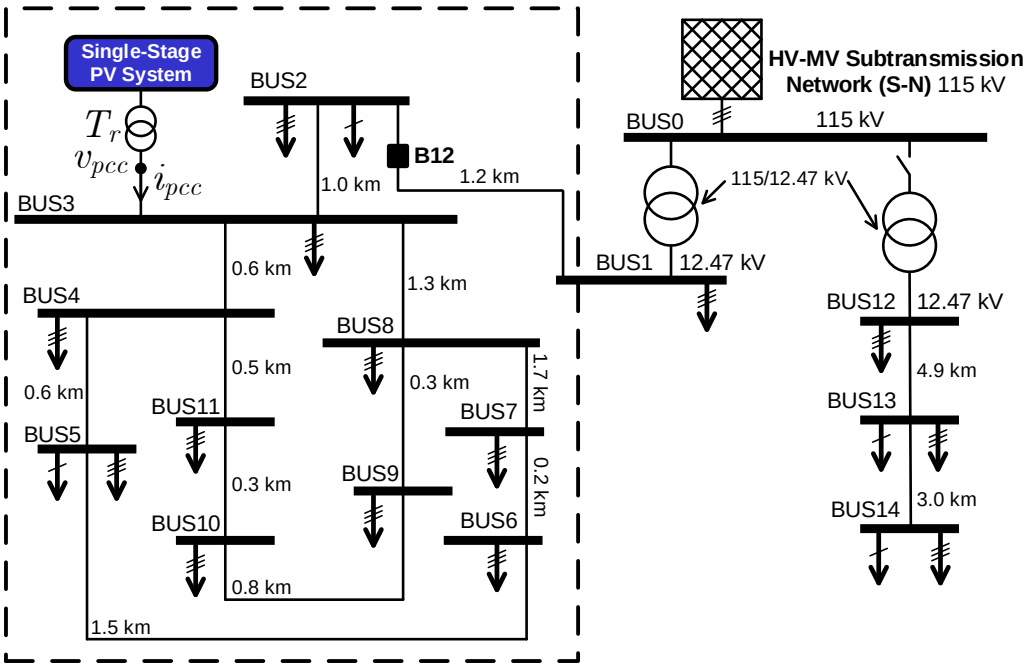

Figure 2.8: Single-stage PV system is connected to the BUS 3 of the test CIGRE benchmark MV distribution network.

Furthermore, this thesis conducts a comprehensive set of case studies to evaluate the TOV caused by the conventional single-stage PV system due to a single-line-to-ground fault and an islanding incident. The conventional single-stage PV system and controller parameters are given in Appendix B. The PV system relay settings are listed in Table D.1 of Appendix D.

2.4.1 Case 1: Simulated Performance of the Single-Stage PV System Under the Startup Process and Normal Operation

This case study demonstrates the conventional single-stage PV system response to the start-up process, followed by stepwise changes in the solar irradiation, G while the MPPT scheme is exercised. Initial solar irradiation of the PV *generator* is $G = 1.0\ kW/m^2$. Until $t = 0.3\ s$, all the controllers are disabled and the gate pulses of the VSI are blocked. However, the dc-link capacitor are pre-charged by the open-circuit voltage of the PV *generator*.

Figure 2.9 illustrates the simulated response of the PV system. As Figure 2.9(a) shows, at $t = 0.45\ s$, the solar irradiation is stepped down to $G = 0.6\ kW/m^2$, and is stepped up to $G = 0.8\ kW/m^2$ at $t = 0.65\ s$. Figure 2.9(b) shows that the output power,

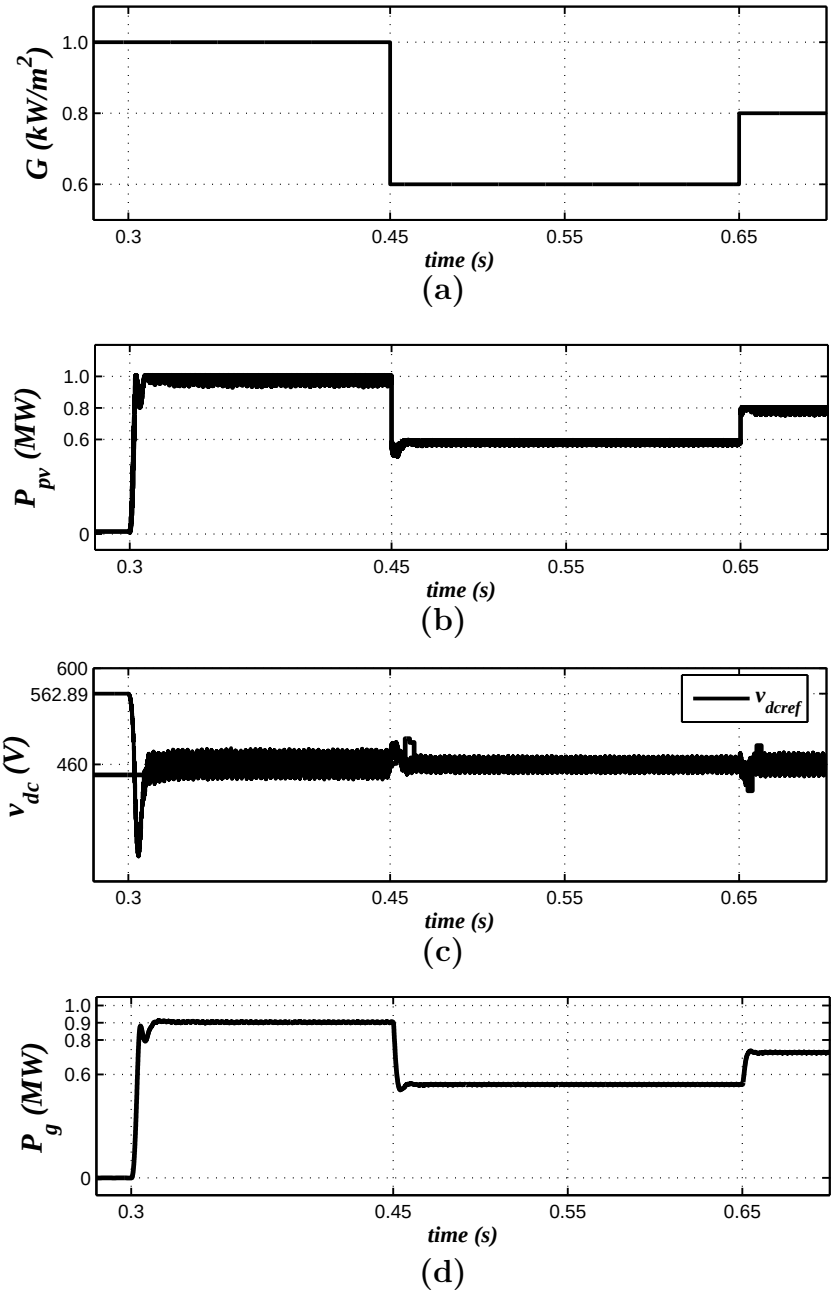

Figure 2.9: Conventional single-stage PV system response to startup and stepwise change in solar irradiance with the MPPT scheme is enabled.

P_{pv}, delivered by the PV *generator* is approximately proportional to the solar irradiation. As Figure 2.9(c) indicates, until $t = 0.3\ s$, the measured dc-link voltage is about $v_{dc} = 563\ V$. Thereafter it tracks v_{dcref} set by the MPPT scheme. Also, v_{dc} is automatically corrected by the MPPT scheme due to the stepwise change in solar irradiation. As can be seen from Figure 2.9(d), the initial output power delivered to the grid is about 0.92 MW; thereafter it changes according to the solar irradiation.

Furthermore, Figure 2.10 illustrates the inverter phase terminal and grid-side phase currents, inverter ac-side and grid-side voltages, and the phase relationship between the grid-side current and voltage (phase–a only). Subsequent to each step change in solar irradiation, the changes are observed in the inverter phase terminal and grid-side phase currents from Figure 2.10(a) and (b). However, as Figure 2.10(c) and (d) indicate, the inverter ac-side and grid-side voltages remain unchanged. Figure 2.10(e) shows that the phase-a voltage and current of the grid are always in-phase, which demonstrates that the reactive power is zero at all times i.e. the unity power factor is maintained at the PCC by the inverter.

2.4.2 Case 2: Single-Stage PV System Response to a Three-Phase-to-Ground Fault

This test demonstrates the response of the conventional single-stage PV system to a three-phase-to-ground fault at BUS 4 of the network of Figure 2.8. Initially, the single-stage PV system is assumed to be in a steady state while the PV *generator* receives a solar irradiation of 1.0 kW/m^2 and v_{dcref} is determined by the MPPT scheme. The first fault is incepted at $t = 0.45\ s$ by grounding all three phases through 1 mH inductances and lasts for 0.1 s; the second permanent fault takes place at $t = 0.95\ s$. As Figure 2.11(a) shows, subsequent to each fault inception, the magnitude of the inverter phase terminal current increases due to the significant drop of the grid-side voltage (not shown in Figure 2.11). However, the current magnitude is limited due to the current-mode control of the inverter. Consequently, the dc-link voltage v_{dc} rises and the PV system output power drops, as shown in Figure 2.11(b) and (c), respectively.

As Fig. 2.11 indicates, the permanent fault results in the isolation of the PV system from BUS 3, at around 1.05 s, due to the intervention of the low- and high-voltage relay of the single-stage PV system.

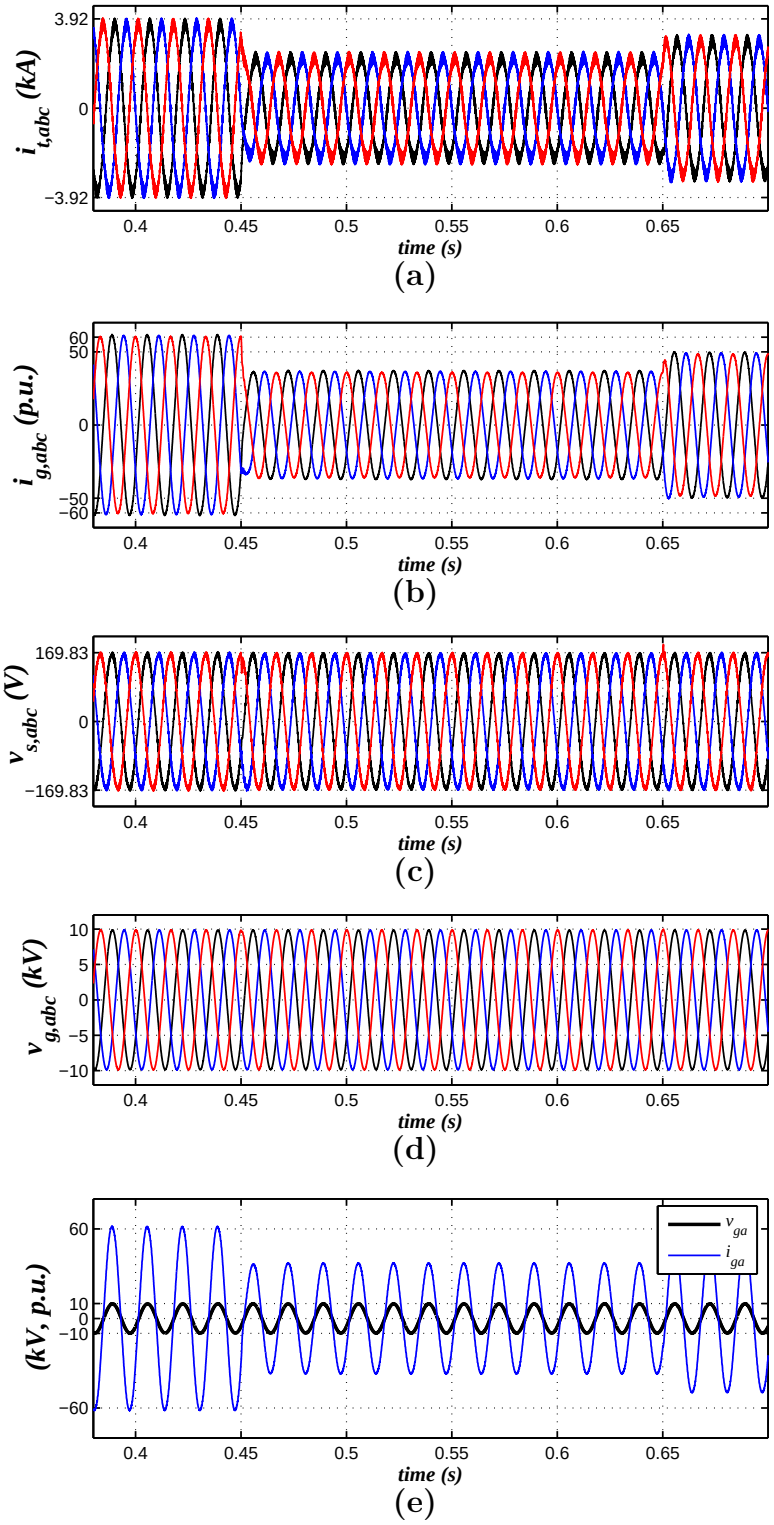

Figure 2.10: Conventional single-stage PV system startup response under Case #1.

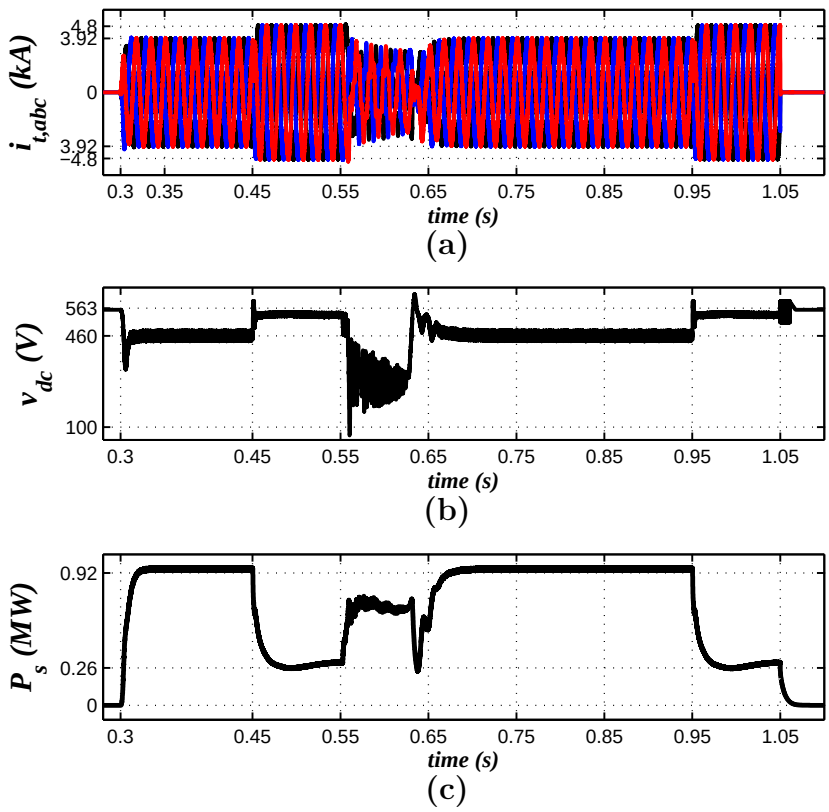

Figure 2.11: Conventional single-stage PV system response to a three-phase-to-ground fault.

2.4.3 Case 3: TOVs Caused by the Conventional Single-Stage PV System due to an Asymmetrical AC Fault

This case study demonstrates the TOVs caused by the conventional single-stage PV system due to a single-line-to-ground fault. Prior to the fault, the PV system is assumed to be in a steady state with $G = 1.0\ kW/m^2$ and the MPPT scheme is enabled. Two single-line-to-ground (phase-c is bolted to the ground) faults take place at BUS 4 of the distribution network of Figure 2.8. The first fault strikes at $t = 0.55\ s$ and lasts for 0.1 s; the second fault is permanent and takes place at $t = 0.8\ s$.

Figure 2.12 illustrates the conventional single-stage PV system response. Figure 2.12(a) shows the voltages of BUS 3. The fault results in the significant drop in the magnitude of the grid-side faulted phase and the voltage rise in the healthy phases of about 1.12 *p.u.* (and hence, they are called *ground-fault over-voltages*). In this case, the TOV on the healthy phases is limited since the conventional PV system uses a YG winding configuration of the transformer, T_r at the grid-side [32]. As shown in Figure 2.12(b), limited increase in the inverter phase terminal currents, i_{tabc} is observed. However, the current retains its pre-disturbance sinusoidal form. The aforementioned behavior is ex-

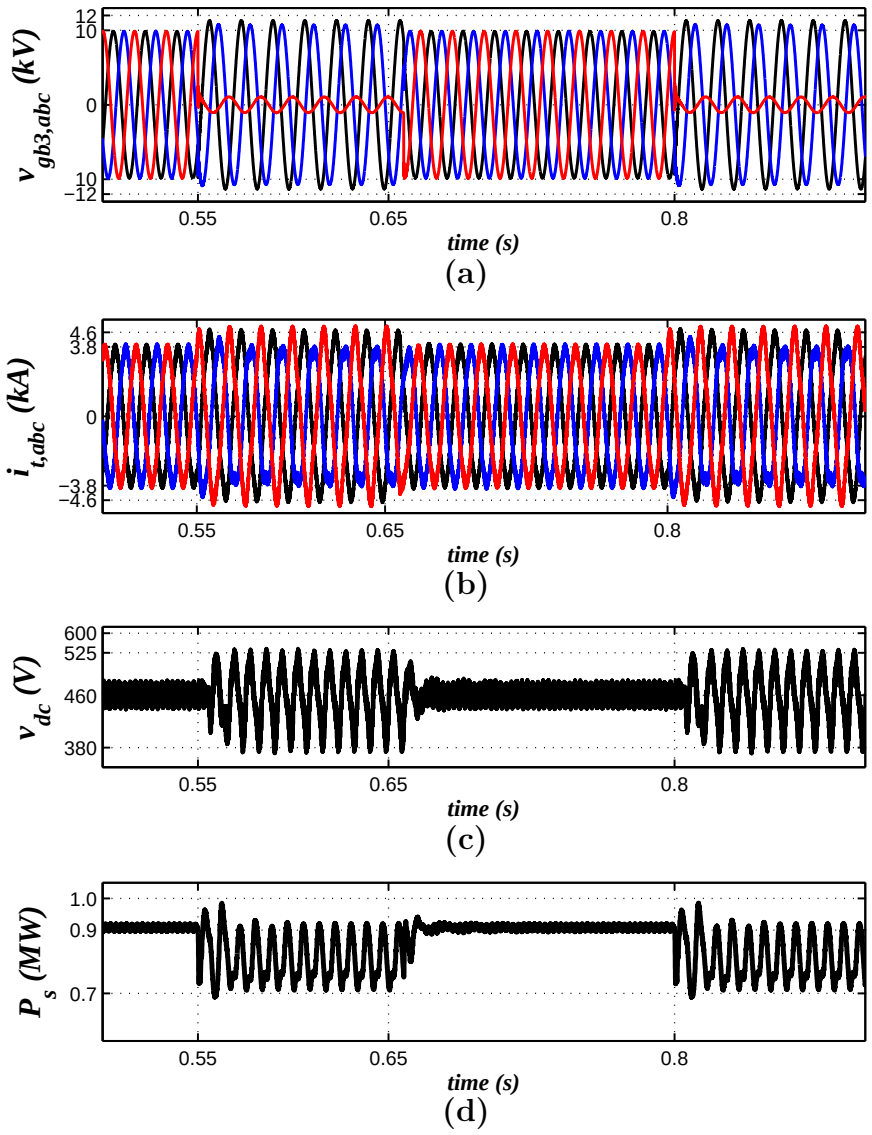

Figure 2.12: Conventional single-stage PV system response and TOVs due to a single-line-to-ground fault.

pected since the current-mode control is adopted for the PV system. Figure 2.12(d) indicates that, the imbalance of the grid-side voltage causes double-frequency pulsation in the PV system output power [71]. Similarly, as Figure 2.12(c) demonstrates, the dc-link voltage also fluctuates. As can be seen from Figure 2.12, the PV system resumes its normal operation when fault is cleared at $t = 0.65\ s$. However, due to the inception of permanent fault at $t = 0.8\ s$, the PV system behaves exactly the same way as it is during the post-disturbance time.

Figure 2.12(a) further shows that the TOV on the healthy phase due to the permanent fault is limited to about 1.12 $p.u.$ Although not shown, due to the permanent fault, low-

and high-voltage relay (connected at the low-voltage side of T_r) isolates the single-stage PV system from BUS 3, in about 1.0 s.

2.4.4 Case 4: TOVs Caused by the Conventional Single-Stage PV System during an Unintentional Islanding Incident

This test case demonstrates the second TOV mechanism (explained in Subsection 2.2.1) through which a PV system causes temporary over-voltages. Initially, the single-stage PV system is in a steady state, with $G = 1.0\ kW/m^2$ while the MPPT is in process. At $t = 0.65\ s$, the breaker B_{12} of the network of Figure 2.8 is disconnected, leading to an islanding incident. The single-stage PV system is now in the islanded zone and connected to the BUS 3.

Figure 2.13 illustrates the single-stage PV system response to an unintentional islanding incident. It can be seen from Figure 2.13(a) that, subsequent to the island formation, the grid-side voltages experience TOVs of about 1.68 $p.u.$ The reason behind the formation of TOVs is that, prior to the islanding incident, the single-stage PV system delivers about 0.92 MW [see Figure 2.13(d)], while the aggregate local load within the islanded zone is about 0.57 MW; implies that the PV system causes severe TOVs when the generation exceeds load (high PV generation to load ratio) [29], [47], [69]. In order to produce the pre-disturbance power, the PV system decreases the amplitude of the grid currents, as Figure 2.13(b) shows. Figure 2.13(c) illustrates that, due to the distortions in the grid-side voltages and currents, the dc-link voltage slightly deviates from the setpoint but remains under 600 V. As Figure 2.13(e) indicates, due to the frequency deviation, the low- and high-frequency relay intervenes and isolates the PV system, at $t = 0.75\ s$. Consequently, the dc-link voltage settles at the open-circuit voltage of the PV *generator* and the power transfer from the single-stage PV system is disrupted.

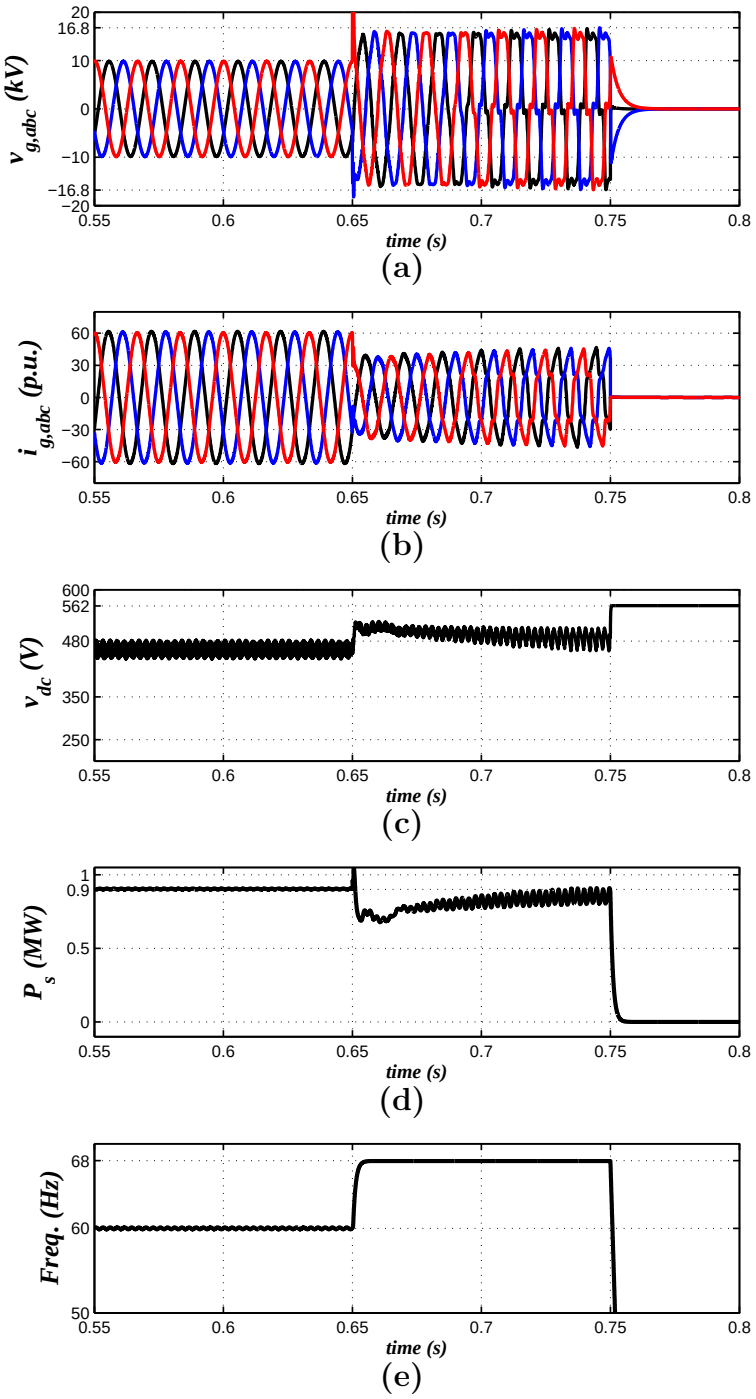

Figure 2.13: Conventional single-stage PV system response and TOV event due to an unintentional islanding incident.

2.4.5 Case 5: TOVs Caused by the Conventional Single-Stage PV System due to an Asymmetrical AC Fault and the following Islanding Incident

This case study demonstrates the TOV caused by the conventional single-stage PV system due to a single-line-to-ground fault and the following islanding incident. Prior to the fault and the following islanding incident, the PV system is in a steady state while the PV *generator* receives a solar irradiation of 1.0 kW/m^2 and the MPPT scheme is enabled. The rating of the local load connected in Figure 2.3 is $0.32+j0.17\ MVA$. The single-stage PV system delivers about 0.92 MW.

At $t = 0.65\ s$, a permanent single-line-to-ground fault (phase-c is bolted to the ground) takes place at the PCC point of the system of Figure 2.3. Afterwards, the upstream grid protection device detects the fault within 3 *cycles* and, as such, opens the breaker B_g at $t = 0.70\ s$, leading to an islanding incident. As a result, all the inverter current flows into the remaining small local load connected in the islanded zone. Consequently, voltage temporarily rises for another 100 ms until the low- and high-frequency relay triggers at $t = 0.80\ s$ and shutdown the inverter. Aforementioned phenomenon is known as TOVs due to the "interruption of significant power export" [29], [31], [46], [47].

Figure 2.14 illustrates the conventional single-stage PV system response. As Figure 2.14(a) and (b) show, the healthy phases of the grid-side and the inverter ac-side experience severe TOVs of about 2.21 $p.u.$ and 2.39 $p.u.$, respectively. A PV system having Δ/YG transformer experiences larger inverter ac-side over-voltages [32]. Moreover, voltages are distorted since a large zero-sequence current circulates in the Δ-connected windings of T_r. As can be seen from Figure 2.14(c) and (d), the dc-link voltage and the single-stage PV system output power experience double frequency pulsation during fault and the following islanding incident. As Figure 2.14(e) indicates, due to the frequency deviation, the low- and high-frequency relay intervenes and isolates the PV system, at $t = 0.80\ s$.

Therefore, the TOV caused by the conventional single-stage PV system is the most severe when there exists a single-line-to-ground fault during an islanding incident. This is not implausible and if the islanding detection scheme is not fast enough then the TOV during that short interval can make substantial damage on the DGs, equipments, and other customer loads [30].

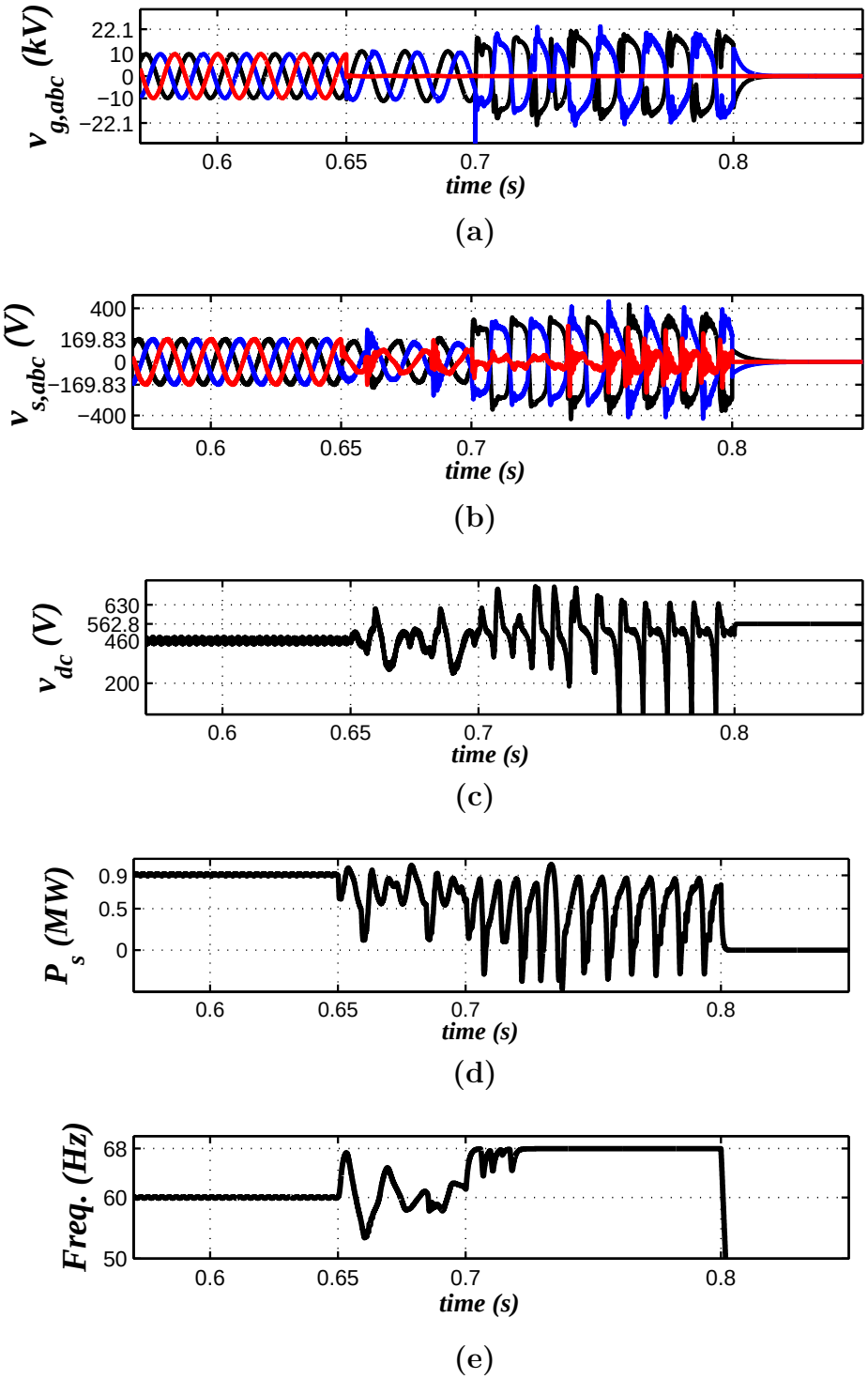

Figure 2.14: Conventional single-stage PV system response and TOV event due to a single-line-to-ground fault and the following islanding incident.

2.5 Modified Single-Stage PV System

2.5.1 System Configuration and Principle of Operation

To investigate the TOV caused by an effectively-grounded PV system, a modified single-stage grid-connected three-phase PV system is adopted in this section. Figure 2.15 illustrates the schematic single-line diagram of the modified single-stage three-phase PV system [46]. As Figure 2.15 shows, the modified system employs a half-bridge converter (HBC) and a Y/YG isolation transformer. As required by the grid codes, isolation transformer, T_r uses a grounded *wye* (YG) winding configuration at its grid-side [29], [50], [51], [70]. To maintain the relationship between the phase terminal voltages of the inverter and the grid-side phase voltages, a *wye* (Y) winding configuration at the inverter side of T_r is adopted [32]. In order to connect the neutral point of T_r at the inverter ac-side and to avoid splitting the dc-link capacitor, the modified system adopts a half-bridge converter (HBC) [75], [76]. Thus, the neutral point of T_r at the inverter ac-side is connected to the midpoint of HBC. A small inductance, L_n connected in series with a resistance, R_n is placed in between the transformer and HBC in order to limit the zero-sequence current that will flow through the neutral point of the transformer during ground faults [32]. The inductance L_n and resistance R_n are acting as effective zero-sequence reactance and resistance, respectively.

The modified PV system uses the same decoupled *dq*-frame current-control scheme and the dc-link voltage controller as those employed for the conventional single-stage PV system (explained in Subsection 2.3.2 and Subsection 2.3.3). However, during network disturbances (such as network faults or unintentional islanding), the modulating signals m_d and m_q from the inverter current- control scheme may get saturated. To circumvent the aforementioned situation, the outputs of the current-control scheme of the inverter are processed in a block that is labeled in Figure 2.15 as the vector magnitude limiter (VML) [60], [87]. Furthermore, the modified PV system uses a TOV limiting scheme block to mitigate/reduce the TOV. Figure 2.16 illustrates the zero-sequence current controller of the modified single-stage PV system which regulates the zero-sequence current of the inverter. The setpoint of this controller is $i_{0ref} = 0$. It should be pointed out that, the aforementioned zero-sequence current controller is a part of the inverter current-control scheme of the modified PV system. As can be seen from Figure 2.15, the TOV limiting scheme block can issues two commands. If the block issues the command $m_{dq,max}$, the block will be used for the conventional single-stage PV system. On the other hand, if the TOV limiting scheme block issues the command $m_{abc,max}$, the block will be used for the modified single-stage PV system.

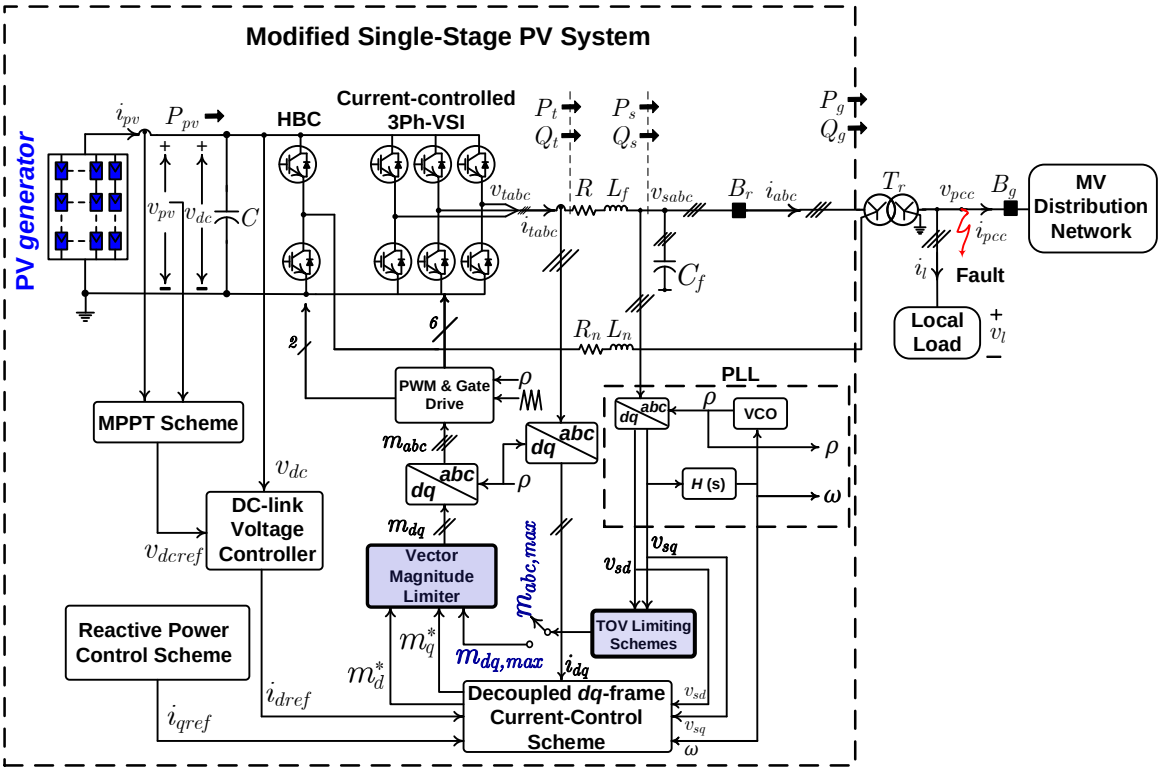

Figure 2.15: Schematic diagram illustrating the modification to the conventional single-stage PV system.

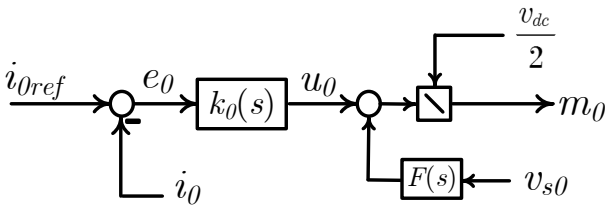

Figure 2.16: Block diagram of the zero-sequence current controller of the modified single-stage PV system.

2.6 Proposed TOV Limiting Schemes

This section proposes two TOV limiting schemes. One is for the conventional single-stage PV system and another one is for the modified single-stage PV system. Each scheme has its own advantage. Governing principle behind the TOV limiting scheme is explained by using the equations of three-phase terminal voltages, v_{tabc} of the VSI, which are based on [76]

$$v_{ta}(t) = \frac{v_{dc}}{2} m_a(t)$$
$$v_{tb}(t) = \frac{v_{dc}}{2} m_b(t) \tag{2.14}$$
$$v_{tc}(t) = \frac{v_{dc}}{2} m_c(t)$$

where, v_{ta}, v_{tb}, and v_{tc} are the phase terminal voltages of the VSI, v_{dc} is the dc-link voltage, and m_a, m_b, m_c are the modulating signals of the inverter. According to (2.14), the phase terminal voltages, v_{tabc} of the VSI and, as such, the grid-side voltages, $v_{g,abc}$ can be controlled by controlling the inverter modulating signals, m_{abc}. The aforementioned concept is utilized in the proposed TOV limiting schemes.

2.6.1 TOV Limiting Scheme 1 for the Conventional Single-Stage PV System

In the conventional single-stage PV system with Δ/YG isolation transformer of Figure 2.3, each grid-side voltage (v_{ga}, v_{gb}, or v_{gc}) is related by an inverter ac-side line-to-line voltage. This implies that, each grid-side voltage depends on two phase voltages of the inverter . Due to the aforementioned reason, this thesis proposes a TOV limiting scheme for the conventional single-stage PV system which is shown in Figure 2.17. As the Figure 2.17(a) shows, at first, the inverter ac-side voltages, v_{sabc} are transformed to v_{sd} and v_{sq} by using the *abc*- to *dq*-frame transformation block. The magnitude of v_{sabc} ($\hat{v}_s = \sqrt{v_{sd}^2 + v_{sq}^2}$) is then normalized by the nominal peak value, $\hat{v}_{nominal}$ of the inverter ac-side voltage (low-voltage side of the isolation transformer). The normalized value, $\hat{v}_s$ (in *p.u.*) is processed through a low-pass filter (LPF) and then used to compare with a maximum voltage setpoint, $\hat{v}_{slimit}$. The maximum voltage setpoint, $\hat{v}_{slimit}$ is the maximum permissible limit of the TOV imposed by some grid codes, like the one in [20]. The $\hat{v}_{slimit}$ is set to as 1.3 *p.u.* Thereafter, the error, e_s is processed through an anti-wind-up technique based PI controller. This controller produces the selection value, e_{so}. Based on the selection value, a non-linear transfer characteristics block produces the required maximum saturation limit, $m_{dq,max}$ of m_d and m_q.

Aforementioned non-linear transfer characteristics block is responsible to produce the maximum saturation limit of m_d and m_q. The non-linear transfer characteristics is illustrated in Figure 2.17(b). This can be explained as, follows. Input range of the transfer characteristics is selected in such a way that, if $\hat{v}_s$ (in *p.u.*) during the TOV

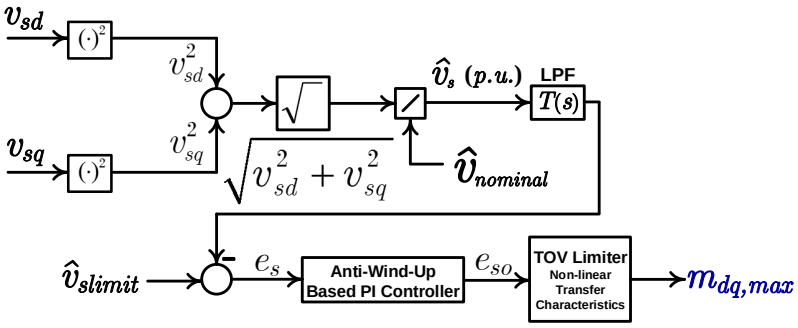

(a) TOV limiting Scheme 1

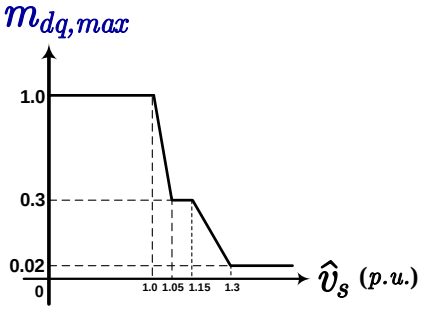

(b) Non-linear transfer characteristics

Figure 2.17: (a) Block diagram of the TOV limiting Scheme 1 for the conventional single-stage PV system. (b) Non-linear transfer characteristics of the TOV limiter.

incident goes beyond $\hat{v}_{slimit}$, anti-wind-up technique based PI controller processes the error and issues the command for producing the required $m_{dq,max}$. For example, if $\hat{v}_s$ (in $p.u.$) goes above 1.3 $p.u.$, then $m_{dq,max}$ would be 0.02, but if $\hat{v}_s$ (in $p.u.$) goes above $\hat{v}_{nominal}$ but below $\hat{v}_{slimit}$ such as 1.15 $p.u.$, then $m_{dq,max}$ would be 0.3. This implies that, the controller issues command to produce smaller limit of the modulating signal during larger over-voltage incident. The slope and the input and output range of the non-linear transfer characteristics can be tuned for an acceptable performance. Figure 2.18 illustrates the anti-wind-up technique based PI controller. This is implemented in the PSCAD environment by using standard component blocks available in the software master library. If the output is saturated then this controller reduces the output of the integrator by adjusting the input of the integrator. Its parameters, such as proportional gain, k_p, anti-wind-up gain, k_{aw}, and the limiter value are design choice and can be carefully tuned for an acceptable performance.

Figure 2.19 illustrates the VML for the conventional single-stage PV system. During

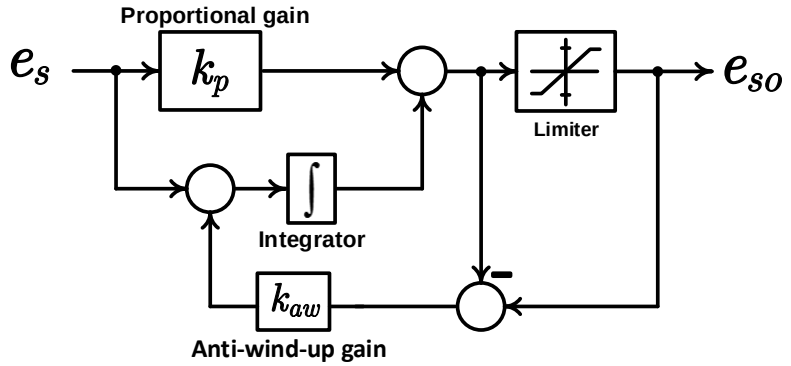

Figure 2.18: Block representation of the anti-wind-up technique based PI controller.

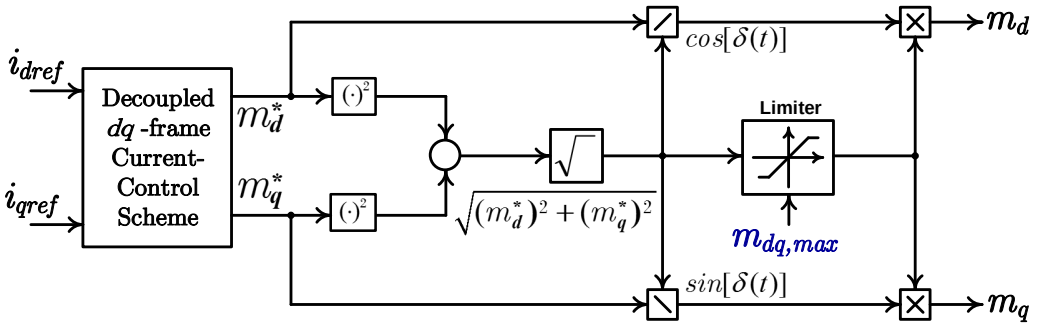

Figure 2.19: Block diagram of vector magnitude limiter of the conventional single-stage PV system.

network faults or over-voltage incident modulating signal components of the inverter may get saturated, which in turn, makes the inverter operates abnormally. Therefore, during such incident and to operate the inverter in its linear modulation region, dq-frame modulating signals are limited by the VML. However, the VML does not change the ratios $m_d^*/\sqrt{(m_d^*)^2+(m_q^*)^2}$ and $m_q^*/\sqrt{(m_d^*)^2+(m_q^*)^2}$ (i.e., it does not change the phase angle of $m_{abc}(t)$. The VML also ensures that $\sqrt{(m_d^*)^2+(m_q^*)^2} \leqslant m_{dq,max}$. As can be seen from Figure 2.19, the TOV limiting Scheme 1 issues $m_{dq,max}$ which is used in the VML. The inverter modulating signals, m_{abc} are obtained from m_d and m_q by using the dq- to abc-frame transformation block.

2.6.2 TOV Limiting Scheme 2 for the Modified Single-Stage PV System

The modified single-stage PV system presented in Figure 2.15 uses Y/YG isolation transformer and, as such, each grid-side voltage (v_{ga}, v_{gb} and v_{gc}) is related to the respective inverter ac-side voltage (v_{sa}, v_{sb} and v_{sc}). This suggests that, grid-side phase voltages can be independently controlled by their respective inverter ac-side voltages. Therefore, as Figure 2.20(a) shows, for the modified single-stage PV system, the TOV limiting Scheme 2 uses inverter ac-side voltages in order to produce the modulating signal limit, $m_{a,max}$, $m_{b,max}$ and $m_{c,max}$ for m_a, m_b and m_c respectively. The peak values of the inverter ac-side voltages (v_{sa}, v_{sb} and v_{sc}) are measured and normalized to the nominal peak value, $\hat{v}_{nominal}$ of the inverter ac-side voltage (low-voltage side of the isolation transformer). Figure 2.20(b) demonstrates the non-linear transfer characteristics of the TOV limiting Scheme 2. For achieving acceptable performance, however, the non-linear transfer characteristic curve for the TOV limiting Scheme 2 uses slightly different value than that is used for the TOV limiting Scheme 1. Other than that, the mechanism uses in the modulating signal limit processing block of Figure 2.20(a) is the same as that explained for the TOV limiting Scheme 1. Figure 2.21 illustrates the VML of the modified PV system. When VML is applies in the modified PV system, maximum and minimum saturation level of the limiter can be set to 1 and -1, respectively.

It should be pointed out that, the TOV limiting schemes also reacts to steady-state over-voltage. To avoid the aforementioned circumstances, in practice, a monostable multivibrator with a predefined set time can be incorporated in the TOV limiting schemes. In the case of detected over-voltage, the monostable multivibrator should be turned on and started to operate till the set time. After the predefined set time, the monostable multivibrator will be disabled. If the over-voltage is still present, the inverter should be shuts down indefinitely.

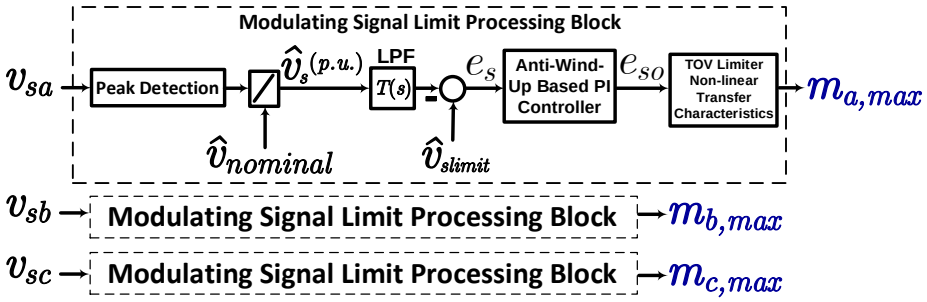

(a) TOV limiting Scheme 2

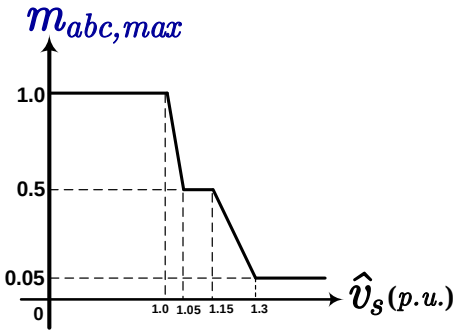

(b) Non-linear transfer characteristics

Figure 2.20: (a) Block representation of the TOV limiting Scheme 2 for the modified single-stage PV system. (b) Non-linear transfer characteristics of the TOV limiter.

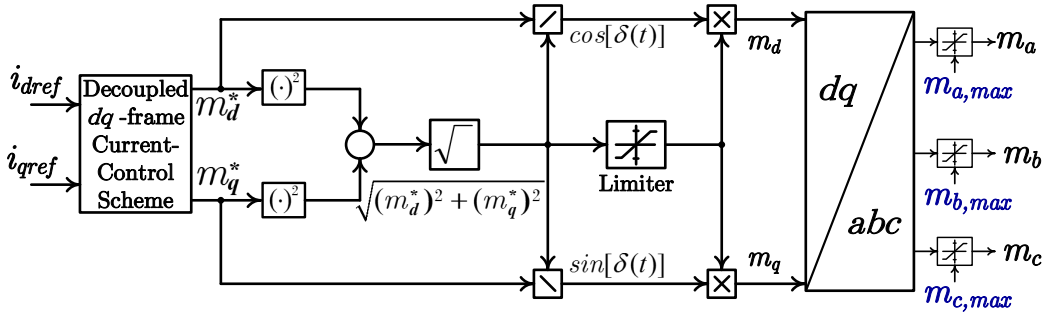

Figure 2.21: Block representation of VML of the modified single-stage PV system.

2.7 Simulation Results and TOV Mitigation

To evaluate the effectiveness of the TOV limiting schemes, a detailed switched model of the modified single-stage PV system of Figure 2.15 and the conventional single-stage PV system of Figure 2.3 are simulated in the PSCAD/EMTDC software environment. The rated power of the PV *generator* is 1.0 MW. Other parameters of the PV *generator* are listed in Table A.1. The VSI and isolation transformer T_r of the modified PV system are all assumed to have a power rating of 1.0 MVA. The modified PV system is interfaced with a CIGRE benchmark MV distribution network of Figure 2.8, which is the same as that employed for the conventional PV system. The modified PV system and controller parameters are given in Appendix B. The PV system relay settings are listed in Table D.1 of Appendix D.

To investigate the TOV caused by the modified single-stage PV system, a simulation case study without using the proposed TOV limiting Scheme 2 is performed. Then, this section, compares TOVs caused by the modified PV system and the conventional PV system. Afterwards, this section studies both the modified and the conventional PV system response under the proposed TOV limiting schemes.

2.7.1 Case 1: TOVs Caused by the Modified Single-Stage PV System due to an Asymmetrical AC Fault and the following Islanding Incident

This simulation case study demonstrates the TOV caused by the modified single-stage PV system without exercising the proposed TOV limiting Scheme 2. Prior to the disturbance, the modified PV system is assumed to be in a steady state and delivers about 0.92 MW while the MPPT scheme is enabled and the PV *generator* receives a solar irradiation of G = 1.0 kW/m^2. The rating of the local load connected in Figure 2.15 is 0.32+j0.17 MVA. Figure 2.22 illustrates the modified single-stage PV system response without using the proposed TOV limiting Scheme 2.

A permanent single-phase-to-ground fault (phase-c is bolted to the ground) takes place at t = 0.65 s at the PCC point of the system of Figure 2.15. The fault incident is detected by the upstream grid protection relay within 3 *cycles* and thereafter opens the breaker B_g at t = 0.70 s; leading to an islanding incident. Figure 2.22(a) and (b) indicate that, due to the fault and the following islanding incident, the grid-side and the inverter ac-side healthy phase voltages experience over-voltages of about 2.55 $p.u.$ and 2.04 $p.u.$, respectively. Despite using the Y/YG isolation transformer, the modified

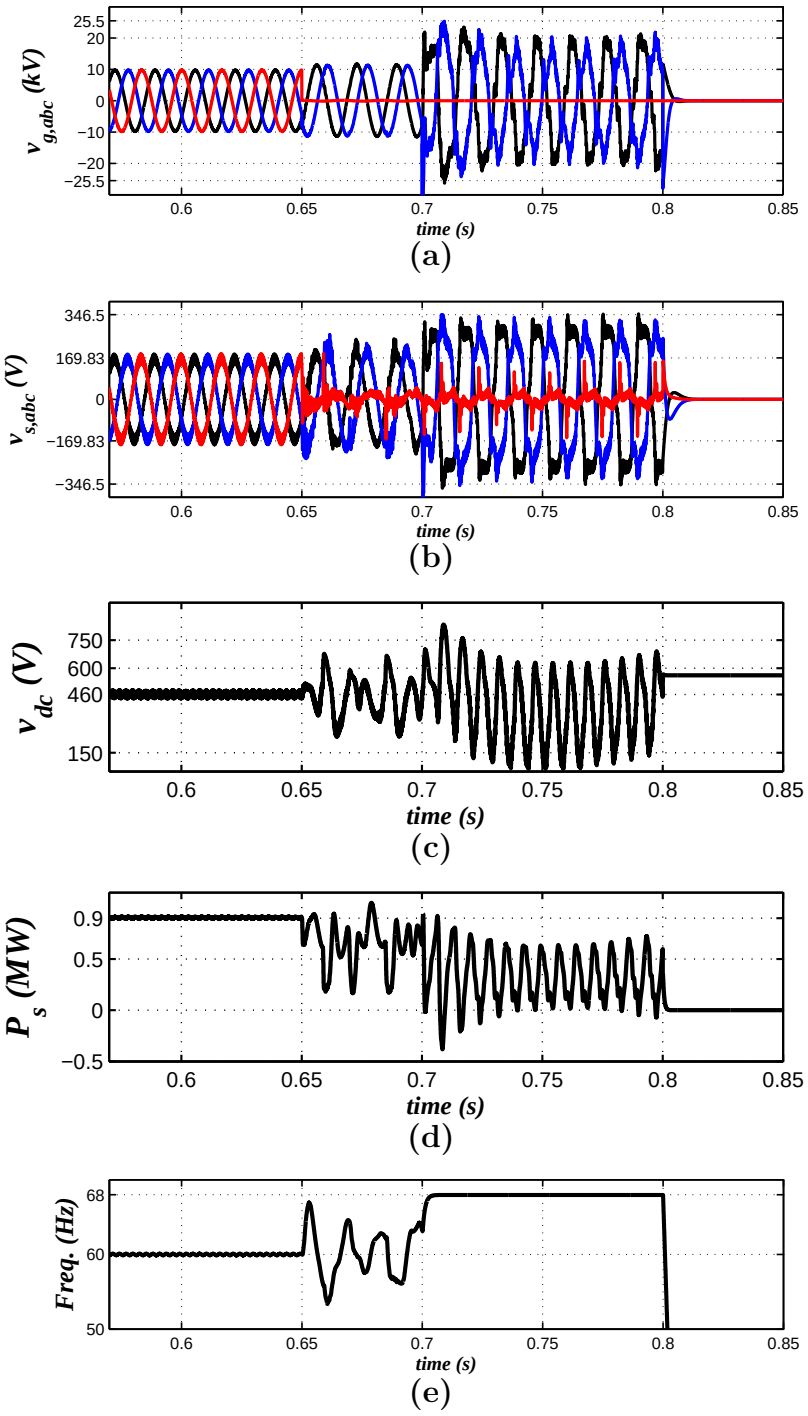

Figure 2.22: Modified single-stage PV system response due to an asymmetrical fault and the following islanding incident without using the proposed TOV limiting Scheme 2.

PV system also experiences severe TOVs. The aforementioned problem also reported in [31], [49]. As demonstrated in Case #5 [see Figure 2.14], it can be concluded that, during a single-line-to-ground fault and the following islanding incident, the conventional

PV system with a Δ/YG isolation transformer experiences smaller grid-side over-voltages, but slightly larger inverter ac-side over-voltages. Figure 2.22(c) and (d) show that the voltage imbalance due to the fault and the following islanding incident results in the double frequency pulsations on the dc-link voltage and the power output [71]. Figure 2.22(c) further indicates that, the dc-link voltage exceeds the maximum dc-link voltage level (600 V) due to the fault and the following islanding incident. As Figure 2.22(e) shows, frequency relay of the PV system detects larger deviation of the frequency and isolates the PV system, at $t = 0.80$ s.

2.7.2 Case 2: Conventional Single-Stage PV System Response under the Proposed TOV Limiting Scheme 1

This test case demonstrates the effectiveness of the proposed TOV limiting Scheme 1. The TOV limiting Scheme 1 applies to the conventional single-stage PV system of Figure 2.3. This case study is similar to Case #5 which is demonstrated in Subsection 2.4.5, with the exceptions that the conventional PV system is under the proposed TOV limiting Scheme 1. Prior to the fault and the following islanding incident, the PV system is in a steady state while the PV *generator* receives a solar irradiation of 1.0 kW/m^2 and the MPPT scheme is enabled. The rating of the local load connected in Figure 2.3 is $0.32+j0.17$ MVA. The single-stage PV system delivers about 0.92 MW. Figure 2.23 represents the response of the conventional PV system under the proposed TOV limiting Scheme 1. As Figure 2.23(a) and (b) indicate, after the formation of island, magnitude of over-voltages of the two sides of the isolation transformer are significantly reduced (below 1.3 $p.u.$) and are limited to about 1.23 $p.u.$ (grid-side) and 1.24 $p.u.$ (inverter ac-side). Figure 2.23(c) also depicts that, line-to-line grid-side over-voltages are limited to about $\sqrt{3}$ of 1.23 $p.u.$ due to the TOV limiting Scheme 1 for providing the required saturation limit of d and q components of the inverter modulating signals in the case of detected over-voltage. As can be seen from Figure 2.23(d) and (e), double frequency pulsations on the dc-link voltage and the PV system output power are also reduced. The maximum magnitude of the dc-link voltage is below 600 V. Although not shown, both the fault and the islanding incident result in the isolation of the conventional PV system from BUS 3, at $t = 0.8$ s. Consequently, the PV system output power is disrupted and the dc-link voltage settles at the measured open-circuit voltage of the PV *generator*.

It can be observed from Figure 2.24 that, before fault and the following islanding incident, $m_{dq,max}$ from non-linear transfer characteristics curve is close to 1 (in this case 0.95). However, due to the fault, $m_{dq,max}$ drops down to 0.3 and after islanding incident

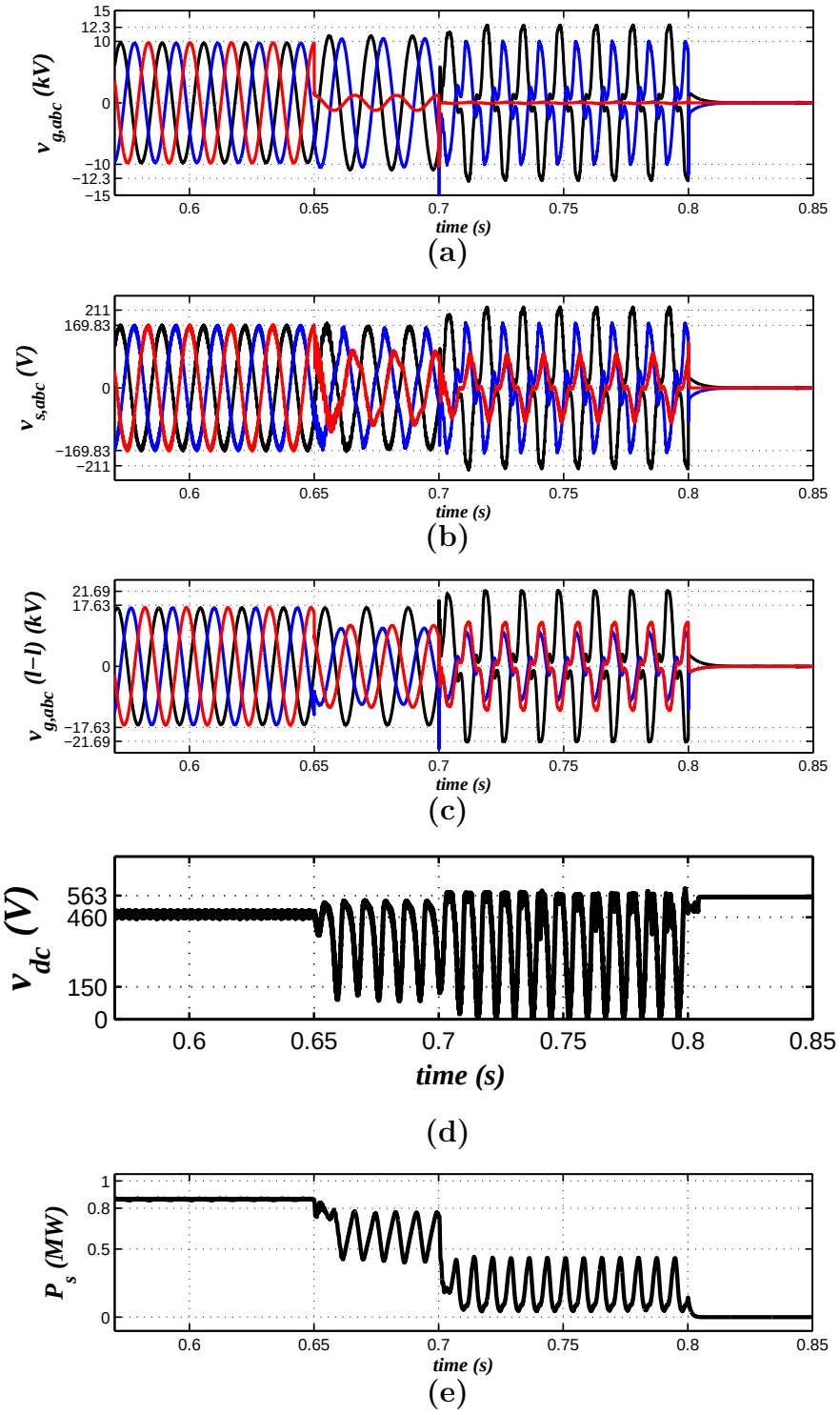

Figure 2.23: Conventional single-stage PV system response under the proposed TOV limiting Scheme 1.

it becomes very low value of 0.02 in order to limit the TOVs. This implies that, the larger the over-voltage, the smaller the limit of the modulating signal limit. Therefore,

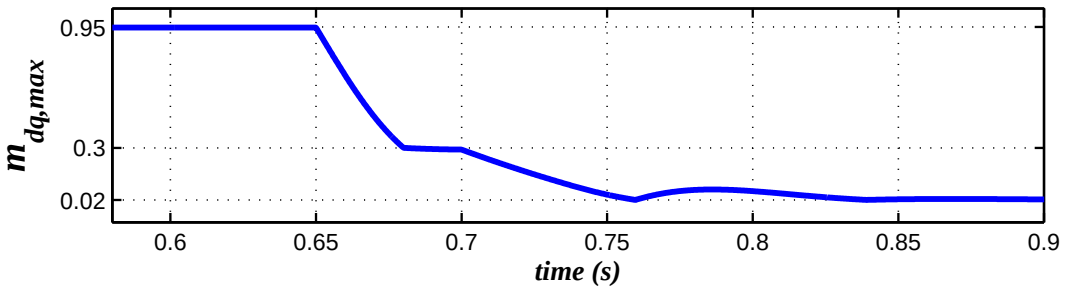

Figure 2.24: Non-linear transfer characteristics for the TOV limiting Scheme 1 of the conventional single-stage PV system.

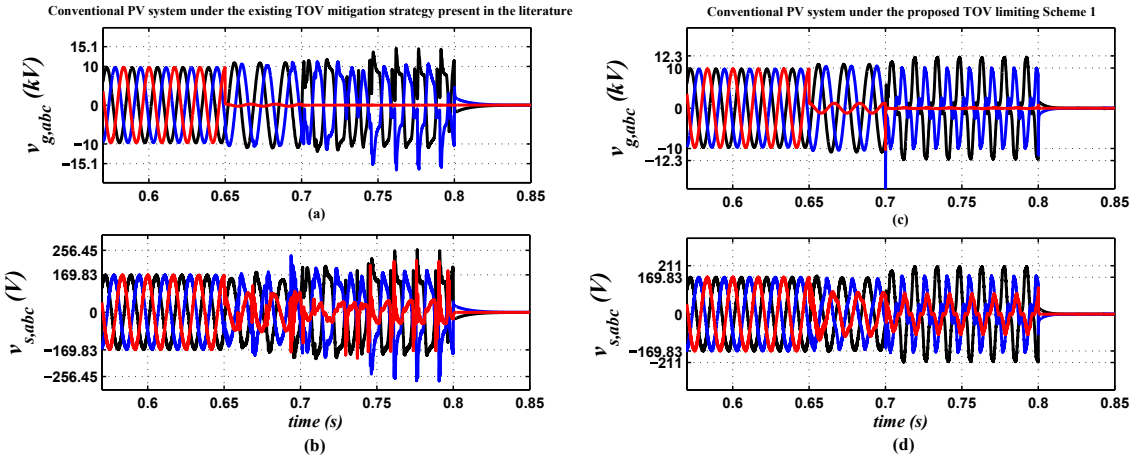

Figure 2.25: Conventional single-stage PV system's voltages (grid-side and inverter ac-side) under the existing TOV mitigation strategy and the proposed TOV limiting Scheme 1.

the TOV limiting Scheme 1 offers a better capability for limiting TOVs caused by the conventional PV system.

Figure 2.25 illustrates the conventional single-stage PV system's voltages (grid-side and inverter ac-side) under the existing TOV mitigation strategy proposed in the literature [46] and the proposed TOV limiting Scheme 1. Figure 2.25 (a) and (b) represent the grid-side and the inverter ac-side phase voltages under the existing TOV mitigation strategy which is proposed in the literature [46]. Under the existing TOV mitigation strategy, the TOVs at the grid-side and the inverter ac-side are limited to about 1.5 *p.u.* Moreover, the voltages exhibit larger steady-state distortions. Figure 2.25 (c) and (d) represent the grid-side and the inverter ac-side phase voltages under the proposed TOV limiting Scheme 1. Under the proposed TOV limiting Scheme 1, the TOVs are limited to about 1.23 *p.u.* (grid-side) and 1.24 *p.u.* (inverter ac-side).

2.7.3 Case 3: Modified Single-Stage PV System Response under the Proposed TOV Limiting Scheme 2

This case study is similar to Case #1 which is demonstrated in Subsection 2.7.1, with the exceptions that the TOV limiting Scheme 2 is exercised in the modified single-stage PV system of Figure 2.15. The non-linear transfer characteristics curve uses slightly different values to determine the saturation limits of the modulating signals, as illustrated in Figure 2.20(b). Prior to the disturbance, the modified PV system is assumed to be in a steady state and delivers about 0.92 MW while the MPPT scheme is enabled and the PV *generator* receives a solar irradiation of $G = 1.0\ kW/m^2$. The rating of the local load connected in Figure 2.15 is $0.32+j0.17\ MVA$.

Figure 2.26 illustrates the response of the modified PV system under the proposed TOV limiting Scheme 2, to a single-line-to-ground fault and the following islanding condition. As Figure 2.26(a) and (b) indicate, under the TOV limiting Scheme 2, the over-voltages of the healthy phases are significantly limited. The grid-side over-voltages are limited to about 1.16 *p.u.*, whereas the inverter ac-side voltages are limited to about 1.20 *p.u.* Unlike Case #1, the modified PV system under the proposed TOV limiting Scheme 2 provides considerable improvement. Also Figure 2.26(c) and (d) depict that, double frequency pulsation range is significantly reduced in the output power and the dc-link voltage waveforms. As it can be seen from Figure 2.26(e), zero-sequence current controller of Figure 2.16 regulates the inverter zero-sequence current close to zero before the fault inception, however, the zero-sequence current increases after the fault, for a few cycles before the PV system is isolated from the grid by the inverter protective relays.

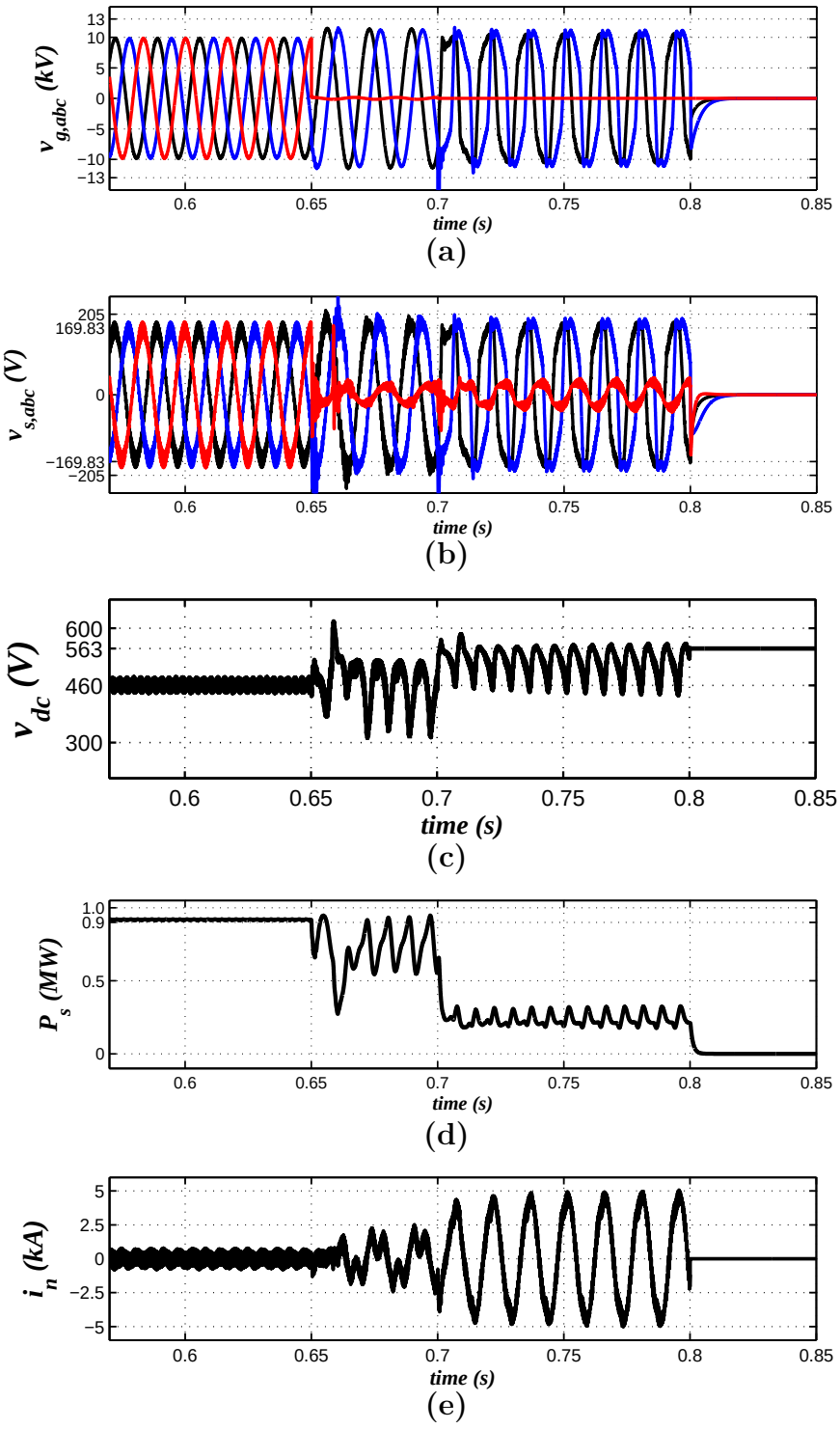

Figure 2.26: Modified single-stage PV system response under the proposed TOV limiting Scheme 2.

2.8 Summary and Conclusions

In this chapter, the mechanisms, and characteristics behind the temporary over-voltage (TOV) were explained. Two mechanisms have been identified by which a distributed PV system can causes temporary over-voltages (TOVs). The first mechanism is known as neutral voltage displacement, whereas the second mechanism is called interruption of significant power export. A comprehensive conventional single-stage grid-connected three-phase PV system with a widely used Δ/YG isolation transformer was modeled. The model adopted a decoupled *dq*-frame current-control scheme, and a dc-link voltage controller for the inverter. The developed model was used to analyze the TOV through a fairly comprehensive set of case studies. Furthermore, a modified single-stage grid-connected three-phase PV system with a Y/YG isolation transformer was modeled. The modified PV system model was also used to analyze the TOV. A vector magnitude limiter (VML) block is used for the both PV systems in order to prevent saturation of the d and q components of the modulating signals of the inverter. Additionally, two TOV limiting schemes were proposed to limit the most severe TOVs caused by the both PV systems due to a single-phase-to-ground fault and the following islanding incident. The proposed TOV limiting scheme used an anti-wind-up technique based PI controller. Proposed TOV limiting schemes produced the required saturation limit of the modulating signals and, as such, the inverter ac-side and grid-side voltages were controlled. The performance of the single-stage PV systems and the effectiveness of the proposed TOV limiting schemes were demonstrated by time-domain simulation studies in the PSCAD/EMTDC environment.

The following conclusions can be made from the simulation results:

- The TOV can occur either during a single-line-to-ground fault or subsequent to an islanding incident. In the conventional PV system, the healthy phases of the grid-side voltage experiences TOV of about 1.12 *p.u.* due to a single-line-to-ground fault, whereas the grid-side voltage experiences TOV of about 1.68 *p.u.* due to an unintentional islanding incident.

- The magnitude of the TOV is proportional to the ratio of the total PV power generation to the total load in the islanded zone.

- The TOV is the most severe during a single-line-to-ground fault and the following islanding incident. It is shown from the simulation results that, the grid-side and the inverter ac-side experience over-voltages of about 2.21 *p.u.* and 2.39 *p.u.*, respectively. By a proper control strategy, the TOV caused by the PV system can be limited. It is shown that, under the proposed TOV limiting Scheme 1, the grid-side

and the inverter ac-side over-voltages are limited to about 1.23 *p.u.* and 1.24 *p.u.*, respectively.

- An effective grounding system may not mitigate the TOV. It is shown from the simulation results that, the modified single-stage PV system experiences grid-side and inverter ac-side over-voltages of about 2.55 *p.u.* and 2.04 *p.u.*, respectively. However, under the proposed TOV limiting Scheme 2, the grid-side and the inverter ac-side over-voltages are limited to about 1.16 *p.u.* and 1.20 *p.u.*, respectively.

Chapter 3

TOV Analysis: Two-Stage PV System

3.1 Introduction

The standard maximum dc voltage for PV modules and PV systems installed in North America is 600 volts [88]. Moreover, according to the national electrical code, NEC 490.2, the PV *generator* open-circuit voltage must never exceed 600 V. The maximum voltage from the PV *generator* can be extracted by using the MPPT scheme. However, in the PV system, most of the power production occurs at significantly lower voltages. The ratio between the highest voltage and the typical power production voltage can range from 1.6 to 1 to greater than 2 to 1 [89]. While widely adopted large-scale PV system employs a central inverter as the only power processing stage, the aforementioned issue prevents central inverter to operate optimally. Hence, in power conversion, as the operating voltage range increases, it is typical to move to a two-stage power conversion architecture. Thus, the controlled dc voltage from the output of the PV *generator* is first boosted using a dc-dc converter to a fixed value, for the subsequent inverter stage, which can then be optimized [89].

This chapter, uses a two-stage grid-connected three-phase PV system for the temporary over-voltage (TOV) analysis. The two-stage PV system uses a Δ/YG isolation transformer. This chapter also uses the proposed TOV limiting scheme 1 in order to mitigate the TOV. The two-stage PV system employs a dc-dc boost converter as the first power-processing stage, which can boost a low-voltage of the PV *generator* up to a specific high dc-link voltage and also responsible for the MPPT. The second power-processing stage uses a three-phase VSI, which can stabilize the dc-link voltage and shape

the output current of the PV system. Moreover, the boost converter uses an output voltage controller in order to control its output terminal voltage, particularly during network faults. The purpose of the boost converter output terminal voltage controller is to keep the dc-link voltage within the specific range and prevent from rising. At last, the TOV limiting scheme 1 which is proposed in Chapter 2 is employed in the two-stage PV system to limit the TOV during a single-line-to-ground fault and the following islanding incident.

3.2 Two-Stage PV System

3.2.1 System Structure

A schematic diagram is shown in Figure 3.1 which represents a two-stage grid-connected three-phase PV system interfaced with a CIGRE benchmark MV distribution network at the point of common coupling (PCC). The PV *generator* is connected to the dc-link of the inverter through a traditional unidirectional dc-dc boost converter [75]. To obtain the required power rating, the PV *generator* is composed of the parallel connection of N_p PV strings. Moreover, to ensure that the open-circuit voltage of the PV *generator* is within the maximum voltage limit of 600 V, each PV string consists of the series connection of N_s PV modules. The aforementioned condition and definitions are adopted from [88] and [90], respectively. As can be seen from Figure 3.1, P_{pv} refers to the PV power injected into the boost converter. For extracting maximum power from the PV *generator*, an incremental conductance (IC) algorithm based MPPT scheme is used [84] and [85]. Under normal operation, the boost converter is controlled to regulate the voltage, v_{pv} at the PV *generator* terminal. The MPPT scheme of the boost converter issues the setpoint, v_{pvref} of the controlled PV *generator* terminal voltage. As Figure 3.1 shows, P_{bo} and P_{inv} represent the power output from the boost converter and the power drawn by the inverter from the dc-link, respectively.

Under normal operating conditions, the current-controlled three-phase VSI regulates the dc-link voltage through the dc-link voltage controller. However, during network faults, another controller of the boost converter takes control of its output terminal voltage, which prevents the dc-link voltage from rising. Figure 3.1 further shows that, the inverter is interfaced with the MV distribution network through a low-pass filter, L_fC_f and an isolation transformer, T_r. The function of the filter is to prevent current harmonics from penetrating into the network. The VSI employs the conventional dq-frame current-control scheme [76]. The inverter phase terminal currents, i_{tabc} and ac-side voltages, v_{sabc} are transformed into corresponding dq-frame signals. Synchronization of

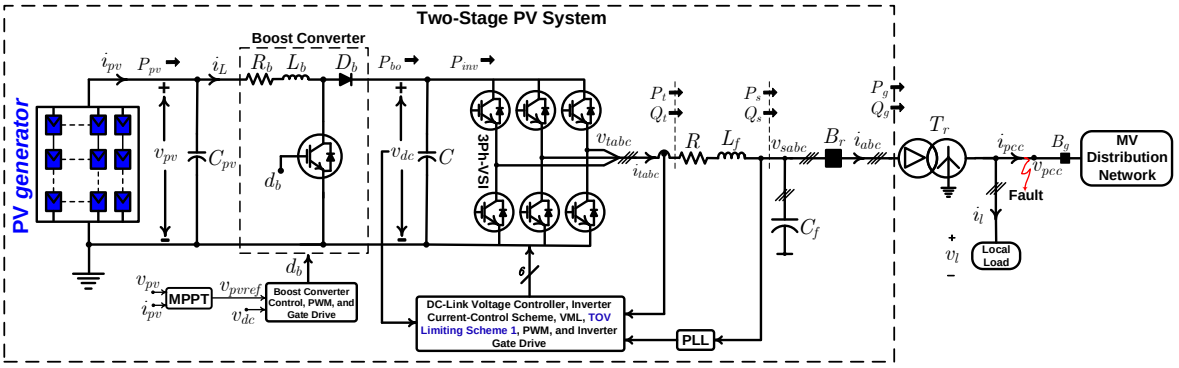

Figure 3.1: Single-line schematic diagram of a two-stage grid-connected three-phase PV system interfaced with a distribution network.

v_{sabc} is done by the phase-locked loop (PLL) [71]. Since, the main focus is to analyze and mitigate the TOV during a single-line-to-ground fault and an islanding incident, the vector magnitude limiter (VML) and the proposed TOV limiting Scheme 1 discussed in Chapter 2 are introduced in the PV system of Figure 3.1.

3.2.2 Control System of DC-DC Boost Converter

The two-stage PV system uses a dc-dc boost converter as the first power-processing stage, which can boost a low voltage of the PV *generator* up to a specific high dc-link bus voltage. Control strategies for the PV boost converter have been proposed in [91–94]. As shown in Figure 3.2, the PV *generator* is connected to the PV boost converter through a capacitor, C_{pv}. The capacitor, C_{pv} prevents the current ripples produced by the boost converter from disturbing v_{pv}. The MPP of the PV *generator* is achieved through the controlling of v_{pv}. Thus, a closed loop control structure regulates v_{pv} at the setpoint, v_{pvref} issued by the MPPT block. For this control structure, the dynamics of the PV *generator* terminal voltage and the boost converter inductor current are described as

$$\frac{dv_{pv}}{dt} = \frac{1}{C_{pv}}(i_{pv} - i_L) \tag{3.1}$$

$$\frac{di_L}{dt} + \frac{1}{L_b}R_b i_L = \frac{1}{L_b}[v_{pv} - (1 - m_b)v_{dc}] \tag{3.2}$$

where i_{pv} is the PV *generator* output current, i_L is the inductor current, R_b and L_b are the boost converter resistance and inductance, m_b is the modulating signal, and v_{dc} is the dc-link capacitor voltage seen by the boost converter.

Figure 3.3 represents the closed loop control structure which can regulates v_{pv} at the

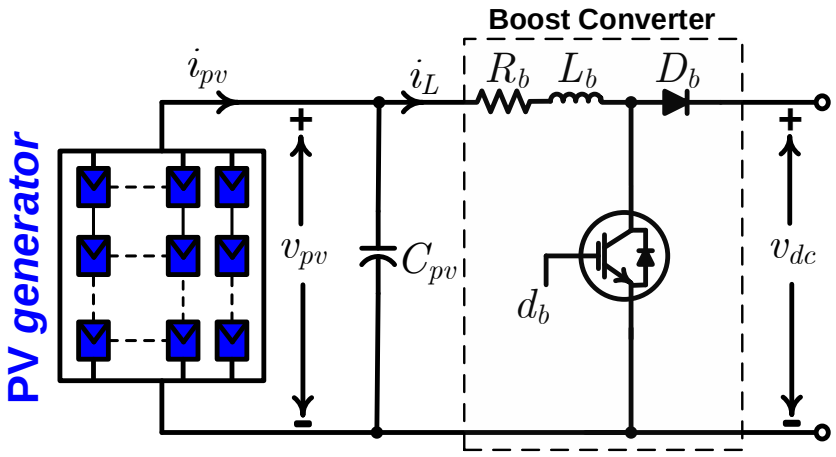

Figure 3.2: Schematic representation of the PV DC-DC boost converter.

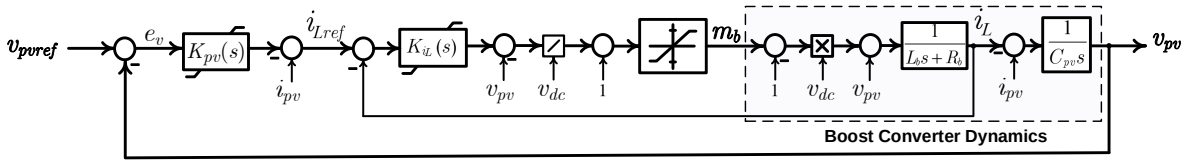

Figure 3.3: Block representation of the two-loop averaged current-control method of the boost converter.

setpoint, v_{pvref} issued by the MPPT block. The aforementioned control loop is established by using (3.1) and (3.2) and based on the two-loop averaged current control method of boost converter [92] and [95]. As can be seen from Figure 3.3, based on (3.2), inner inductor current regulating loop controls i_L such that it follows the following transfer function:

$$\frac{I_L(s)}{I_{Lref}(s)} = \frac{1}{\tau_b s + 1} \tag{3.3}$$

where the time constant, τ_b should be made small for a fast control response. The outer v_{pv} control loop issues the reference i_{Lref} for the inner inductor current control loop. The outer v_{pv} control loop is based on (3.1). Under normal operating conditions, control loop of Figure 3.3 controls v_{pv}, while the dc-link voltage regulation is done by the inverter dc-link voltage controller. However, during network faults, the dc-link voltage rises and to prevent the dc-link voltage from rising and maintain the voltage level within a specific range, boost converter uses an output voltage control loop for controlling its output

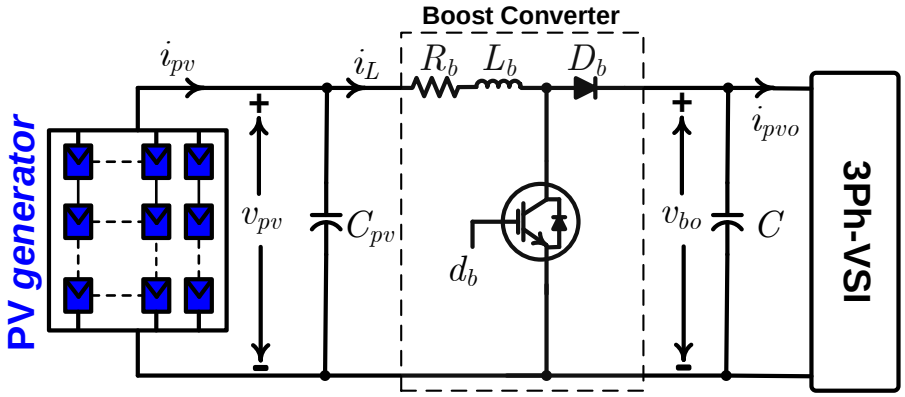

Figure 3.4: Schematic representation of the PV DC-DC boost converter.

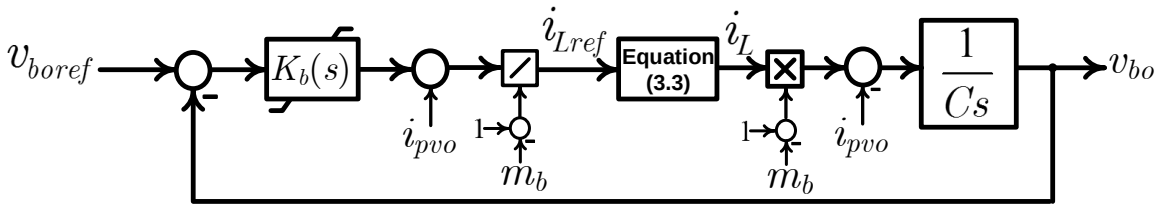

Figure 3.5: Output terminal voltage control loop of the boost converter.

terminal voltage, v_{bo}. Figure 3.4 represents the PV dc-dc boost converter circuit. The dynamics of v_{bo} can be written as

$$\frac{dv_{bo}}{dt} = \frac{1}{C}[(1 - m_b)i_L - i_{pvo}] \tag{3.4}$$

Figure 3.5 illustrates the output terminal voltage controller of the boost converter of Figure 3.4. During networks faults, the purpose of this controller is to control i_{Lref} to regulate v_{bo}. The setpoint, v_{boref} for this controller is chosen slightly smaller than 600 V (for example, about 585 V). Compensators $K_{pv}(s)$, K_{i_L}, and $K_b(s)$ are all of the proportional-integral (PI) type and the generic form is $K(s) = (k_p s + k_i)/s$.

3.2.3 Inverter Control Architecture

Inverter Current-Control Scheme

The current-control of the inverter of Figure 3.1 is performed in a dq-frame of coordinates rotating in synchronism with the space phasor corresponding to v_{sabc} by utilizing a phase-

locked loop (PLL) [71] and [76]. The d- and q-axis components of the inverter ac current, i_d and i_q, independently track their respective setpoints, i_{dref} and i_{qref}, based on the following transfer function

$$\frac{I_d(s)}{I_{dref}(s)} = \frac{I_q(s)}{I_{qref}(s)} = \frac{1}{\tau_i s + 1} \tag{3.5}$$

where the time constant, τ_i is a design choice. It should be noted that for the fast current-control response, τ_i should be made small. This can be done by proper tuning of the current-controlled parameters [76]. In turn, i_d and i_q enable the control of real-power, P_s and the reactive-power, Q_s of the inverter, respectively. Thus, the equation of power components P_s and Q_s can be written as

$$P_s = \frac{3}{2} v_{sd} i_d \tag{3.6}$$

$$Q_s = -\frac{3}{2} v_{sd} i_q \tag{3.7}$$

where v_{sd} denotes the d-axis components of v_{sabc}. The control structure of the inverter current-control scheme is discussed in the Subsection 2.3.2 of Chapter 2. More details about the inverter ac current-control can be found in [76].

Inverter DC-Link Voltage Controller

Inverter dc-link voltage controller of the two-stage PV system is based on the following equation:

$$\begin{aligned} \frac{1}{2} C \frac{dv_{dc}^2}{dt} &\approx P_{bo} - P_{inv} \\ &\approx P_{bo} - \frac{3}{2} v_{sd} i_d \\ &\approx P_{bo} - \frac{3}{2} v_{sd} i_{dref} \end{aligned} \tag{3.8}$$

Equation (3.8) indicates that the inverter dc-link voltage can be controlled by i_d. If it is assumed that the value of τ_i is so small then $i_d \approx i_{dref}$ holds. The dc-link voltage control of the two-stage PV system can be accomplished by the controller demonstrated in Figure 3.6. The fundamental concept of the inverter dc-link voltage controller is adopted from [76]. As Figure 3.6 shows, dc-link voltage compensator, $K_v(s)$, processes the error between v_{dc}^2 and its setpoint, v_{dcref}^2 and issues the command i_{dref}. In turn, the

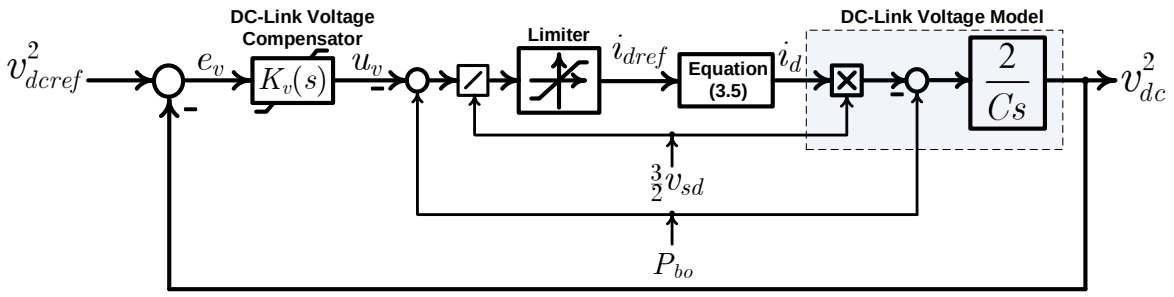

Figure 3.6: DC-link voltage controller of the two-stage PV system.

controller responds to the command based on (3.5).
To mitigate the nonlinear effects on the control, the signals $(3/2)v_{sd}$ and P_{bo} are delivered as feedforward compensation. Therefore, the approximate control plant can be formulated as

$$\frac{1}{2}C\frac{dv_{dc}^2}{dt} \approx u_v \tag{3.9}$$

where u_v is new control input from the dc-link voltage compensator. From (3.9) it can be realized that the control plant becomes an integrator and $K_v(s)$ can be utilized a proportional-integral (PI) type which is written as follows

$$K_v(s) = \frac{k_1 s + k_2}{s} \tag{3.10}$$

where k_1 and k_2 are the proportional and integral gains, respectively.

VML and The Proposed TOV Limiting Scheme

To evaluate the TOV caused by the two-stage PV system during a single-line-to-ground fault and the following islanding incident, the VML and the proposed TOV limiting Scheme 1 are introduce in the two-stage two-stage PV system of Figure 3.1. Figure 3.7 (a) and (b) illustrate the TOV limiting Scheme 1 and the non-linear transfer characteristics curve for the TOV limiter. Figure 3.8 demonstrates the block diagram of the VML. The operation of the TOV limiting Scheme 1 and the VML are extensively discussed in Subsection 2.6.1.

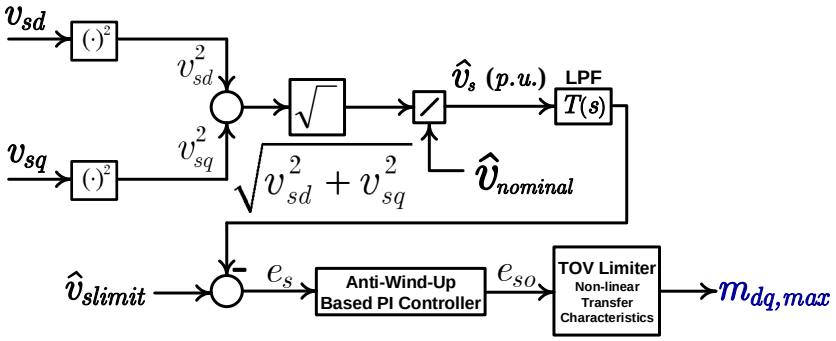

(a) TOV limiting Scheme 1

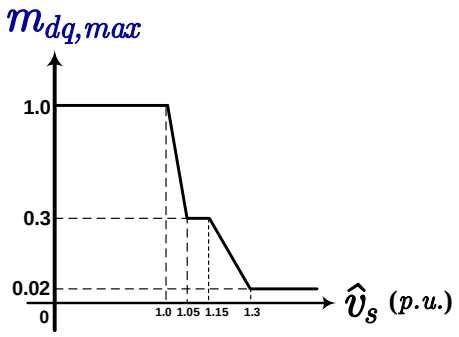

(b) Non-linear transfer characteristics

Figure 3.7: (a) Block representation of the TOV limiting Scheme 1 for the two-stage PV system. (b) Non-linear transfer characteristics of the TOV limiter.

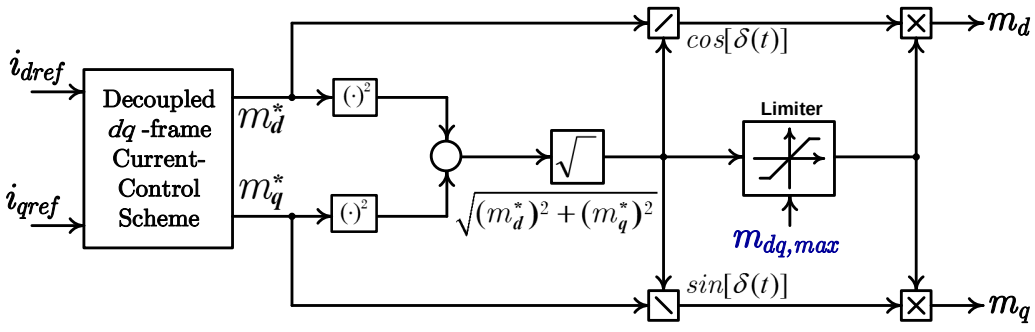

Figure 3.8: Block diagram of VML of the the two-stage PV system.

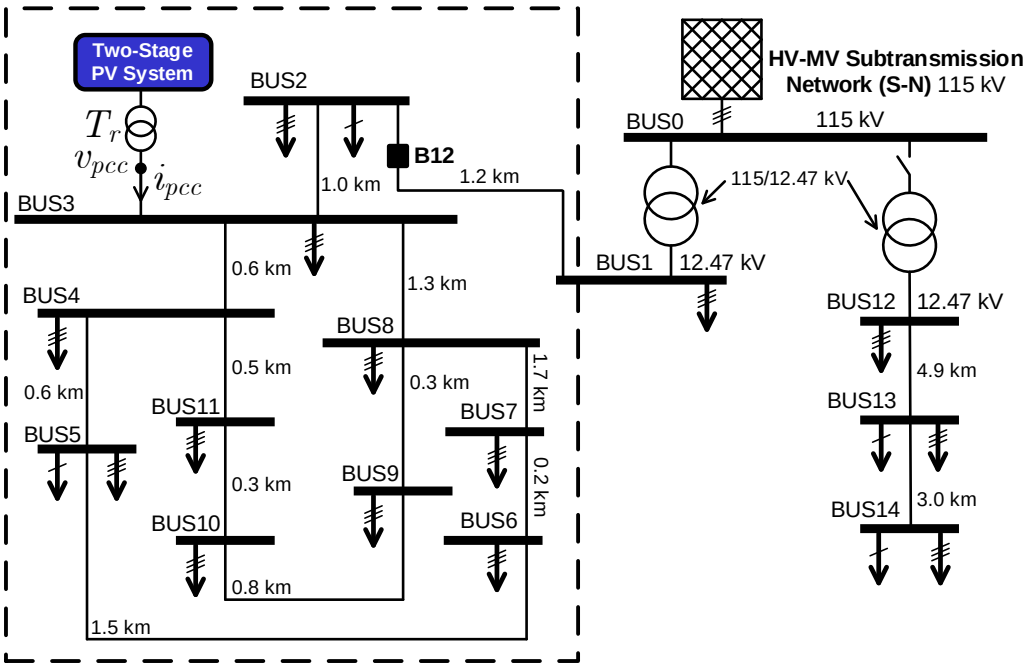

Figure 3.9: Two-stage PV system is connected to the BUS 3 of the test CIGRE benchmark MV distribution network.

3.3 Study Cases and TOV Mitigation

To demonstrate the performance of the two-stage PV system, and to evaluate the effectiveness of the proposed TOV limiting Scheme 1, a number of study cases have been conducted on a detailed switched model of the system of Figure 3.1 in the PSCAD/EMTDC software environment [83]. The rated power of the PV *generator* is 1.0 MW and that is composed of $N_p = 300$ parallel-connected PV strings. To ensure that the open-circuit voltage of the PV *generator* is within the maximum voltage limit of 600 V, each PV string consists of the series connection of $N_s = 18$ PV modules; each module is, in turn, assumed to be composed of $M_s = 54$ identical basic PV cells. Other parameters of the PV *generator* are given in Appendix A. The VSI and isolation transformer T_r of the two-stage PV system are all assumed to have a power rating of 1.0 MVA. For the two-stage PV system, boost converter output terminal voltage setpoint is, $v_{boref} = 585\ V$, and the dc-link voltage setpoint is, $v_{dcref} = 570\ V$. As shown in Figure 3.9, the two-stage PV system is interfaced with a CIGRE benchmark MV distribution network. The network and the load parameters can be found in [64] and [86]. The two-stage PV system and controller parameters are listed in Table C.1 of Appendix C.

3.3.1 Case 1: Simulated Performance of the Two-Stage PV System Under the Startup Process and Step Change in Solar Irradiation

This case study demonstrates the overall performance of the two-stage PV system under the start-up process and step change in solar irradiation. The MPPT scheme is based on the incremental conductance (IC) algorithm [84], [85]. Under the start-up process, the PV *generator* is exposed to a solar irradiation of $G = 1.0\ kW/m^2$. During the start-up period, the PV *generator* terminal voltage setpoint, v_{pvref} is issued by the MPPT scheme with a constant value of about 0.86 times the measured open-circuit voltage of the PV *generator*. The MPPT scheme starts running at $t = 0.3\ s$. Until $t = 0.3\ s$, all the system controllers and inverter gate drive circuits are disabled. During this time interval, dc-link capacitor of the inverter are pre-charged by the open-circuit voltage of the PV *generator*.

At $t = 0.5\ s$, the solar irradiation assumes a stepwise decrease to $0.6\ kW/m^2$ and remains for $0.2\ s$. Again, at $t = 0.7\ s$, solar irradiation is increased from $0.6\ kW/m^2$ to $0.8\ kW/m^2$, and finally at $t = 0.8\ s$, the solar irradiance assumes a stepwise increase from $0.8\ kW/m^2$ to $1.0\ kW/m^2$. Figure 3.10 and Figure 3.11 illustrate the two-stage PV system response under the aforementioned conditions. Figure 3.10(a) indicates the step-wise changes in solar irradiation. Figure 3.10(b) indicates that the steady-state value of the PV *generator* output current, i_{pv} is proportional to the corresponding solar irradiations. However, as Figure 3.10(c) shows, until $t = 0.3\ s$, v_{pv} is approximately equal to the measured open-circuit voltage (about $564\ V$) of the PV *generator*. Thereafter, v_{pv} remains regulated by the boost converter control loop of Figure 3.3. The MPPT scheme issues the PV *generator* terminal voltage setpoint, $v_{pvref} = 484\ V$. Due to the boost converter control loop, the PV *generator* terminal voltage remains regulated. The reason behind is that, the change in solar irradiance does not impact significantly on the open-circuit and MPP voltage. As can be seen from Figure 3.10(d), stepwise changes in solar irradiance causes proportional change in the PV *generator* power, P_{pv}. As Figure 3.10(e) shows, except slight transient excursion, dc-link voltage remains regulated at its setpoint by the dc-link voltage controller of the inverter.

Figure 3.11(a) and Figure 3.11(b) show the inverter phase terminal current i_{tabc}, and the dq-transformed current, i_{dq}, respectively. The magnitude of i_d at $G = 1.0\ kW/m^2$ can be determined by using (3.6), whereas i_q remains regulated at zero. It can also be observed that, i_d, i_{tabc}, and grid side current, i_{gabc} [shown in Figure 3.11(c)] are changing according to the solar irradiation. Figure 3.11(d) shows the PV system output power, P_s under the stepwise change in solar irradiation. For the solar irradiation of $1.0\ kW/m^2$,

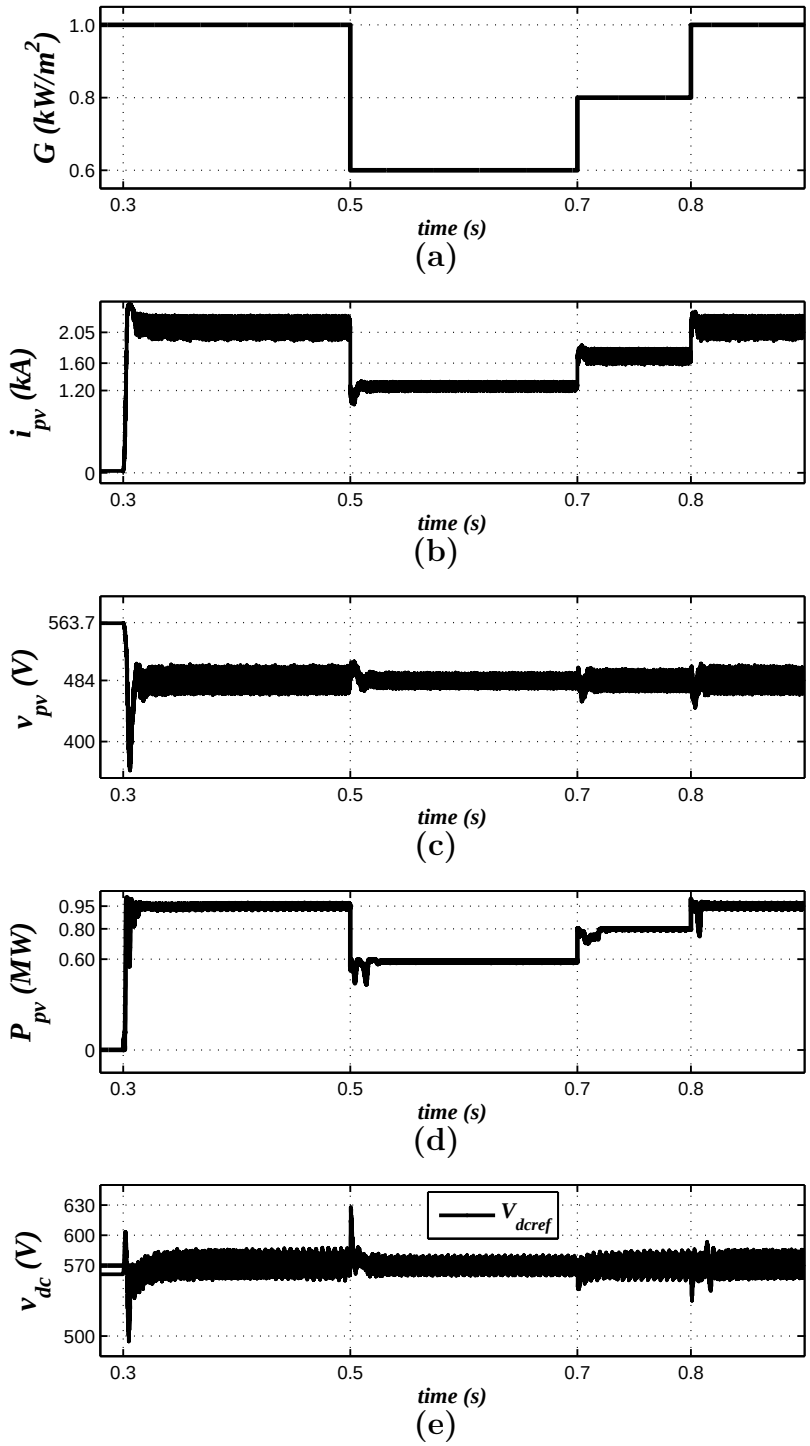

Figure 3.10: Two-stage PV system overall response under the startup process and stepwise changes in solar irradiation, with the MPPT scheme is enabled.

the two-stage PV system delivers about 0.85 MW.

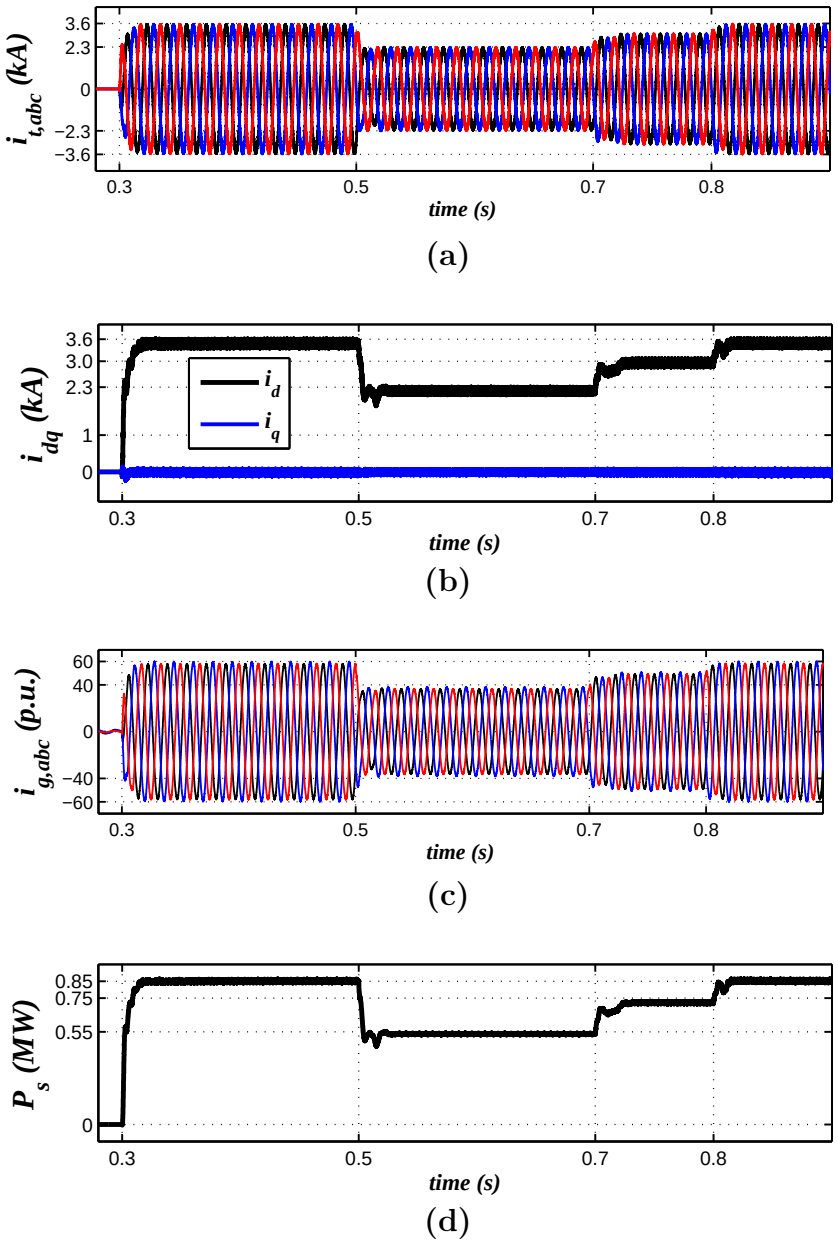

Figure 3.11: Two-stage PV system response under Case #1.

3.3.2 Case 2: Two-Stage PV System Response to a Three-Phase to Ground Fault

The two-stage PV system is connected to BUS 3 of the CIGRE benchmark for MV distribution network which is shown in Figure 3.9. The performance of the two-stage system and its associated controllers in response to a symmetrical ac fault is shown in Figure 3.12. Prior to the fault, the two-stage PV system is assumed to be in a steady state while the PV *generator* receives a solar irradiance of 1.0 kW/m^2. At $t = 0.7$ s, a

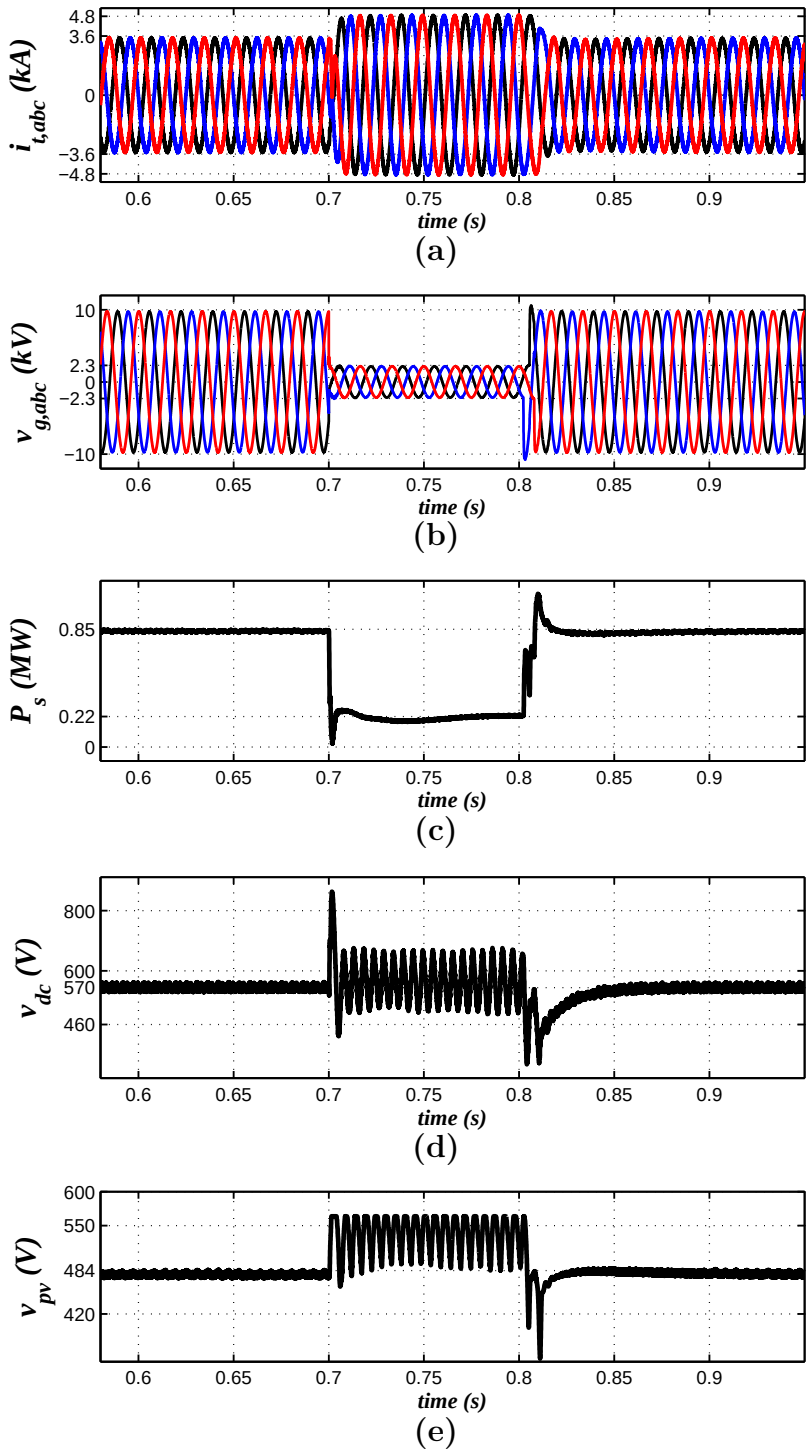

Figure 3.12: Two-stage PV system response to a three-phase-to-ground fault condition.

temporary three-phase-to-ground fault is incepted at BUS 4 and lasts for 0.1 s.

As Figure 3.12(a) and Figure 3.12(b) show, the fault results in a limited, smooth increase in the inverter phase terminal current, i_{tabc} and significant drop in the grid-

side voltages, v_{gabc}, respectively. This scenario results in the reduction of the inverter system output power, P_s, as shown in Figure 3.12(c). The boost converter output voltage controller [refer to Figure 3.5] is responsible for taking action during the fault interval time and keeping the dc-link voltage level within the specific range and prevents from rising. The dc-link voltage waveform is shown in Figure 3.12(d). It can be observed from Figure 3.12(e) that, when the boost converter output terminal voltage controller takes control, v_{pv} voltage is operated at higher value of about 564 V. Thus, the dc and ac power balance can be achieved. Figure 3.12 also shows that the system tolerates the fault and that, subsequent to the fault clearance, i_{tabc}, v_{gabc}, and P_s revert to their pre-disturbance forms and qualities. Consequently, the boost converter output terminal voltage controller stops its operation and the control loop of Figure 3.3 starts to control v_{pv} according to the setpoint, v_{pvref}.

3.3.3 Case 3: TOVs Caused by the Two-Stage PV System due to an Asymmetrical AC Fault

This case study demonstrates the TOVs caused by the two-stage PV system due to a single-line-to-ground fault. Prior to the fault, two-stage PV system is assumed to be in a steady state with $G = 1.0\ kW/m^2$ and the MPPT scheme is enabled. Then, two single line-to-ground (phase-c is bolted to the ground) faults take place at BUS 4 of the distribution network of Figure 3.9. The first fault strikes at $t = 0.55\ s$ and lasts for 0.1 s; the second fault is permanent and takes place at $t = 0.8\ s$.

Figure 3.13 illustrates the two-stage PV system response. Figure 3.13(a) shows the voltage of BUS 3. The fault results in significant drop in the magnitude of the grid-side faulted phase and the voltage rise in the healthy phases of about 1.12 $p.u.$ The TOV on the healthy phases are limited since the PV system uses a YG winding configuration of the isolation transformer, T_r, at the grid side. As shown in Figure 3.13(b), limited increase in the inverter phase terminal current, i_{tabc} is observed. Moreover, the current retains its pre-disturbance sinusoidal form. The aforementioned behavior is expected since the current-mode control is adopted for the two-stage PV system. As Figure 3.13(c) and (d) indicate, the imbalance of the grid-side voltage causes double-frequency pulsation in the inverter dc-link voltage and PV system output power, respectively. However, during the fault interval time, the dc-link voltage and PV system output power fluctuate within a limited range. As can be seen from Figure 3.13, the two-stage PV system resumes its normal operation when the fault is cleared at $t = 0.65\ s$. As Figure 3.13(a) shows, the TOV on the healthy phases, due to the permanent fault is limited to about 1.12 $p.u.$

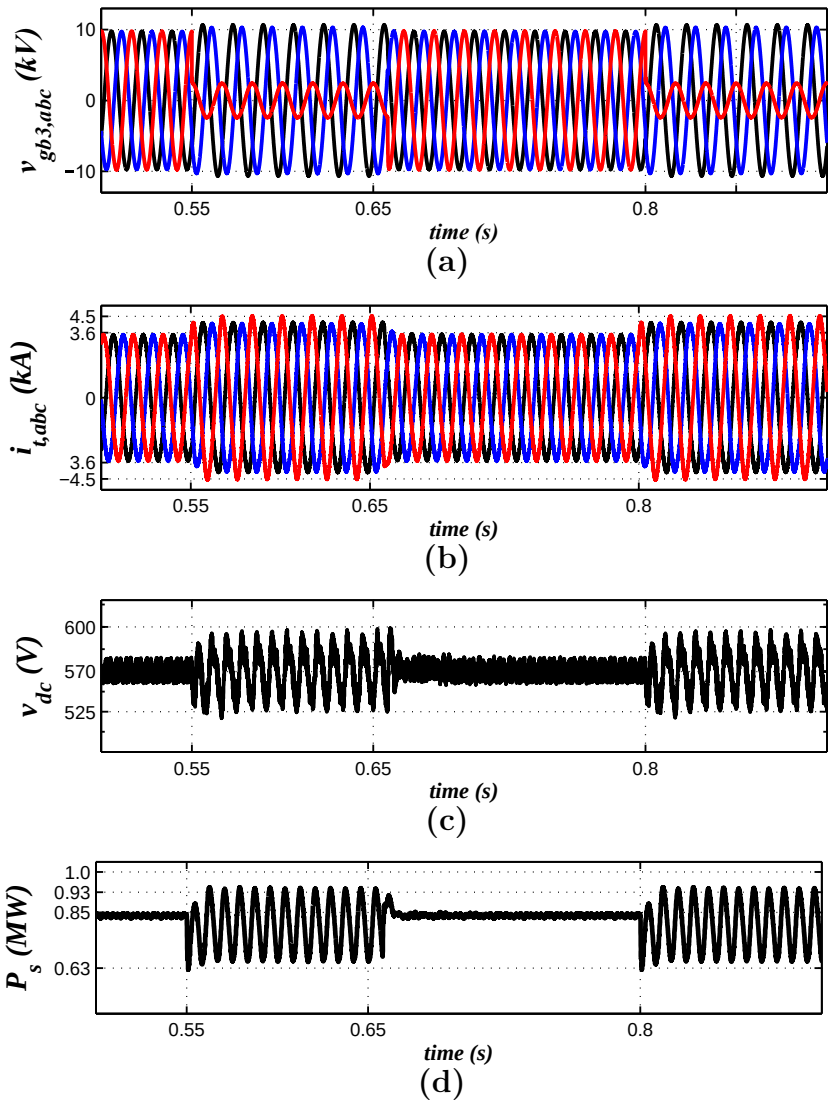

Figure 3.13: Two-stage PV system response and TOVs due to a single-line-to-ground fault.

Although not shown, due to the permanent fault, low- and high-voltage relay (connected at the low-voltage side of T_r) isolates the two-stage PV system from BUS 3, in about 1.0 s.

3.3.4 Case 4: TOVs Caused by the Two-Stage PV System during an Unintentional Islanding Incident

In this test case, prior to the islanding incident, the two-stage PV system is assumed to be in a steady state, with $G = 1.0\ kW/m^2$, while the MPPT scheme is enabled. Figure 3.14 illustrates the two-stage PV system response to an unintentional islanding incident.

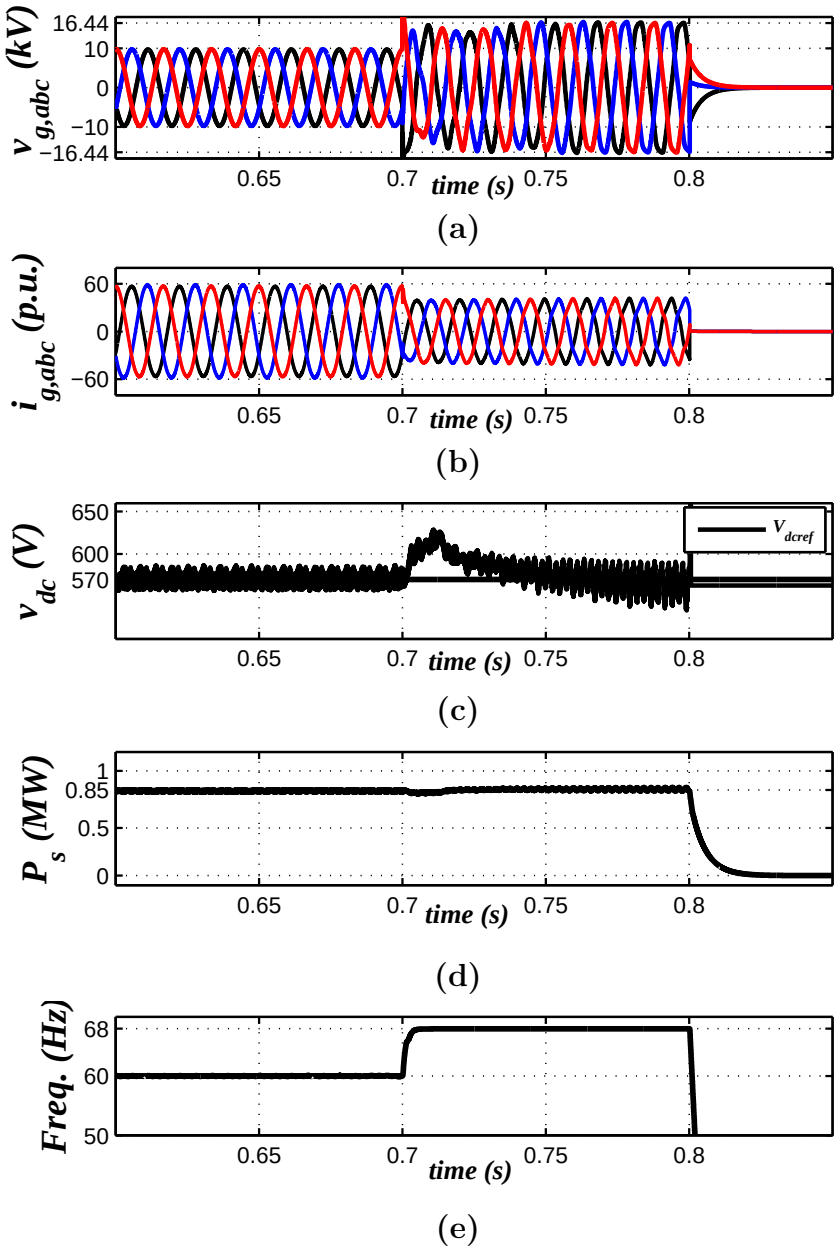

Figure 3.14: Two-stage PV system response and TOVs due to an unintentional islanding incident.

At $t = 0.7\ s$, the breaker B_{12} of the network of Figure 3.9 is disconnected and an island forms. The two-stage PV system is now in the islanded zone and, connected to the BUS 3. As Figure 3.9 indicates, the islanded zone is demonstrated by a dashed box. As can be seen from Figure 3.14(a), subsequent to the island formation, the grid-side voltage experience TOVs of about 1.64 $p.u.$ The aforementioned over-voltage behavior can be explained as follows.

Prior to the islanding incident, the two-stage PV system delivers about 0.85 MW

[refer to Figure 3.14(d)], while the aggregate load within the islanded zone is about 0.57 MW; implies that the PV system can cause severe TOVs when generation exceeds load (high PV generation to load ratio) [29], [31]. In order to produce pre-disturbance power, grid current, i_{gabc} decreases, as Figure 3.14(b) shows. Figure 3.14(c) illustrates that, due to the distortions in the grid-side voltages and currents, the dc-link voltage of the inverter slightly deviates from the setpoint, however remains under 600 V. As Figure 3.14(e) shows, the low- and high-frequency relay detects the frequency deviation and isolates the two-stage PV system from BUS 3, at $t = 0.8$ s. Consequently, the dc-link voltage settles at the open-circuit voltage of the PV *generator* and the power transfer from the inverter system is disrupted.

3.3.5 Case 5: TOVs Caused by the Two-Stage PV System due to an Asymmetrical AC Fault and the following Islanding Incident

This case study demonstrates the TOVs caused by the two-stage PV system due to a single-line-to-ground fault and the following islanding incident. Prior to the disturbance, the two-stage PV system is assumed to be in a steady state while the PV *generator* receives a solar irradiation of 1.0 kW/m^2. The rating of the local load connected in Figure 3.1 is $0.32+j0.17$ MVA.

Figure 3.15 illustrates the two-stage PV system response. Prior to the fault and the following islanding incident, the two-stage PV system delivers about 0.85 MW. At $t = 0.75$ s, a permanent single-phase-to-ground fault (phase-c is bolted to the ground) takes place at the PCC point of the system of Figure 3.1. Afterwards, the upstream grid protection device detects the fault within 3 *cycles* and opens the breaker B_g, at $t = 0.8$ s, leading to an islanding incident. As a result, all the inverter current flows into the remaining small local load connected in the islanded zone. Consequently, voltage temporarily rises for another 100 ms until the low- and high-frequency relay triggers at $t = 0.9$ s and shuts down the inverter. Aforementioned phenomenon is known as TOVs due to the "interruption of significant power export" [29], [31], [47]. As Figure 3.15(a) and (b) show, the healthy phases of the grid-side and the inverter ac-side experience severe TOVs of about 1.82 $p.u.$ and 1.87 $p.u.$, respectively. Moreover, voltages are distorted since a large zero-sequence current circulates in the Δ-connected windings of T_r. As can be seen from Figure 3.15(c) and (d), the dc-link voltage and output power of the two-stage PV system experience double-frequency pulsation during fault and the following islanding incident. Since the inverter dc-link voltage pulsations exceed the maximum limit (600

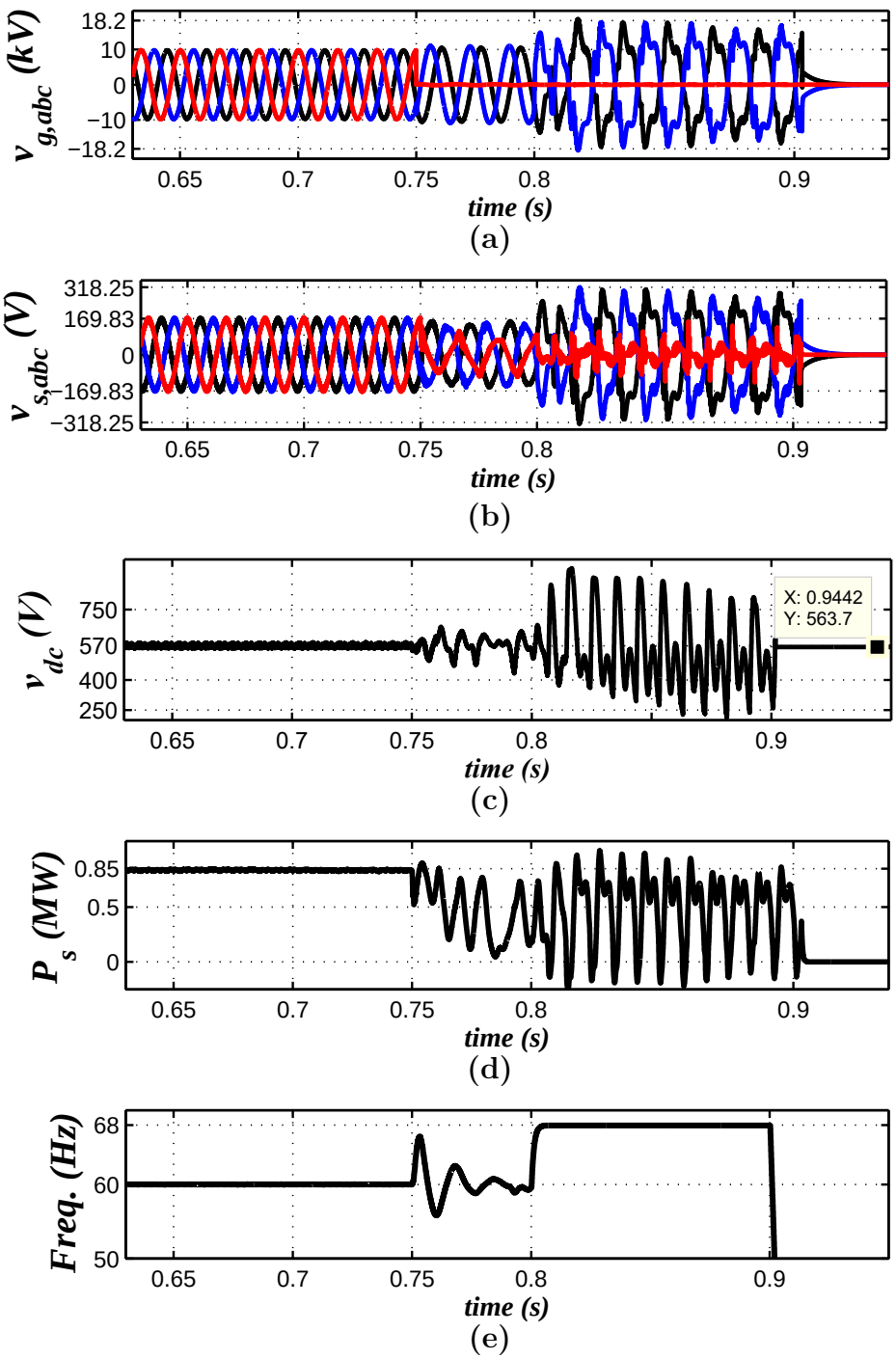

Figure 3.15: Two-stage PV system response due to a single-line-to-ground fault and the following islanding incident, without any mitigation measures.

V), and due to the frequency deviation, the low- and high-frequency relay intervenes and shuts down the inverter, at $t = 0.9\ s$, as Figure 3.15(e) shows.

3.3.6 Case 6: Two-Stage PV System Response under the Proposed TOV Limiting Scheme 1

To evaluate the effectiveness of the proposed TOV limiting Scheme 1, this case study demonstrates the two-stage PV system response under the proposed TOV limiting 1. In the case of a detected over-voltage, the TOV limiting Scheme 1 issues the required maximum saturation limit, $m_{dq,max}$ for m_d and m_q [refer to Figure 3.7(a) and (b)]. Consequently, m_d and m_q will be controlled and transformed to m_{abc} by *dq*- to *abc*- frame transformation block. In turn, the inverter ac-side voltage, v_{sabc} and, as such, the grid-side voltage, v_{gabc} can be limited during any over-voltage incident.

Prior to the fault inception and the following islanding incident, the two-stage PV system is assumed to be in a steady state while the PV *generator* is exposed to a solar irradiation of $G = 1.0\ kW/m^2$. The boost converter controls the PV *generator* terminal voltage. A local load of $0.32 + j0.17\ MVA$ is connected at the point in between the transformer, T_r and the breaker, B_g, as shown in Figure 3.1. A permanent single-line-to-ground fault (phase-*c* is bolted to the ground) is incepted at $t = 0.75\ s$ at the PCC of Figure 3.1. This incident is detected by the upstream grid protection circuitry within 3 *cycles* and opens the breaker B_g, at $t = 0.80\ s$, leading to an islanding scenario.

Figure 3.16 illustrates the two-stage PV system response. As can be seen from Figure 3.16(a), before islanding incident, the fault results in the limited drop on the inverter ac-side healthy phase voltages and significant voltage drop of the faulted phase. This is due to the limited increase of the inverter phase terminal current, i_{tabc} (not shown). Figure 3.16(b) also depicts that, before islanding incident, due to the fault, the grid-side voltages of the healthy phases increase but they are limited to about 1.12 *p.u.* However, as shown in Figure 3.16(a) and (b), even after the islanding incident, the inverter ac-side and the grid-side voltages of the healthy phases are limited to about 1.17 *p.u.* and 1.14 *p.u.*, respectively. Due to the proposed TOV limiting Scheme 1, the TOV is limited during the most severe over-voltage condition. Thus, the TOV limiting Scheme 1 offers a better capability for limiting over-voltages caused by the two-stage PV system. Figure. 3.16(c) and 3.16(d) show that, the double-frequency pulsations on the inverter dc-link voltage and output power are also limited.

Figure 3.16(e) indicates that, during fault and the following islanding incident, the measured v_{pv} is limited to about open-circuit voltage of the PV *generator*. As Figure 3.16(f) shows, due to the frequency deviation, the low- and high-frequency relay detects larger deviation of the frequency and shuts down the inverter, at $t = 0.90\ s$.

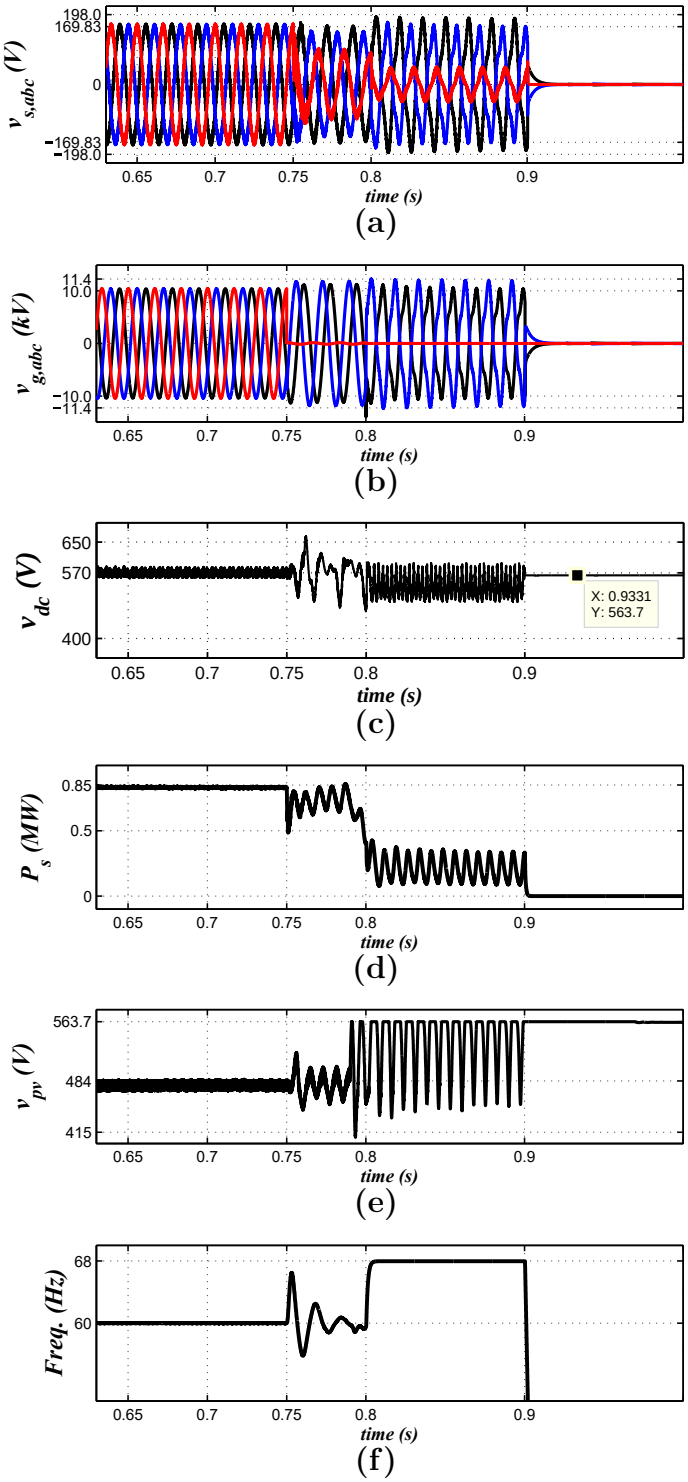

Figure 3.16: Two-stage PV system response under the proposed TOV limiting Scheme 1.

Table 3.1: Comparative Study of TOVs Caused by the PV Systems

TOV Event (worst–case scenario)	**PV System**	**Region**	**TOV Limiting Scheme**	**TOV (*p.u.*)**
single-line-to-ground fault and the following islanding incident	conventional single-stage	grid-side	absent	2.21
			with TOV limiting Scheme 1	**1.23**
		inverter ac-side	absent	2.39
			with TOV limiting Scheme 1	**1.24**
	modified single-stage	grid-side	absent	2.55
			with TOV limiting Scheme 2	**1.16**
		inverter ac-side	absent	2.04
			with TOV limiting Scheme 2	**1.20**
	two-stage	grid-side	absent	1.82
			with TOV limiting Scheme 1	**1.12**
		inverter ac-side	absent	1.87
			with TOV limiting Scheme 1	**1.17**

3.4 Comparative Study of TOVs Caused by the PV Systems

This section presents a comparative study of TOVs caused by single-stage and two-stage grid-connected PV systems. Simulation results from different case studies show that the TOV caused by the PV systems is the most severe during a single-line-to-ground fault and the following islanding incident. Thus, the main focus of this section is to compare the single- and two-stage PV systems from the viewpoint of the most severe TOV condition, with and without the proposed TOV limiting schemes. Table 3.1 provides a summary of the study results, reporting the TOV caused by the PV systems during the worst-case scenario. Figure 3.17 and Figure 3.18 provide a graphical illustration of the study results.

Figure 3.17 indicates that, under the aforementioned condition, the TOV on the grid-side is about 2.21 *p.u.* However, when the conventional single-stage PV system employs the proposed TOV limiting Scheme 1, the TOV is limited to about 1.23 *p.u.* Furthermore, the grid-side experiences TOV caused by the modified single-stage PV system of about 2.55 *p.u.* Under the proposed TOV limiting Scheme 2, however, the TOV on the grid-side

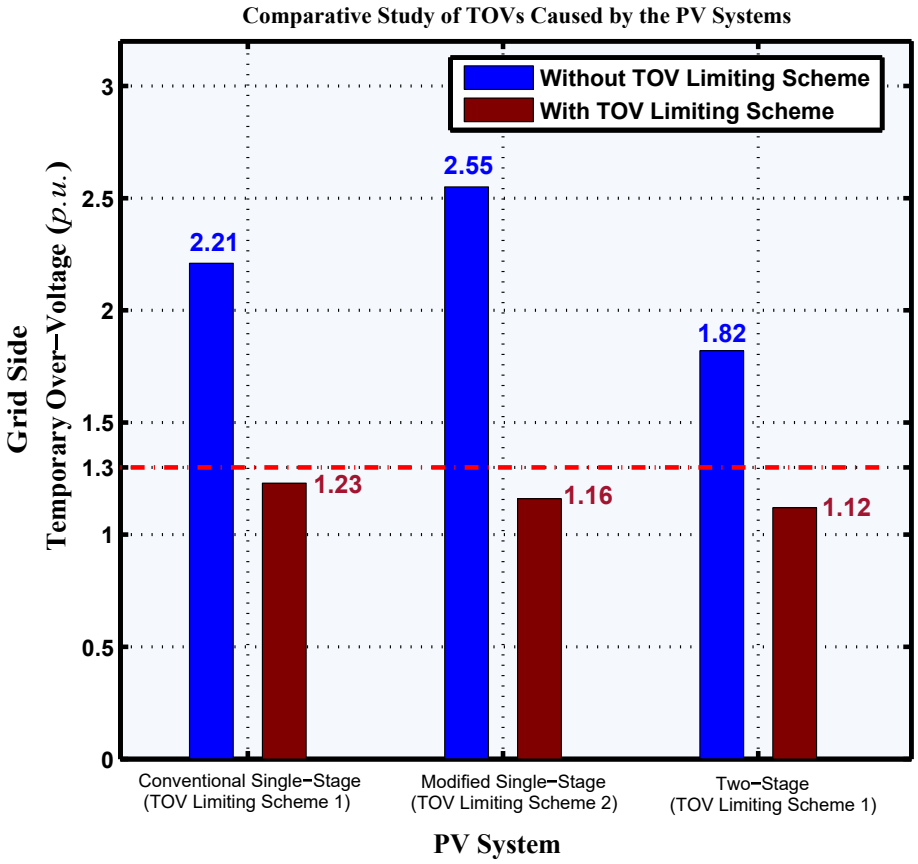

Figure 3.17: Grid-side TOVs caused by the PV systems due to a single-line-to-ground fault and the following islanding incident.

is limited to about 1.16 *p.u.* As compared with the conventional and modified single-stage PV systems, the two-stage PV system experiences much smaller grid-side over-voltages, which is about 1.82 *p.u.* The reason for the smaller TOV is explained by the fact that using two power processing stages results in lower power output from the two-stage PV system as compared to the conventional and modified single-stage PV systems. The TOV limiting Scheme 1 is employed in the two-stage PV system. Again the grid-side TOV is significantly limited to about 1.12 *p.u.* As can be seen from Figure 3.17, the grid-side TOVs caused by the single- and two-stage PV systems are always smaller than 1.3 *p.u.*, under the proposed TOV limiting schemes. Therefore, the DG interconnection requirement about to maintain the TOV limit during network faults, like the one reported in [20], is not violated.

Figure 3.18 indicates that the conventional single-stage PV system experiences larger inverter ac-side TOVs (about 2.39 *p.u.*) than the TOVs (about 2.04 *p.u.*) caused by the modified single-stage PV system, when the proposed TOV limiting schemes are not

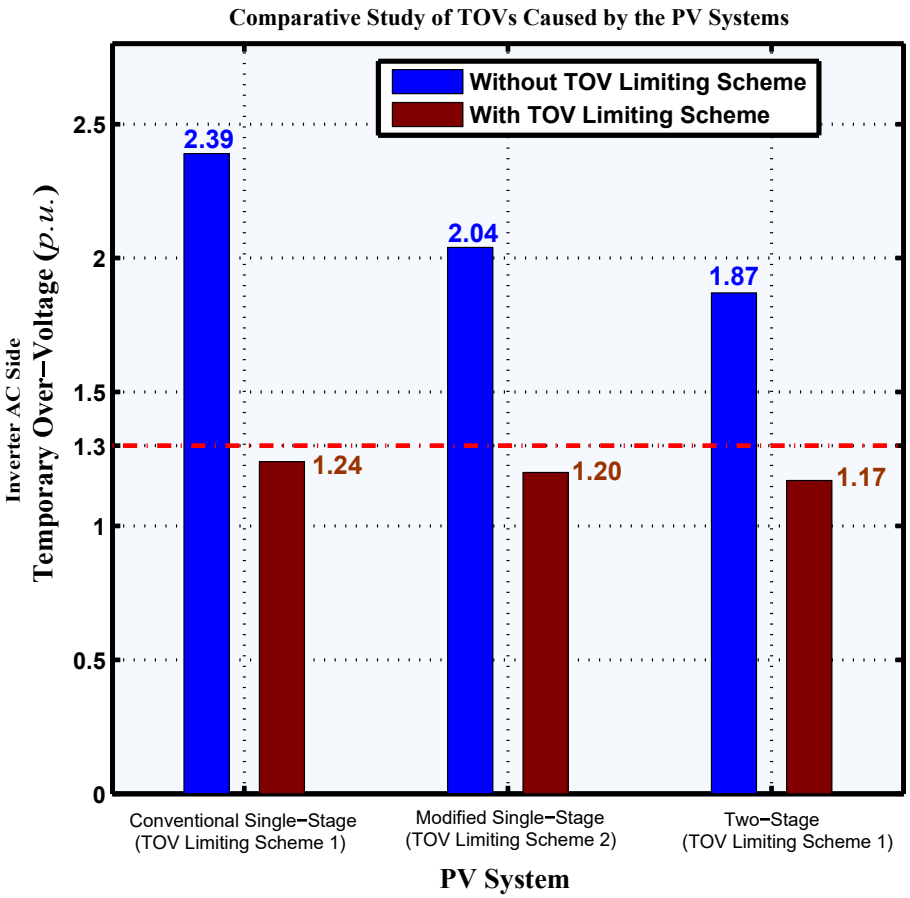

Figure 3.18: Inverter ac-side TOVs caused by the PV systems due to a single-line-to-ground fault and the following islanding incident.

exercised. As compared with the conventional and modified PV systems, the two-stage PV system experiences much smaller inverter ac-side over-voltages, which is about 1.87 *p.u.* Figure 3.18 also indicates that the advantage is preserved under the proposed TOV limiting schemes; as Figure 3.18 shows, the inverter ac-side TOVs caused by each PV system is lower than 1.3 *p.u.*

3.5 Summary and Conclusions

This chapter presented a two-stage grid-connected three-phase PV system and investigated the temporary over-voltage (TOV) caused by the two-stage PV system.

Firstly, the two-stage PV system configuration was discussed. A dc-dc boost converter and one central inverter were used in order to process the PV generated power. The PV *generator* parameters were selected in such a way that, for maximum operating

conditions, the open-circuit voltage of the PV *generator* remains marginally under 600 V. The boost converter control strategy adopted the popular two-loop average control structure, where the boost converter inductor current was controlled by the faster inner current control loop and the PV *generator* terminal voltage was controlled by the slower outer voltage control loop. During network faults, the dc-link voltage of the VSI may rises and, as such, violate the national standard dc-link voltage limit of 600 V [88]. In order to prevent the aforementioned situation, the boost converter was adopted an output terminal voltage controller which controlled the boost converter output terminal voltage during a network fault. The central inverter employed the decoupled dq-frame current-control scheme and the dc-link voltage controller as those employed for the conventional and modified single-stage PV systems. However, the power extracted from the boost converter was used for feedforward compensation.

Secondly, the two-stage PV system employed the proposed TOV limiting Scheme 1 in order to limit the damaging TOV during a single-line-to-ground fault and the following islanding incident. In the case of a detected over-voltage, the TOV limiting Scheme 1 issued the maximum saturation limit for dq components of the modulating signals. Therefore, the dq components of the inverter ac-side voltages were controlled and, as such, the grid-side voltages were controlled.

The effectiveness of the TOV limiting Scheme 1 and the two-stage PV system performance in the presence of various types of disturbance were demonstrated by time-domain simulations conducted in the PSCAD/EMTDC software environment.

The following were demonstrated by the simulation studies:

- The performance of the boost converter controller were demonstrated. During normal operating conditions, the boost converter controlled the terminal voltage of the PV *generator*. However, during network faults, e.g. during a three-phase-to-ground fault, the output terminal voltage controller of the boost converter prevented the dc-link voltage from rising.

- The system response to a single-line-to-ground fault, an unintentional islanding incident, and a single-line-to-ground fault followed by an islanding incident were demonstrated. It was shown that the TOV is the most severe due to a single-line-to-ground fault and the following islanding incident.

- It was shown that, under the proposed TOV limiting Scheme 1, the TOVs on the inverter ac-side and the grid-side were significantly limited. It was also shown that the proposed TOV limiting Scheme 1 meets one of the requirements imposed by [20], in terms of limiting the TOV.

- A comparative study of TOVs caused by single-stage and two-stage grid-connected PV systems was demonstrated. It was shown that the two-stage PV system experienced much smaller grid-side and inverter ac-side over-voltages, as compared to the conventional and modified single-stage PV systems. Moreover, under the proposed TOV limiting schemes, the grid-side and the inverter ac-side TOVs caused by each PV system is lower than 1.3 $p.u.$

Chapter 4

Conclusions and Future Work

4.1 Conclusions

The overall aim of this thesis was to study and characterize temporary over-voltages (TOVs) caused by grid-connected PV systems, and to propose corrective measures to mitigate the TOV problem through the built-in software of the PV system. The thesis, however, was focused on PV systems with single-stage and two-stage three-phase central dc-ac inverters. In this thesis, the mechanisms behind the TOVs caused by the PV systems were described. This thesis discussed that the neutral voltage displacement and the interruption of significant power export were the two important reasons behind TOVs. Furthermore, in this thesis, single- and two-stage PV systems were studied and appropriate control schemes for the inverter and for limiting the TOV caused by the PV system were used. The single- and two-stage PV systems were modeled in detail in the PSCAD/EMTDC software environment. The general conclusions drawn from the studies reported in this thesis are:

- For TOV analysis, the thesis studied a conventional single-stage grid-connected three-phase PV system with a widely used Δ/YG isolation transformer. The single-stage system adopted a decoupled dq-frame current-control scheme, and a dc-link voltage controller for the inverter. The thesis showed that, the TOV can occur either during a single-line-to-ground fault or subsequent to an islanding incident. In the conventional single-stage PV system, the healthy phases of the grid-side voltage experience a TOV of about 1.12 $p.u.$ due to a single-line-to-ground fault, whereas the grid-side voltage experience a TOV of about 1.68 $p.u.$ due to an unintentional islanding incident. The magnitude of the TOV is proportional to the ratio of the total PV power generation to the total load in the islanded zone.

- The TOV is most severe during a single-line-to-ground fault and the following islanding incident. The thesis showed from the simulation results that, without proper TOV mitigation measures, the grid-side and the inverter ac-side experience over-voltages of about 2.21 *p.u.* and 2.39 *p.u.*, respectively.

  The thesis proposes a TOV limiting scheme for the conventional single-stage PV system in order to reduce the magnitude of the damaging TOV during the most severe condition. A PI controller with an anti-wind-up technique is utilized in the proposed TOV limiting scheme. The thesis showed that, the conventional single-stage PV system, under the proposed TOV limiting Scheme 1, the grid-side and the inverter ac-side over-voltages are limited to about 1.23 *p.u.* and 1.24 *p.u.*, respectively.

- A modified single-stage grid-connected PV system is adopted to further investigate the TOV. The modified system employs a half-bridge converter (HBC) and a Y/YG isolation transformer. Through time-domain simulation studies, the thesis showed that an effectively-grounded PV system may not mitigate TOVs. This is in agreement with the findings reported in [29], [31], [49].

  Further, a TOV limiting scheme for the modified single-stage PV system is proposed to reduce the magnitude of the TOV. The proposed TOV limiting Scheme 2 issues the maximum saturation limit for the three-phase set of modulating signals in order to control the three-phase voltages, in the case of detected over-voltage. The effectiveness of the TOV limiting schemes are evaluated by time-domain simulation studies in the PSCAD/EMTDC software environment. The thesis showed that, the modified PV system, under the proposed TOV limiting Scheme 2, the grid-side and the inverter ac-side over-voltages are limited to about 1.16 *p.u.* and 1.20 *p.u.*, respectively.

- The TOV caused by the two-stage PV system is also investigated. The study showed that the two-stage PV system experiences much smaller grid-side and inverter ac-side over-voltages, as compared to the conventional and modified single-stage PV systems. The proposed TOV limiting Scheme 1 is employed in the two-stage PV system. The thesis showed that, under the proposed TOV limiting Scheme 1, the grid-side and the inverter ac-side over-voltages are limited to about 1.12 *p.u.* and 1.17 *p.u.*, respectively.

- Finally, a comparative study of TOVs caused by single-stage and two-stage grid-connected PV systems is presented. The study showed that, under the proposed

TOV limiting schemes, the grid-side and the inverter ac-side TOVs caused by each PV system is lower than 1.3 *p.u.* Thus, the proposed TOV limiting schemes meet the requirements imposed by [20], in terms of limiting the TOV.

4.2 Future Work

The following is a list of potential future research topics, related to the subject of this thesis:

- Studying the performance of, and making refinements to the proposed TOV limiting schemes, considering more realistic transformer models that include saturation characteristics.
- Studying the applicability of, and modifying, the proposed TOV limiting schemes for the PV systems interfaced with European MV distribution networks through a transformer with a YG/Δ winding configuration. A TOV analysis at the high-voltage side (Δ-side) of the transformer can be performed and, as such, modifications to the proposed TOV limiting schemes may be required for limiting the TOV.
- Studying the performance of the proposed TOV mitigation strategies when an islanding detection algorithm is also incorporated into the PV system.
- Adding a battery storage to the system, thus creating a PV/battery unit that can balance the PV generated power with the load. A PV power curtailment strategy can be adopted that enables the PV unit to curtail the PV generated power and autonomously match the local load in the islanded zone. Thus, the TOV caused by the PV system can be avoided. The excess energy can be utilized for charging the battery.

Appendix A

PV *generator* Model and Parameters

Parameters of the PV *generator* used in the single- and two-stage PV systems are taken from KC200GT data sheet and can be found in [96] and Table A.1.

Table A.1: PV *generator* Parameters

Parameter	Value	Remarks
number of series-connected PV cells per module	54	M_s
number of parallel-connected PV strings	300	N_p
number of series-connected PV modules per string	18	N_s
module short-circuit current (STC)	8.21 A	$\tilde{I}_{sc,r}$
module open-circuit voltage (STC)	32.9 V	$\tilde{V}_{oc,r}$
module maximum-power current (STC)	7.61 A	$\tilde{I}_{mp,r}$
module maximum-power voltage (STC)	26.3 V	$\tilde{V}_{mp,r}$
voltage temperature coefficient	-0.1 V/K	$\tilde{K}_V$
current temperature coefficient	0.003 A/K	$\tilde{K}_I$
diode ideality factor	1.3	a
module reference solar irradiation	1.0 kW/m^2	G_r
module reference p-n junction temperature	298 K	T_r
equivalent series resistor	0.231 Ω	R_s
equivalent parallel resistor	597.38 Ω	R_p
PV *generator* maximum power	1.0 MW	P_{pv}

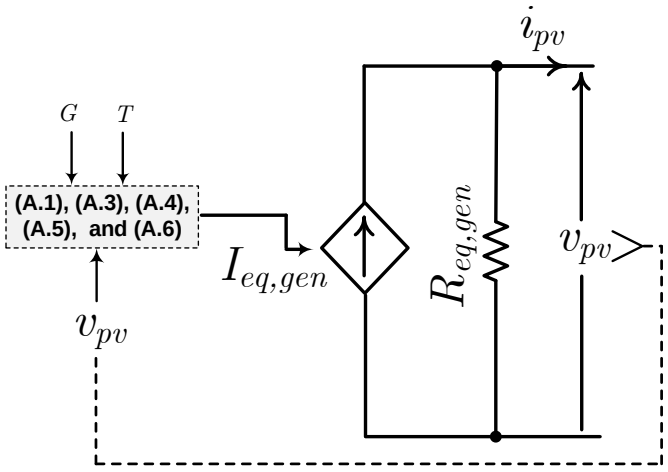

Figure A.1: An equivalent PSCAD circuit of the PV *generator*.

In this thesis, the PV *generator* model is adopted from [71]. The PV *generator* uses the single-diode model of a real PV cell or module. An equivalent PSCAD circuit of the PV *generator* is demonstrated in Figure A.1. As can be seen from the circuit of Figure A.1, v_{pv} and i_{pv} are the terminal voltage and current of the PV *generator*, $I_{eq,gen}$ is the equivalent current source, $R_{eq,gen}$ is the equivalent resistance, G is the solar irradiation, and T is the p-n junction temperature. The PV *generator* model is governed by the following two equations [71]

$$I_{eq,gen} = N_p I_i \left(\frac{R_P}{R_s + R_p} \right) \tag{A.1}$$

$$R_{eq,gen} = (R_s + R_p) \frac{N_s}{N_p} \tag{A.2}$$

where N_p is the number of parallel-connected PV strings, N_s is the number of series-connected PV modules per string, R_s and R_p are the series and parallel resistance of the PV module, and I_i is the terminal current of the ideal PV module.

As discussed in [71], I_i can be for formulated as

$$I_i = I_g(G,T) - \left[I_o(T) \left(e^{\frac{\beta(v_{pv} + i_{pv} R_s)}{a}} - 1 \right) \right] \tag{A.3}$$

where I_g is the photo-generated current, I_o is the diode reverse saturation current which depends on T, a is the diode ideality factor, and β is the inverse thermal voltage defined as

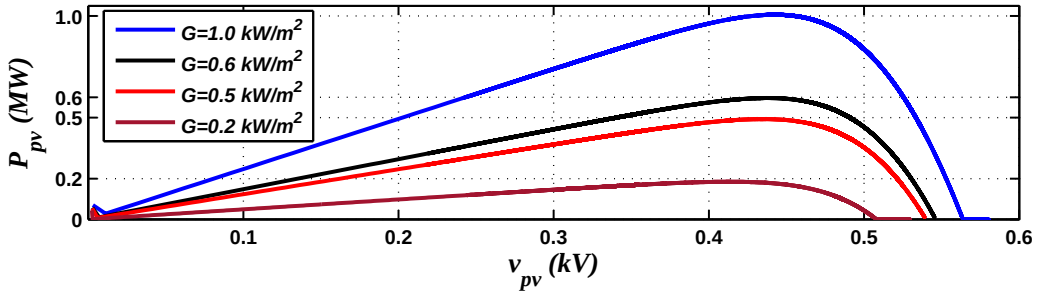

Figure A.2: Power-voltage characteristics curve of the PV *generator*.

$$\beta(T) = \frac{q}{M_s k T} \tag{A.4}$$

where q is the electron charge ($1.60217646 \times 10^{-19} C$), k is Boltzmann's constant ($1.3806503 \times 10^{-23} J/K$), and M_s is the number of series-connected PV cells per module.

In the short-circuit condition, I_g can be formulated as

$$I_g \simeq \left[\tilde{I}_{sc,r} + \tilde{K}_I (T - T_r)\right] \left(\frac{G}{G_r}\right) \tag{A.5}$$

where $\tilde{I}_{sc,r}$ is the PV module short-circuit current at STC, $\tilde{K}_I$ is the current temperature coefficient, and T_r and G_r are the reference p-n junction temperature and reference solar irradiation of the PV module, respectively.

In the open-circuit condition, I_o can be formulated as

$$I_o = \frac{\tilde{I}_{sc,r} + \tilde{K}_I (T - T_r)}{e^{\frac{\beta\left(\tilde{V}_{oc,r} + \tilde{K}_V (T - T_r)\right)}{a}} - 1} \tag{A.6}$$

where $\tilde{V}_{oc,r}$ and $\tilde{K}_V$ are the open-circuit voltage and the voltage temperature coefficient of the PV module, respectively.

The PV *generator* parameters are given in Table A.1. Figure A.2 illustrates the power-voltage characteristics curve of the PV *generator*, for different levels of the solar irradiation. As can be seen from Figure A.2, the maximum output power from the PV *generator* at $G = 1.0\ kW/m^2$ is about $1.0\ MW$.

Appendix B

Single-Stage PV System Parameters for Chapter 2

The single-stage PV system and controller parameters are listed in Table B.1 and Table B.2, respectively.

Table B.1: Single-Stage PV System Parameters

Parameter	Value	Remarks
PV *generator* rating	1.0 MW	
dc-link capacitance	5000 μF	C
maximum dc-link voltage	600 V	
inverter rating	1.0 MVA	
inverter switching frequency	3060 Hz	51×60 Hz
interface resistance	2.0 $m\Omega$	R
filter inductance	30 μH	L_f
filter capacitance	$200\Delta + 750Y$ μF	C_f
transformer nominal power	1.0 MVA	T_r
transformer voltage ratio	0.208/12.47 kV	Δ/Y (Figure 2.3)
transformer voltage ratio	0.208/12.47 kV	Y/Y (Figure 2.15)
transformer leakage inductance	0.1 $p.u.$	
transformer ohmic resistance	0.02 $p.u.$	
transformer copper losses	0.005 $p.u.$	
L_n	5 μH	Figure 2.15
R_n	15 $m\Omega$	Figure 2.15
τ_i	0.5 ms	Equation (2.7)

Table B.2: Controller Parameters for Chapter 2

Controller Parameter	k_p and k_i	Saturation limits	Remarks
k_d	0.06, 4	–7, 7	Figure 2.4
k_q	0.06, 4	–7, 7	Figure 2.4
k_0	0.009, 10	–0.3, 0.3	Figure 2.16
K_v	1.667, 370	–2.36, 2.36	Figure 2.6

The transfer function of the PLL filter is as follows:

$$H(s) = 685.42 \times 10^2 \left(\frac{s^2 + 568.516 \times 10^3}{s^3 + 1508s^2 + 568.516 \times 10^3 s} \right) \times \left(\frac{s^2 + 166s + 6889}{s^2 + 964s + 232.324 \times 10^3} \right) \quad [(rad/s)/V]. \tag{B.1}$$

The transfer function of the current-controller feed-forward filter of Figure 2.4 is as follows:

$$F(s) = \frac{1}{0.00005s + 1}. \tag{B.2}$$

The transfer function of the low-pass filter (LPF) of Figure 2.17(a) and Figure 2.20(a) are as follows:

$$T(s) = \frac{1}{0.005s + 1}. \tag{B.3}$$

The anti-wind-up technique based PI controller [Figure 2.18] parameters are: the proportional gain, $k_p = 5$, the anti-wind-up gain, k_{aw} is the design choice, and the integrator time constant is equal to 0.5 ms.

Appendix C

Two-Stage PV System Parameters for Chapter 3

The two-stage PV system parameters for Chapter 3 are listed in Table C.1. The PV *genereator* parameters can be found in Appendix A.

Table C.1: Two-Stage PV System Parameters

Parameter	Value	Remarks
rated power of PV *generator*	1.0 MW	
C_{pv}	1000 μF	
R_b	2 $m\Omega$	
L_b	100 μH	
boost converter switching frequency	3420 Hz	57×60 Hz
dc-link capacitance	8000 μF	C
maximum dc-link voltage	600 V	
inverter switching frequency	3060 Hz	51×60 Hz
inverter rating	1.0 MVA	
R	2 $m\Omega$	
L_f	30 μH	
C_f	200 μF	Δ connection
transformer nominal power	1.0 MVA	T_r
transformer voltage ratio	0.208/12.47 kV	Δ/YG (Figure 3.1)
K_{pv}	$1.67 + 909.09/s$	Figure 3.3
K_{iL}	$0.51 + 14.993/s$	Figure 3.3
K_b	$6.82 + 7043.742/s$	Figure 3.5
τ_i	0.5 ms	Equation (3.5)
K_v	$5.2 + 333.333/s$	Figure 3.6

Appendix D

PV System Relay Parameters

The PV system uses a voltage and a frequency relay. The function of the voltage relay is to detect the PCC voltage excursions, whereas the frequency relay detects the frequency excursions. Both relays isolate the PV system from the grid if the voltage and frequency exceed the normal operation limits. IEEE standards [36] define the minimum requirements of the voltage and frequency relays. The relay settings are adopted from [71] and given in Table D.1. The voltage and frequency relays are applied at the primary side of the isolation transformer, T_r.

Table D.1: Voltage and Frequency Relay Parameters

Voltage Relay Parameter	Value
first lower threshold	0.181 $p.u.$
under threshold first time delay	1.0 s
second lowest threshold	0.104 $p.u.$
under threshold second time delay	0.1 s
first higher threshold	0.229 $p.u.$
over threshold first time delay	1.0 s
second highest threshold	0.283 $p.u.$
over threshold second time delay	0.1 s
Frequency Relay Parameter	**Value**
lower threshold	59.3 Hz
under threshold time delay	0.1 s
upper threshold	60.5 Hz
over threshold time delay	0.1 s
minimum voltage to enable frequency relay	0.12 $p.u.$

Bibliography

[1] G. Pepermans, J. Driesen, D. Haeseldonckx, R. Belmans, and W. D'haeseleer, "Distributed generation: definition, benefits and issues," *Energy Policy*, vol. 33, no. 6, pp. 787–798, April 2005.

[2] B. Owens, "The Rise of Distributed Power," *Technical Report*, General Electric, 2014.

[3] H. L. Willis, and W. G. Scott, *Distributed power generation: planning and evaluation*. New York: Marcel Dekker, 2000.

[4] M. Oprisan, and S. Pneumaticos, "Potential for electricity generation from emerging renewable sources in Canada," in *Proc. IEEE EIC Climate Change Technology Conf.*, May 2006, pp. 1–9.

[5] N. Asano, and T. Saga, "PV technology trends and industry's role," in *Proc. IEEE Int. Electron Devices Meeting (IEDM)*, Dec. 2008, pp. 1–6.

[6] A. Labouret, and M. Villoz, *Solar Photovoltaic Energy*. Institution of Engineering and Technology (IET), ISBN: 978-1-84919-154-8, 2010.

[7] J. Schoene, V. Zheglov, D. Houseman, J. Smith, and A. Ellis, "Photovoltaics in distribution systems; integration issues and simulation challenges," in *Proc. IEEE Power Energy Soc. Gen. Meeting*, pp. 1–5, July 2013.

[8] C. Winneker, "Highlight: Worlds solar photovoltaic capacity passes 100-gigawatt landmark after strong year," EPIA, Tech. Rep., Feb. 2013.

[9] "Annual Report 2015," IEA Photovoltaic Power Systems Programme (PVPS), May 2016.

[10] "Global Market Outlook for Solar Power 2015-2016," European Photovoltaic Industries Association, EPIA, Tech. Rep., June 2015.

[11] R. K. Varma, G. Sanderson, and K. Walsh, "Global PV incentive policies and recommendations for utilities," in *Proc. 24th Can. Conf. Elect. Comput. Eng. (CCECE)*, pp. 001158–001163, May 2011.

[12] Y. Poissant and P. Bateman, "National Survey Report of PV Power Applications in Canada 2014," *IEA, NRCan & CanSIA*, Sept. 2015.

[13] "Roadmap 2020: Powering Canada's Future with Solar Electricity," *Canadian Solar Industries Association (CanSIA)*, Aug. 2015. [Online]. Available: `http://www.cansia.ca/uploads/7/2/5/1/72513707/cansia_roadmap_2020_final.pdf`

[14] F. Katiraei and J. R. Agüero, "Solar PV integration challenges," *IEEE Power Energy Mag.*, vol. 9, no. 3, pp. 62–71, May 2011.

[15] R. Passey, T. Spooner, I. MacGill, M. Watt, and K. Syngellakis, "The potential impacts of grid-connected distributed generation and how to address them: A review of technical and non-technical factors," *Energy Policy*, vol. 39, no. 10, pp. 6280-6290, Oct. 2011.

[16] A. Woyte, V. V. Thong, K. Purchala, R. Belmans, and J. Nijs, "Quantifying the occurrence and duration of power fluctuations introduced by photovoltaic systems," in *Proc. IEEE Power Tech Conference*, Bologna, vol.3, 7p. , 23-26 June 2003.

[17] R. K. Varma, J. Berge, I. Axente, V. Sharma and K. Walsh, "Determination of Maximum PV Solar System Connectivity in a Utility Distribution Feeder," in *IEEE Power & Energy Society Transmission and Distribution Conference and Exposition*, Orlando, Florida, May 2012.

[18] R. M. Jameel, S. U. Hani and T. Aziz, "Impact study of integrating solar plant in an 11kV urban distribution system," in *Proc. IEEE Power Energy Soc. Gen. Meeting Conference & Exposition*, National Harbor, MD, pp. 1–5, July 2014.

[19] S. Steffel, "Electric Grid Impact of PV and Mitigation Strategies," in *UVIG 2012 Fall Technical Workshop*, Omaha, Nebraska, October 2012.

[20] *Distributed Generation Technical Interconnection Requirements: Interconnections at Voltages 50kV and Below*, Hydro One Networks Inc., DT-10-015 R3, March 2013.

[21] M. Thomson and D. G. Infield, "Impact of widespread photovoltaics generation on distribution systems," *IET Renew. Power Generation*, vol. 1, no. 1, pp. 33–40, Mar. 2007.

[22] M. McGranaghan, T. Ortmeyer, D. Crudele, T. Key, J. Smith and P. Barker, "Renewable systems interconnection study: Advanced grid planning and operations," *Sandia National Laboratories*, Feb. 2008.

[23] G. L. Campen, "An analysis of the harmonics and power factor effects at a utility intertied photovoltaic system," *IEEE Trans. Power App. Syst.*, vol. PAS 101, no. 12, pp. 4632–4639, Dec. 1982.

[24] J. H. R. Enslin and P. J. M. Heskes, "Harmonic interaction between a large number of distributed power inverters and the distribution network," *IEEE Trans. Power Electron.*, vol. 19, no. 6, pp. 1586–1593, Nov. 2004.

[25] I. T. Papaioannou, A. S. Bouhouras, A. G. Marinopoulos, M. C. Alexiadis, C. S. Demoulias, D. P. Labridis, "Harmonic impact of small photovoltaic systems connected to the LV distribution network," in *Proc. European Electricity Market (EEM)*, pp.1–6, 28-30 May 2008.

[26] M. C. Benhabib, J. M. A. Myrzik, and J. L. Duarte, "Harmonic effects caused by large scale PV installations in LV network," in *Proc. Int. Conf. Electrical Power Quality and Utilization*, Barcelona, Spain, pp. 1–6, 9-11 Oct. 2007.

[27] P. Barker, "Overvoltage considerations in applying distributed resources on power systems," in *Proc. IEEE Power Eng. Soc. Summer Meeting*, vol. 1, Jul. 2002, pp. 109–114.

[28] S. Chen, and H. Yu, "A review on overvoltages in microgrid," in *Proc. Asia-Pacific Power Energy Eng. Conf.*, Mar. 2010, pp. 1–4.

[29] A. S. Energy, USA, "Neutral connections and effective grounding," in *White paper*, ENG-TOV-270-01 3/13.

[30] F. J. Pazos, A. Barona, J. Amantegui, E. Azcona, and S. Fernández, "Power frequency overvoltage generated by solar plant inverters," in *Proc. Int. Conf. Renew. Energies Power Quality*, Valencia, Spain, Apr. 15–17, 2009, pp. 1–8.

[31] M. E. Ropp, D. Schutz, and S. Cozine, "Temporary overvoltage issues in distribution-connected photovoltaic systems and mitigation strategies," in *Proc. 47th Minnesota Power Systems Conf*, Nov. 1–3, 2011, pp. 1–10.

[32] J. Balakrishnan, A. Atputharajah, and J. Ekanayake, "Review of the effects of transformer configuration on distributed generator interconnection," in *Proc. IEEE 3rd Int. Conf. Ind. Inf. Systems*, Dec. 2008, pp. 1–6.

[33] W. E. Feero, and W. B. Gish, "Overvoltages Caused by DSG Operation: Synchronous and Induction Generators," *IEEE Trans. Power Del.*, vol.1, no. 1, pp. 258–264, Jan. 1986.

[34] W. B. Gish, W. E. Feero, and S. Greuel, "Ferroresonance and Loading Relashionships for DSG Installations," *IEEE Trans. Power Del.*, vol. 2, no. 3, pp. 953–959, July 1987.

[35] *IEEE Standard for Interconnecting Distributed Resources With Electric Power Systems*, IEEE Std. 1547-2003.

[36] *IEEE Standard for Interconnecting Distributed Resources With Electric Power Systems*, IEEE Std. 1547.2-2008.

[37] *IEEE Recommended Practice for Utility Interface of Photovoltaic (PV) Systems*, IEEE Standard 929, 2000.

[38] *Interconnection of Distributed Resources and Electricity Supply Systems*, CAN/CSA-C22.3 No. 9-08, June 2008.

[39] E. Caamano, J. Thornycroft, H. De Moor, and S. Cobben, "State-of-the-art on dispersed PV power generation: Publications review on the impacts of PV distributed generation and electricity networks," *Technical Report, International Energy Agency (IEA)*, Jul. 2007.

[40] A. F. Povlsen, "Impacts of power penetration from photovoltaic power systems in distribution networks," *Technical Report, IEA PVPS*, T5-10, 2002.

[41] T. Funabashi, K. Koyanagi and R. Yokoyama, "A review of islanding detection methods for distributed resources," in *Proc. IEEE Power Tech Conf.*, Jun. 2003, vol. 2, pp. 23–26.

[42] A. Woyte, R. Belmans, and J. Nijs, "Testing and islanding protection function of photovoltaic inverters," *IEEE Trans. Energy Convers.*, vol. 18, no. 1, pp. 157–162, Mar. 2003.

[43] J. Yin, L. Chang, and C. Diduch, "Recent development in islanding detection for distributed power generation," in *Proc. Large Engineering Systems Conf. Power Engineering*, Jul. 2004, pp. 124–128.

[44] C. Schauder, "Impact of FERC 661-A and IEEE 1547 on photovoltaic inverter design," in *Proc. IEEE Power Energy Soc. Gen. Meeting*, Jul. 2011, pp. 1–6.

[45] J. Romero, A. F. Katiraei and B. Kruimer, "Impact studies and mitigation measures for integration of solar photovoltaic distributed generation," *Technical Report, Quanta Technology*, 2013.

[46] H. Ghoddami and A. Yazdani, "A mitigation strategy for temporary overvoltages caused by grid-connected photovoltaic systems," *IEEE Trans. Energy Convers.*, vol. 30, pp. 413–420, June 2015.

[47] R. Bravo, R. Salas, R. Yinger, and S. Robles, "Solar photovoltaic inverters transient over-voltages," in *Proc. IEEE Power Eng. Soc. General Meeting*, July 2013, pp. 1–5.

[48] *IEEE Recommended Practice for Grounding of Industrial and Commercial Power Systems*, IEEE Std 142-2007 (Revision of IEEE Std 142-1991), pp. 1–225, Nov. 2007.

[49] M. E. Ropp, M. Johnson, D. Schutz, and S. Cozine, "Effective grounding of distributed generation inverters may not mitigate transient and temporary overvoltage," in *Proc. Western Protective Relay Conf.*, Spokane, WA, USA, Oct. 16–18, 2012, pp. 1–8.

[50] A. Dexters, T. Loix, J. Driesen, and R. Belmans, "A comparison of grounding techniques for distributed generators implemented in four-wire distribution grids, UPS systems and microgrids," in *Proc. 19th Int. Conf. Elect. Distrib.*, pp. 1–4, 2007.

[51] R. Arritt and R. Dugan, "Distributed generation interconnection transformer and grounding selection," in *Proc. IEEE Power Energy Soc. Gen. Meeting,*, pp. 1–7, July 2008.

[52] S. Hong, D. Yoo and M. Z.-Martinson, "Effective grounding for PV plants," in *White Paper, Solectria Renewables*, SRCW00101. [Online]. Available: `https://solectria.com//site/assets/files/1484/solectria_effective_grounding_for_pv_plants.pdf`

[53] R. Walling, "TOV issues in renewable plant collectors and application of grounding transformers," *IEEE PES Presentation*, 2014. [Online]. Available: `http://www.ieee-pes.org/presentations/td2014/td2014p-000647.pdf`

[54] M. Reno, R. Broderick, and S. Grijalva, "Smart inverter capabilities for mitigating over-voltage on distribution systems with high penetrations of PV," in *IEEE Photovoltaic Specialists Conference*, pp. 3153–3158, June 2013.

[55] T. Aziz, T. Saha, and N. Mithulananthan, "Analysis and mitigation of transient overvoltage with integration of small scale power-electronic interfaced DG," in *Proc. IEEE Power Energy Soc. Gen. Meeting*, pp. 1–8, July 2012.

[56] M. B. Delghavi and A. Yazdani, "A control strategy for islanded operation of a distributed resource (DR) unit," in *IEEE Power & Energy Soc. Gen. Meeting*, Calgary, AB, Canada, 2009.

[57] H. Mahmood, and J. Jiang, "A control strategy of a distributed generation unit for seamless transfer between grid connected and islanded modes," in *Proc. International Symposium on Industrial Electronics (ISIE)*, pp. 2518–2523, Jun. 2014.

[58] A. C. Mahendra, "Novel Control of PV Solar and Wind Farm Inverters as STATCOM for Increasing Connectivity of Distributed Generators" (2013). *University of Western Ontario - Electronic Thesis and Dissertation Repository.* Paper 1241.

[59] H. Mahmood, D. Michaelson, and J. Jiang, "Strategies for independent deployment and autonomous control of PV and battery units in islanded microgrids," *IEEE Trans. Emerg. Sel. Topics Power Electron.*, vol. 3, pp. 742–755, Sept 2015.

[60] H. Ghoddami, M. B. Delghavi, and A. Yazdani, "An integrated wind-photovoltaic-battery system with reduced power-electronic interface and fast control for grid-tied and off-grid applications," *Renew. Energy*, vol. 45, pp. 128–137, 2012.

[61] M. Mirhosseini, J. Pou and V. G. Agelidis, "Single- and two-stage inverter-based grid-connected photovoltaic power plants with ride-through capability under grid faults," *IEEE Trans. Sustainable Energy*, vol. 6, no. 3, pp. 1150–1159, 2015.

[62] T. M. Blooming and D. J. Carnovale, "Application of IEEE Std 519-1992 Harmonic Limits," *Conference Record of Annual Pulp and Paper Industry Technical Conference*, pp. 1–9, 2006.

[63] E. Troester, "New German Grid Codes for Connecting PV Systems to the Medium Voltage Power Grid," in *Proc. 2nd Int. Workshop Conc. Photovoltaic Power Plants Opt. Des. Product., Grid Connect.*, pp. 1–4, Mar. 2009.

[64] Benchmark systems for network integration of renewable and distributed energy resources, *CIGRE Technical Brochure*, CIGRE Task Force C6.04.02, 2011.

[65] C. Mozina, "Impact of green power inverter-based distributed generation on distribution systems," in *Proc. 67th Annu. Conf. Protective Relay Eng.*, pp. 264–278, March 2014.

[66] M. Vaziri, S. Vadhva, F. Tavatli, and S. Vaziri, "Volt/var regulation and issues with high penetration of renewables on distribution systems," in *IEEE 13th International Conference on Information Reuse and Integration (IRI)*, pp. 519–524, Aug. 2012.

[67] M. Farhoodnea, A. Mohamed, H. Shareef, and H. Zayandehroodi, "Power quality impacts of high-penetration electric vehicle stations and renewable energy-based generators on power distribution systems," *Measurement*, vol. 46, no. 8, pp. 2423–2434, 2013.

[68] M. Thomson and D. Infield, "Impact of widespread photovoltaics generation on distribution systems," *Renewable Power Generation, IET*, vol. 1, pp. 33–40, March 2007.

[69] V. Schwarzer and R. Ghorbani, "Transient Over-Voltage Mitigation and its Prevention in Secondary Distribution Networks with High PV-to-Load Ratio," *Tech. Rep.*, Hawaii Natural Energy Institute, 2015.

[70] S. Darie,"Guidelines for large photovoltaic system integration," in *Proc. IEEE Transmission and Distribution Conference and Exposition*, pp. 1–6, May 2012.

[71] A. Yazdani, A. R. Di Fazio, H. Ghoddami, M. Russo, M. Kazerani, J. Jatskevich, K. Strunz, S. Leva and J. A. Martinez, "Modeling Guidelines and a Benchmark for Power System Simulation Studies of Three-Phase Single-Stage Photovoltaic Systems," *IEEE Trans. Power Del.*, vol. 26, pp. 1247–1264, April 2011.

[72] M. Singh, V. Khadkikar, A. Chandra, and R. K. Varma, "Grid Interconnection of Renewable Energy Sources at the Distribution Level With Power-Quality Improvement Features," *IEEE Trans. Power Del.*, vol. 26, pp. 307–315, April 2011.

[73] M. B. Delghavi and A. Yazdani, "A control strategy for islanded operation of a Distributed Resource (DR) unit," in *Proc. IEEE Power Eng. Soc. General Meeting*, pp. 1–8, July 2009.

[74] H. Ghoddami and A. Yazdani, "A Single-Stage Three-Phase Photovoltaic System With Enhanced Maximum Power Point Tracking Capability and Increased Power Rating," *IEEE Trans. Power Del.*, vol. 26, pp. 1017–1029, April 2011.

[75] N. Mohan, T. M. Undeland, and W. P. Robbins, *Power Electronics: Converters, Applications, and Design*, 3rd ed. Hoboken, NJ: Wiley, 2003.

[76] A. Yazdani and R. Iravani, *Voltage-Sourced Converters in Power Systems*. IEEE/John-Wiley, ISBN: 978-0-470-52156-4, 2010.

[77] A. Yazdani and P. P. Dash, "A Control Methodology and Characterization of Dynamics for a Photovoltaic (PV) System Interfaced With a Distribution Network," *IEEE Trans. Power Del.*, vol. 24, pp. 1538–1581, July 2009.

[78] S. A. Rahman and R. K. Varma, "PSCAD/EMTDC model of a 3-phase grid connected photovoltaic solar system," in *Proc. 43rd North Amer. Power Symp.*, pp. 1–7, August 2011.

[79] M. Manojkumar, K. Porkumaran, and C. Kathirvel, "Power electronics interface for hybrid renewable energy system – A survey," in *Proc. International Conference on Green Computing Communication and Electrical Engineering* , pp. 1–9, March 2014.

[80] E. Romero-Cadaval, G. Spagnuolo, L. G. Franquelo, C. A. Ramos-Paja, T. Suntio and W. M. Xiao, "Grid-Connected Photovoltaic Generation Plants: Components and Operation," *IEEE Ind. Electron. Mag.*, vol. 7, no. 3, pp. 6–20, Sept 2013.

[81] H. Tian, F. M. David, K. Ellis, P. Jenkins and E. Muljadi, "Detailed Performance Model for Photovoltaic Systems," *National Renewable Energy Laboratory (NREL)*, July 2012.

[82] A. D. Rajapakse and D. Muthumuni, "Simulation tools for photovoltaic system grid integration studies," in *Proc. Electr. Power Energ. Conf. (EPEC 2009)*, pp. 1–5, Oct 2009.

[83] *PSCAD/EMTDC v. 4.6*, Manitoba HVDC Research Centre. Winnipeg, MB, Canada, 2015.

[84] A. R. Reisi, M. H. Moradi and S. Jamasb, "Classification and comparison of maximum power point tracking techniques for photovoltaic system: A review," *Renewable Sustain. Energy Rev.*, vol. 19, pp. 433–444, 2013.

[85] T. Esram and P. L. Chapman, "Comparison of Photovoltaic Array Maximum Power Point Tracking Techniques," *IEEE Trans. Energy Convers.*, vol. 22, no. 2, pp. 439–449, 2007.

[86] K. Strunz,"Developing benchmark models for studying the integration of distributed energy resources," *IEEE Power Eng. Soc. Gen. Meeting*, Montreal, QC, Canada, 2006.

[87] M. A. Zamani, A. Yazdani and T. S. Sidhu, "A control strategy for enhanced operation of inverter-based microgrids under transient disturbances and network faults," *IEEE Trans. Power Del.*, vol. 27, no. 4, pp. 1737–1747, 2012

[88] B. Brooks, L. Casey and J. Song, "High Voltage Photovoltaics," *SOLARPRO*, issue 2.5, Aug./Sep. 2009.

[89] L. Casey, "The Performance Advantage of Higher Voltage Inverters," *SOLARPRO*, issue 2.5, Aug./Sep. 2009.

[90] *IEEE Recommended Criteria for Terrestrial Photovoltaic Power Systems*, ANSI/IEEE Std. 928–1986.

[91] B. Yang, W. Li, Y. Zhao and X. He, "Design and Analysis of a Grid-Connected Photovoltaic Power System," *IEEE Trans. Power Electron.*, vol. 25, no. 4, pp. 992–1000, 2010.

[92] H. Ghoddami and A. Yazdani, "A Bipolar Two-Stage Photovoltaic System Based on Three-Level Neutral-Point Clamped Converter," in *Proc. IEEE Power Energy Soc. Gen. Meet.*, pp. 1–8, July 2012.

[93] H. Mahmood, D. Michaelson, and J. Jiang, "Control strategy for a standalone PV/battery hybrid system," in *Proc. IEEE Ind. Electron. Conf.*, pp. 3412–3418, Oct. 2012.

[94] K. Kobayashi, I. Takano, and Y. Sawada,"A study of a two stage maximum power point tracking control of a photovoltaic system under partially shaded insolation conditions," *Solar Energy Mater. Solar Cells*, vol. 90, pp. 2975–2988, Nov. 2006.

[95] A. K. Rathore, "Two Loop Average Current Control of Boost Converter," [Online]. Available: `https://www.ece.nus.edu.sg/stfpage/akr/controlboost.pdf`

[96] Kyocera Solar, Inc. "HIGH EFFICIENCY MULTYCRYTAL MODULE," KC200GT, [Online]. Available: `http://www.kyocerasolar.com/assets/001/5195.pdf`.

Curriculum Vitae

Name:	Md Maruful Islam
Post-Secondary Education and Degrees:	University of Western Ontario London, ON, Canada 2014–2016, MESc in Electrical Engineering Khulna University of Engineering & Technology (KUET) Khulna, Bangladesh 2006–2010, B.Sc. in Electrical & Electronic Engineering (EEE)
Honours and Awards:	• Western Graduate Research Scholarship, 2014–16. • Bangladesh-Sweden Trust Fund (BSTF) Travel Award, 2016. • Merit Scholarship Award by Board of Education of Bangladesh, 2006–10. • Named to the Dean's list for scholastic achievement in undergraduate academic session 2007–08, 2008–09, 2009–10. • KUET Technical Scholarship, 2006–10.
Related Work Experience:	• Research and Teaching Assistant, University of Western Ontario, 2014–2016. • University Lecturer, Dept. of Electrical & Electronic Engineering Dhaka University of Engineering & Technology, Dhaka, Bangladesh, 2011–Present.

Publications:

Journal Publication:

- Md Maruful Islam, Md. Rashedul Islam, and Md. Kamal Hossain, "Performance Analysis of a DTC and SVM Based Field-Orientation Control Induction Motor Drive," *International Journal of Power Electronics and Drive Systems (IJPEDS)*, vol. 5, no. 3, pp. 336–343, Feb. 2015.